Radboud University Nijmegen

Faculty of Science (FNWI)

High Energy Physics

Loop-Induced Direct Detection of ALP-Mediated Dark Matter via Nucleon Scattering

Author:
Daniël Mikkers

Supervisors:
Dr. S. Westhoff
Prof. Dr. W.J.P. Beenakker
A. Phan

Second Reviewer:
Prof. Dr. M.E.J. Postma

27th June 2025

Radboud Universiteit

Abstract

Dark matter (DM) remains one of the biggest unresolved mysteries in cosmology and particle physics. Whereas astrophysical and cosmological observations strongly support its existence, direct detection efforts have yet to provide conclusive evidence of its particle nature. This thesis investigates the potential detection of fermionic DM via nucleon scattering mediated by Axion-Like Particles (ALPs). By using effective field theory, we establish a translation between relativistic operators and non-relativistic building blocks, that can be found in literature. The second-order expansion of operators provides an interesting addition, when leading-order terms are suppressed. Next within this effective theory, we examine the scattering amplitude of DM–up-quark scattering at tree-level and find that the cross section is momentum suppressed, as well as suppressed by the ALP decay constant $f_a \sim 1$ TeV. We calculate the scattering amplitude at one-loop order, leveraging the top-quark mass scale to lift the suppression of f_a, and find that the loop contribution dominates the cross section of SI interactions. We examine ultraviolet divergences and renormalization effects, evolving the ALP's vector and axial-vector couplings down to the top-quark mass scale, assuming the ALP is less massive than the top-quark. Based on current experimental bounds on Kaon and B-meson decays, we establish constraints on the coupling for ALP masses below 250 MeV/c^2 and 5 GeV/c^2, respectively. Our findings suggest that current direct detection experiments could probe ALP-mediated dark matter with masses between 10 and 20 GeV/c^2, while heavier DM is excluded by current experiments. Although the neutrino fog may pose a problem and new experiments would be needed to probe these masses, the expectation based on our outcome is within the region where more statistics make detecting small DM masses possible, which make the neutrino fog less problematic. This work highlights the importance of loop-effects in ALP phenomenology and their potential impact on DM detection.

Contents

CHAPTER 1

Introduction

Dark matter (DM) plays a crucial role in our understanding of modern cosmology. Despite its significance, DM has neither been directly detected nor produced in experiments, making it one of the central open questions in cosmology and particle physics. Baryonic matter and the particles of the Standard Model of particle physics cannot explain all the astrophysical observations, which are touched upon later. The ΛCDM model, the standard model of cosmology, is consistent with a wide range of high-quality observations [1]. In this model, Λ represents dark energy, and CDM stands for cold dark matter. Together with inflationary theory, described in ΛCDM, this model provides a detailed picture of the Universe's structure formation [2].

First let us answer why DM needs to be 'cold'. Cold DM refers to particles with insignificant velocity dispersion relative to the Hubble flow and minimal non-gravitational interactions [3]. DM must lack an electric charge to avoid interacting with photons, ensuring it remains "dark". Simulations comparing hot (relativistic) and cold (non-relativistic) DM demonstrate that hot and cold DM lead to significantly different results in large scale structures of the Universe. These simulations lead to the conclusion that hot dark matter could not account for all the DM in the Universe [4]. Cold DM makes, therefore, a more viable candidate.

There are numerous observations supporting cold DM. One of the most compelling pieces of evidence for DM comes from galaxy rotation curves. According to Newtonian gravity, the rotational velocity of stars at a radius r from the galactic center is

$$v(r) = \sqrt{\frac{Gm(r)}{r}} \tag{1.1}$$

where G is the gravitational constant and $m(r)$ is the total mass contained within r [5]. Beyond the galactic disk, the enclosed mass should be approximately constant. Combining information with Eq. (1.1), we see that for distances beyond the galactic disk $v(r) \propto r^{-1/2}$. However, observations show that rotation curves flatten at these radii instead of following Keplerian behavior (see Fig. 1.1) [6]. This flattening of rotation curves implies that $m(r) \propto r$ at large distances. Two explanations have been proposed: either Newtonian mechanics does not apply on these scales (e.g. Modified Newtonian Dynamics) or the discrepancy is caused by DM [7]. As the name suggests, the former theory modifies Newtonian dynamics to make up for the discrepancy with

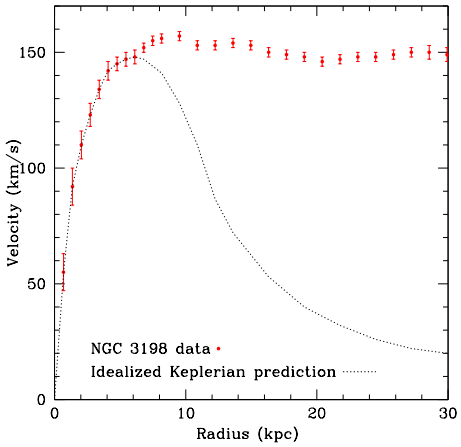

Figure 1.1: Measured rotational speeds of HI regions in NGC 3198 and (dashed) the ideal Keplerian behavior [5].

observations. This thesis focuses on the latter theory, where DM is expected to form halos, i.e. gravitationally bound regions decoupled from the Hubble expansion [8].

Gravitational lensing provides further evidence for DM. In general relativity, massive objects bend light, and in some cases, form Einstein rings with a radius given by

$$\theta_E = \sqrt{\frac{4GM}{c^2}\frac{d_{LS}}{d_L d_S}}.$$

Here c is the speed of light, M is the mass of the lens, d_{LS}, d_L and d_S are the distance between the lens (L) and the source (S), the distance to the lens and the distance to the source, respectively.

Lensing observations allow the mass distribution within galaxies and clusters to be estimated. For instance, in cluster CL 0024+1654 (Fig. 1.2), over 98% of the mass is associated with smoothly distributed DM rather than luminous matter [9]. In Fig. 1.2 the smooth distribution of DM can be seen in galaxy cluster 0024+1654 (in orange). This cluster lenses the background galaxy in eight different subimages.

Similarly, the Bullet Cluster (Fig. 1.3), a colliding cluster of galaxies, provides direct evidence for DM through the separation of baryonic matter (pink) and DM (blue), with DM passing through unaffected by the collision. This effect requires there to be DM [10]. Fig. 1.3 shows that a lot of mass is concentrated in the blue regions, which is not associated with baryonic (luminous) matter and therefore 'dark'.

The last piece of evidence we will address is evidence found in anisotropies in the Cosmic Microwave Background (CMB). The CMB was created about 3×10^5 year ($z \simeq 1100$) after the Big Bang. In this period, known as cosmological recombination, the temperature dropped. The photons in the early Universe no longer scattered with electrons and ions, making ions and electrons able to bind and create atoms, i.e. photons decoupled from baryonic matter. Now photons were able to travel freely, which is what we now detect as the CMB. Small temperature fluctuations in the CMB ($\delta T/\overline{T} \approx 10^{-5}$) encode information about the density and composition of the Universe [12]. A map of the temperature fluctuations in the CMB is given in Fig. 1.4a. From the CMB, the auto-correlation of the temperature fluctuations can be extracted and given in terms of the multipole moments. The associated power spectrum is given in Fig. 1.4b. During

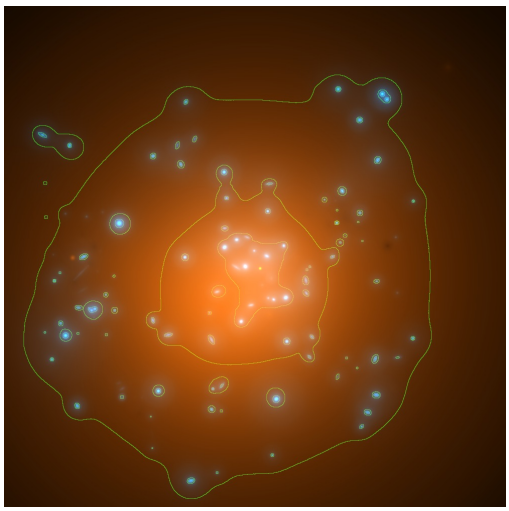

Figure 1.2: The reconstructed total mass density in CL 0024+1654. The DM is shown in orange and the mass associated with luminous matter (the galaxies) is shown in blue. The contours shown are at 0.5, 1, and 1.5 times the critical lensing density [9].

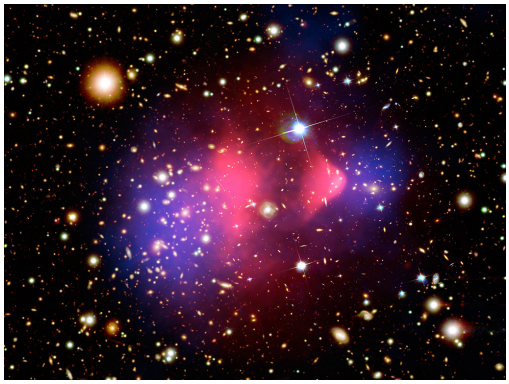

Figure 1.3: Image of the Bullet Cluster taken by Chandra X-Ray Observatory. The hot gas made of baryonic matter is colored in pink. The region where the most mass is concentrated, determined using gravitational lensing, is colored in blue. The mass in the blue regions is associated with dark matter. [11]

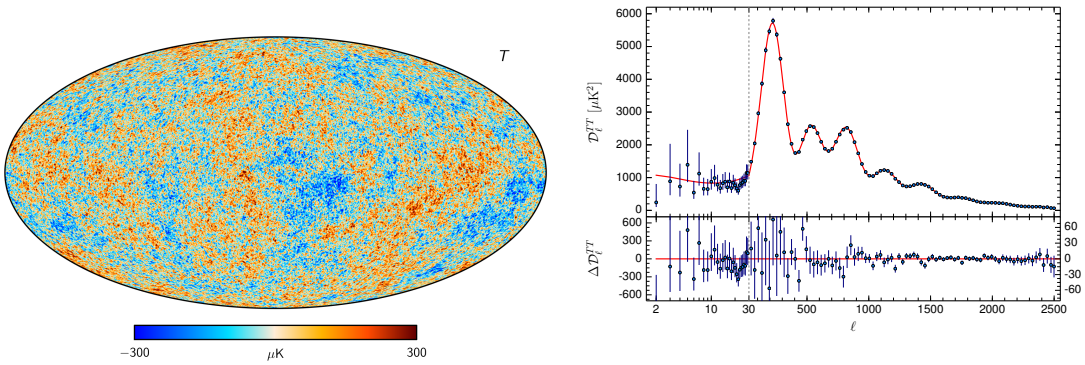

(a) (b)

Figure 1.4: Left: A map of the temperature fluctuations of the CMB made by the Planck telescope in 2020 [13]. Right: The Planck temperature power spectrum in 2015, where the red line is a fit of the ΛCDM model [14]. The residual with respect to the model is plotted in the lower panel.

recombination the interaction between photons and baryonic matter is influenced by DM. Baryonic matter falls into gravitational potential wells created by DM, which in turn heats up the plasma and generates outward pressure. This pressure causes the plasma to expand, cooling the plasma down again. A cycle of compression and expansion induces acoustic oscillations of the baryon-photon fluid. These baryonic acoustic oscillations made an imprint in the peaks of the CMB power spectrum. Changing the abundance of DM in turn changes the power spectrum of the CMB. [15] The ΛCDM model fits well with the CMB power spectrum, as seen in Fig. 1.4b. The Planck data [16] suggests the DM density in the Universe is approximately 24%.

Given this evidence, is there some prediction we can make about the evolution of DM in the Universe? Using the thermal evolution of the Universe, a prediction on the annihilation cross section (or actually the thermally averaged cross section) can be made, assuming that dark matter is made of particles. In the early Universe, the temperatures were high enough that all particles were in thermal equilibrium. We assume that the number density and energy density of a particle i with mass m at temperature T is described by

$$n_{\mathrm{eq},i}(T) = g_i \int \frac{d^3p}{(2\pi)^3} f(p,T), \tag{1.2a}$$

$$\rho_{\mathrm{eq},i}(T) = g_i \int \frac{d^3p}{(2\pi)^3} E(p) f(p,T). \tag{1.2b}$$

Here, g_i are the number of internal degrees of freedom, such as spin, $f(p,T)$ is the phase-space distribution and $E^2(p) = p^2 + m^2$ is the energy of particle i. The phase-space distribution $f(p,T)$ is given by the Fermi-Dirac distribution $(+)$ for fermions and the Bose-Einstein distribution for bosons $(-)$:

$$f(p,T) = \frac{1}{\exp\left((E(p)-p)/T\right) \pm 1}. \tag{1.3}$$

As the Universe expands, the temperature decreases. Assuming that all particles remain in thermal equilibrium, the temperature eventually decreases to a point where it drops below the mass of the particles $m \gg T$. When this happens the phase-space distribution reduces to a

Maxwell-Boltzmann distribution, for both bosons and fermions. The annihilation rate is linearly dependent on the number density $n_{\mathrm{eq},i}$. In order to keep the Universe in thermal equilibrium, the particle's interaction rate must be much larger than the Hubble rate: $\Gamma \gg H$. This interaction rate is defined as

$$\Gamma(T) = n_{\mathrm{eq}}(T)\sigma v_{\mathrm{rel}}(T), \tag{1.4}$$

where σ is the interaction cross section and v_{rel} is the relative velocity between particles. In this situation, particles interact so frequently, they are not bothered by cosmological expansion and any fluctuations in the densities is smoothed out, such that the system returns to equilibrium. This interaction rate is different for various species of particles and different types of interactions. When for some species in the early Universe $\Gamma \sim H$, it decouples from the other particles. Then particles freeze-out from equilibrium and attain some fixed abundance. At freeze-out the particles are no longer in chemical equilibrium, but remain in kinetic equilibrium with the surrounding plasma. [7, 17–19]

Postulating that DM follows the same history as the SM particles, we conclude that DM should be non-relativistic, i.e. CDM, and should have an energy density of $\Omega_\chi h^2 = 0.12$ [16]. The cosmological evolution of DM can be traced using the Boltzmann equation: [17]

$$\frac{dn_\chi}{dt} + 3H(T)n_\chi = -\langle\sigma v\rangle\left(n_\chi^2 - n_{\chi,\mathrm{eq}}^2\right). \tag{1.5}$$

Here, $\langle\sigma v\rangle$ is the thermally averaged annihilation cross section for the process $\chi\chi \to (SM)(SM)$ [20]:

$$\langle\sigma v\rangle = \frac{1}{8m_\chi^4 T K_2^2(m_\chi/T)} \int_{4m_\chi^2}^{\infty} ds\ \sigma(s)\sqrt{s}\left(s - 4m_\chi^2\right) K_1\left(\frac{\sqrt{s}}{T}\right). \tag{1.6}$$

As the Universe expands the number density decreases. It is useful to scale with the expansion instead, and use the comoving number density $Y_\chi = n_\chi/s$, where s is the total entropy density of the Universe. The Boltzmann equation can be rewritten in terms of Y_χ, writing $x = m_\chi/T$, using that sa^3 is constant (where a is the scale-factor), $T \propto 1/a$, and $dx/dt = H(x)x$:

$$\frac{dY_\chi}{dx} = -\frac{xs\langle\sigma v\rangle}{H(m_\chi)}\left(Y_\chi^2 - Y_{\mathrm{eq},\chi}^2\right). \tag{1.7}$$

Solving the equation for CDM (see [7, 17]) results in the following expression for the energy density of DM today

$$\Omega_\chi = \frac{m_\chi s_{\mathrm{today}} Y_{\mathrm{today}}}{\rho_{\mathrm{cr}}}, \tag{1.8}$$

where ρ_{cr} is the critical density of the Universe. This value is often called the relic abundance, because it is the density remaining after freeze-out. To match the experimental results of $\Omega_\chi h^2$, the thermally averaged cross section for a WIMP-like DM candidate has to be of the order of $\langle\sigma v\rangle \sim 10^{-26}$ cm^2 [17].

This prediction has led to the WIMP miracle, with a DM mass around the 100 GeV and coupling of 0.01, which we now know not to be a miracle. Essentisly, the coupling α–not only 0.01–can take any value between 0 and 1, which opens up a wider range of DM masses. With α^2/m_χ^2 remaining constant, m_χ can take any value between approximately 1 keV and 100 TeV, because lighter DM particles have a small coupling and would still be relativistic at freeze-out, while heavier DM particles would have a larger coupling and perturbative calculations are not applicable anymore. [7]

The conlcusion from the above discussion, is that in order to explain the relic abundance of DM, DM must have some kind of interaction with Standard Model particles. Given the strong

evidence for DM, knowing that DM must interact with Standard Model particles and that a wide range of masses m_χ are possible, detecting it directly remains a major goal in physics. Direct detection experiments are still increasing their sensitivity in the cross-section–DM-mass search-space. As we mentioned, different models have been trying to explain DM, but none have been experimentally confirmed, yet. One of these models assumes ALPs as mediators between DM and the SM.. In this thesis we have found a way to make the direct detection of ALP-mediated DM via nucleon scattering work.

First, in Chapter 2 we will focus on direct detection experiments and discuss how they work. Since cold DM is non-relativistic, the predictions from relativistic quantum field theory must be adapted to the non-relativistic regime. In Chapter 2 we discuss the non-relativistic theory from literature and calculate the first and second order non-relativistic expansion of the relativistic theory. Next, in Chapter 3, we examine a specific DM model involving ALPs as a mediator using ALP effective field theory. We then obtain an expression for tree-level scattering in Section 3.2, where we identify some problems involving suppression. This suppression can be lifted by going to one-loop order calculations. So, in Section 3.3 we calculate the loop integral and simplify and approximate it, to obtain the leading order contribution to the loop integral. Since the diagrams are divergent, we identify the operator and diagrams that renormalize our integral in Section 3.4. It was found in literature that meson decay can set constraints on the flavor-changing ALP coupling to quarks. In Section 3.6 we are able to set bounds on the couplings in our loop diagrams for certain ALP masses. Next, we evolve the couplings from the cutoff scale of the ALP effective field theory down to the top-mass in Section 3.5, using RGEs found in literature, where we run into complicating situations. Lastly, in Section 3.7 we estimate the cross section and compare our prediction to experimental results and constraints.

CHAPTER 2

Dark Matter Direct Detection

In the previous chapter we discussed some properties of dark matter (DM) and the evidence for DM. With all this observational evidence, a natural question arises: how can we establish experimental evidence of DM? Various experiments around the world are focused on so-called direct detection to confirm the existence of DM. In this chapter we will first discuss direct detection experiments and their working principles in Section 2.1. Next, in Section 2.2 we discuss effective field theory (EFT) for direct detection of DM with relativistic operators. But, cold DM is non-relativistic (NR), meaning that we must take an NR limit of the relativistic theory in order to make predictions. In Section 2.3 we do this. This chapter will be concluded by Section 2.4, where we go to second order expansion in the NR limit and its caveat of needing the center-of-mass frame.

2.1 Experiments

As discussed in the introduction, numerous gravitational pieces of evidence for DM have been observed, coming to the conclusion that it must be electrically neutral and massive. In Chapter 1 we have seen that in order to explain the relic abundance of DM via a dynamical process, it must have another property; it must have interactions – although weak – with Standard Model (SM) particles. Experimental verification is essential to confirm the existence of DM and probe the properties of these particles, if DM is another type of particle. There are three types of interactions that experiments can observe: DM production, DM annihilation/decay, and DM-SM scattering. These processes are illustrated in Fig. 2.1. The direction of the arrows in the diagram indicates the flow of time, hence, indicating how the diagram should be read and what process is represented by the diagram. Experiments like the Large Hadron Collider (LHC) have prospects producing DM [21]. In such high-energy environments, SM particles may acquire sufficient energy to produce DM through non-SM interactions. Since DM is electrically neutral and detector instruments (like calorimeters) only detect particles via strong or electromagnetic interactions [22], DM would manifest itself as missing energy or momentum in detectors that is not of neutrino origin. However, when this thesis was written, no DM signal has been observed yet at the LHC [23].

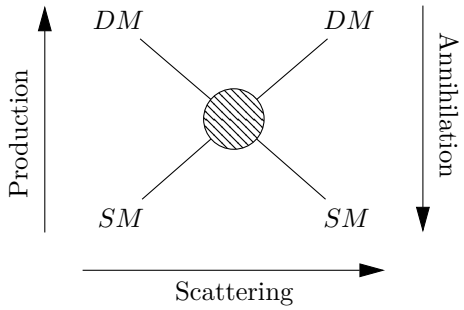

Figure 2.1: Diagram for scattering Standard Model (SM) particles with dark matter (DM), and the production and annihilation of dark matter. The direction of the arrows is the direction time flows in.

The second type of interaction, DM annihilation, involves DM particles annihilating and producing SM particles. The DM present in and around astrophysical objects in or close to our galaxy could self-annihilate into SM particles, which could lead to measurable signatures [24]. The latter is categorized as *indirect detection* and the former as collider-detection of DM.

The third type, DM-SM scattering, constitutes *direct detection*, because the effect of DM is observed with direct interactions with SM particles. DM particles are believed to permeate the Universe and should occasionally scatter with particles on Earth. Such interactions cause nuclear recoil with some recoil energy E_R, that can potentially be measured. If the recoil energy is large enough, it may be possible to detect scatterings and infer the properties of DM from kinematics [7]. The nuclear recoil energy of a nucleus with mass m_N after scattering with a DM particle is given by [7]

$$E_R = \frac{\mathbf{q}^2}{2m_N} \simeq 50 \text{ keV } \left(\frac{m_\chi}{100 \text{ GeV}}\right)^2 \left(\frac{100 \text{ GeV}}{m_N}\right), \tag{2.1}$$

where $|\mathbf{q}| \sim m_\chi v$ is the NR three-momentum transfer in the collision, and $v \sim 10^{-3}$ is the NR average velocity of DM particles in the Milky Way halo. For a nucleus of mass $m_N \sim 100$ GeV/c^2, the recoil energy is less than 1 keV for $m_\chi \leq 10$ GeV/c^2. A recoil energy of this scale is too low for experiments like LZ and XENONnT to detect [25, 26]. However, for DM masses in the range $10 - 10^3$ GeV/c^2, the recoil energy is large enough to produce a detectable signal in these experiments. Other experiments, like DarkSide and PandaX, are specialized in detecting smaller DM masses, in the range of $1 - 10$ GeV/c^2 [27, 28].

A basic quantity of interest in direct detection is the scattering rate between DM and the targets. The differential scattering rate of a DM particle off a nuclear target is [7]

$$\frac{dR}{dE_R} = \frac{\rho_\chi}{m_\chi m_N} \int_{v_{\min}}^{v_{\max}} d^3v \; v f(\mathbf{v} + \mathbf{v}_{\text{obs}}, t) \frac{d\sigma}{dE_R}. \tag{2.2}$$

Here, ρ_χ is the local DM density in the galaxy, f is the DM velocity distribution in the galactic frame, $v_{\max}$ is the Milky Way escape velocity, and $v_{\min}$ is the minimum velocity required to scatter with a nucleus with energy E_R. Assuming that the nucleus is at rest and DM is NR and moving in the x-direction, the four-momenta are $k^\mu = (m_N, \mathbf{0})$ and $p^\mu = (m_\chi + \frac{1}{2}m_\chi v^2, m_\chi v, 0, 0)$, respectively. Defining the momentum transfer in terms of the recoil energy E_R and the scattering angle θ, $q^\mu = (E_R, \sqrt{2m_N E_R}\cos\theta, \sqrt{2m_N E_R}\sin\theta, 0)$, one obtains the minimum velocity for some recoil energy E_R. The density ρ_χ and velocity distribution f are astrophysical parameters. A common distribution-type for f is the Maxwell-Boltzmann distribution. From this differential

rate, two key observables can be extracted: the DM mass m_χ and the cross section σ. If the mediating force is known, one can obtain the cross section and a relation between the mass and the cross section (since the cross section will be dependent on the DM-mass). Hence, direct detection experiments search the mass-cross section parameter space for signals of DM particles.

Direct detection experiments distinguish between spin-independent (SI) and spin-dependent (SD) interactions because their sensitivities differ [29]. It is, therefore, convenient to split the cross section into an SI and SD part. SI cross sections are generally larger than SD cross sections, because SD interactions are always accompanied by momenta, meaning that these are momentum suppressed in the NR-limit. This feature will be discussed further in Section 2.3. Moreover, SI scattering is coherent and experiments detect the coherent recoil energy of the nucleus, resulting in the cross section being enhanced by the atomic number [30]. From the differential cross section $d\sigma/dE_R$, the SI DM-nucleus cross section can be expressed as [7]

$$\frac{d\sigma}{dE_R} = \frac{m_N}{2\mu^2 v^2}\sigma_{\rm SI}F^2(q), \tag{2.3}$$

where μ is the reduced mass of the DM-nucleus system, v is the relative velocity between the DM and nucleus, $F(q)$ is the nuclear form factor and m_N is the mass of the nucleus. We now have a relation for the DM-nucleus cross section, but this is dependent on the type of nucleus (e.g. Xenon or Argon). To make results independent of the nuclear target, it is convenient to relate the SI DM-*nucleus* cross section, $\sigma_{\rm SI}$, to the SI DM-*nucleon* cross section, σ_p, via [7]

$$\sigma_{\rm SI} = \frac{\mu^2}{\mu_p^2}A^2\sigma_p. \tag{2.4}$$

Here, μ_p is the reduced mass of the DM-nucleon system and A is the atomic mass number.

Using a standard quantum field theory approach, one calculates the amplitude $\mathcal{M}$ for DM-nucleus scattering, after which one can obtain the cross section. One can show that the NR amplitude has the following relation to the differential cross section $d\sigma/dE_R$ (see Appendix A.1):

$$\frac{d\sigma}{dE_R} = \frac{m_N}{2\pi v^2}\left\langle|\mathcal{M}_{\rm NR}|^2\right\rangle. \tag{2.5}$$

Combining Eqs. (2.3) to (2.5), the nucleon cross section can be expressed in terms of the NR amplitude [7]

$$\sigma_p F^2(q) = \frac{\mu_p^2}{\pi A^2}\left\langle|\mathcal{M}_{\rm NR}|^2\right\rangle. \tag{2.6}$$

This provides the tools to calculate σ_p if the amplitude is known.

As experimental sensitivities of direct detection experiments improve, they approach the region where coherent elastic neutrino-nucleus scattering (CEνNS) becomes relevant. Neutrino-induced nuclear recoil signals resemble those from DM, complicating detection. Previously this region was considered the "neutrino floor", but is now better understood to be the "neutrino fog". Neutrinos causing the CEνNS have different sources, such as solar neutrinos, atmospheric neutrinos and neutrinos from nuclear reactors. Although the whole mass-cross section search space below the neutrino floor is sensitive to CEνNS, some parts have a larger neutrino-background due to these different sources. Each source has a distinct feature in the search space, as can be seen in Fig. 2.2. Although the background in these regions is very large, outside these neutrino-background soures the neutrino-bakground is much smaller and a distinction between DM and neutrino scattering can be made with sufficient statistics. Hence, the neutrino floor does not remain a hard limit anymore and it is now called a fog, because one can still "see" through the neutrino background (with sufficient statistics) [31]

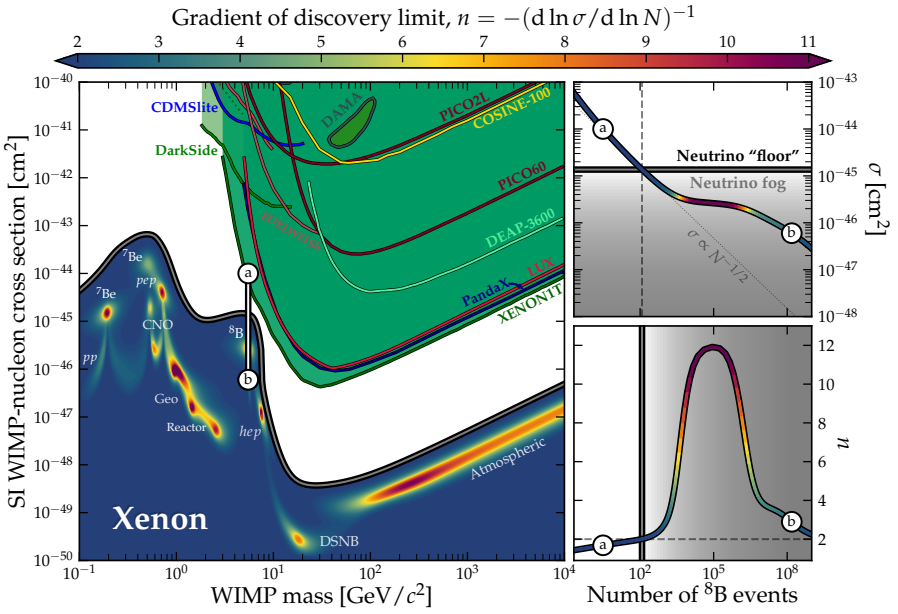

Figure 2.2: In the left panel, the colormap shows the neutrino fog where different sources of the strong neutrino background are indicated. The gray line on top of the neutrino fog is the neutrino floor line, where above $n < 2$ and below $n \geq 2$. The sensitivity of different experiments are given, where the green-shaded region is the search-space that is excluded by experiments. In the top- and bottom-right panel the cross section and gradient of the discovery limit are given as a function of the number of ^8B events, respectively. [31]

Consider that a discovery limit σ decreases as the number of background events N increases. The neutrino fog is quantified by taking the gradient of the discovery limit [31]

$$n = -\left(\frac{d\ln\sigma}{d\ln N}\right)^{-1}. \tag{2.7}$$

Here, n is the index, with $n = 2$ for normal Poissonian statistics, $n > 2$ for saturation and $n < 2$ undefined. However, the neutrino background is dependent on the type of noblegas that is used in the detector. The experiments XENONnT and LZ use liquid Xenon in their detectors. Hence, in the rest of this thesis we will make use of the neutrino background in Xenon, which is also given in Fig. 2.2. For each value of DM mass m_χ, there exists a cross section σ where n crosses 2. This defines the boundary of the neutrino fog and is referred to in the rest of this thesis as the neutrino floor (eventhough it is not an inpenetrable floor).

Apart from knowing the theory behind direct detection experiments, it is good to know how such experiments generally work. Direct detection experiments use dual-phase time projection chambers (TPCs) to detect DM. TPCs contain liquid Xenon (LXe) with a thin layer of gaseous Xenon at the top of the tank. A sketch of the LXe detector is shown in Fig. 2.3. Photomultiplier tube (PMT) arrays are located at the top and bottom of the cylindrical tank. Two signals are generated by the nuclear recoil and caused by secondary effects of scintillation light and ionization electrons. Together, these signals reveal both the position and the recoil energy of the scattering event. In the left panel, an incoming particle interacts with the LXe, producing scintillation light (the S1 signal), which is detected by the PMTs at the top and bottom of the detector, causing

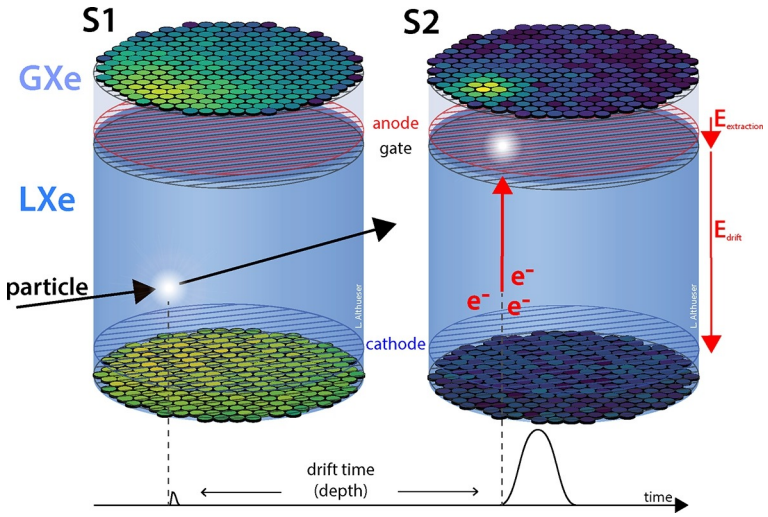

Figure 2.3: Illustration of the principle of a dual-phase liquid Xenon time projection chamber (LXeTPC). In the left figure, S1, an incoming particle deposits energy. The scintillation light of this scattering is detected in the top and bottom photomultiplier tube arrays. On the right, S2, ionized electrons are drifting to the surface, due to the electric field. From the signal of these electrons, information on the position can be extracted. [32]

the small signal bump on the time axis. Ionization electrons that do not recombine, drift toward the liquid surface of the LXe due to an electric field, as shown in the right panel. In the gaseous Xenon region, these electrons gain sufficient energy through the electric field to excite Xenon atoms, generating electroluminescence (the S2 signal). Photons from the electroluminescence are also detected by the PMT arrays. Signal S2 is delayed with respect to the signal S1, because it takes time for the electrons to drift to the gaseous Xenon at the top of the detector. The time delay between S1 and S2 signals provides the depth of the interaction, while the light distribution in the PMT arrays of S2 determines the location of the interaction in the (x, y)-plane.[32, 33]

Direct detection experiments work in the NR regime, because of the low velocity of DM. To quantify DM scattering experiments, one needs a NR theory for DM scattering. For this we have to go to effective field theory.

2.2 Effective Field Theory and Non-Relativistic Building Blocks

The full or more fundamental theory for DM is missing, but it would be good to still be able to make predictions. In these cases effective field theories (EFTs) are a convenient tool to describe new phenomena in physics [34]. EFTs allow one to compute experimental measurable quantities with finite error and uses the separation of energy scales in physics [34, 35]. An example of an effective field theory is Fermi's theory of the weak interaction. Since we know the full theory of the weak force, we know that when the ratio between the momentum transfer and the W-boson mass, q^2/M_W^2, is small, the propagator of the W-boson becomes momentum-independent and the propagator shrinks to a point. In this setting, a diagram with two two-fermion vertices connected with the W-boson, becomes a four-fermion vertex with some effective coupling. This effective coupling is Fermi's coupling and is dependent on the inverse of the W-mass squared,

i.e. the constant is small if $\mathbf{q}^2 \ll M_W^2$.

An EFT is a quantum field theory (QFT) in its own right and, given some Lagrangian, one can compute all the relevant QFT quantities [35]. Like many other QFTs, an EFT needs some ingredients on which it is build: degrees of freedom, symmetries and expansion parameters [34]. In an effective field theory (EFT) the Lagrangian is typically expressed as follows [35]

$$\mathcal{L}_{\text{EFT}} = \sum_{d\geq 4} \sum_i \frac{c_i^{(d)} O_i^{(d)}}{\Lambda^{d-4}}, \tag{2.8}$$

where $\mathcal{O}_i^{(d)}$ are allowed operators of dimension d, $c_i^{(d)}$ are the corresponding Wilson coefficients and Λ is the cutoff scale for the theory. Operators are allowed if they possess the symmetries of the theory. At energies above the cutoff scale Λ the theory ceases to be valid or complete. It serves as a boundary, separating the low-energy phenomena that the EFT is designed to describe from the high-energy physics that is not included in the EFT. Below the cutoff scale high-energy effects factorize from low-energy effects in the EFT. The cutoff suppression of the effective interactions by the cutoff scale also keeps the dimensionality of the Lagrangian at 4.

In this work we are interested in fermion DM-nucleon interaction. The effective interaction Lagrangian in terms the DM and nucleon spinors, is given by [36]:

$$\mathcal{L}_{\text{int}} = \sum_{N=p,n} \sum_i c_i^{(N)} \overline{\chi}\overline{N}\mathcal{O}_i N\chi, \tag{2.9}$$

where c_i are the Wilson coefficients, in which we have absorbed every other object, and therefore having mass dimension -2 such that the Lagrangian has mass dimension 4, because the $\mathcal{O}_i$'s are taken to be dimensionless. From this point onward, all quantities with N are *nucleon* quantities instead of nucleus quantities in the previous section. The operators O_i in Eq. (2.8) and operators $\mathcal{O}_i$ in Eq. (2.9) are different operators, because in the former fields are inside the operator and in the latter the fields are not inside the operator.

The Lagrangian is applicable to the relativistic regime, so Eq. (2.9) still has the spinor-fields χ (DM) and N (nucleon) in it. Since DM-nucleon interactions are NR, the Lagrangian must also have a NR form that looks something like

$$\mathcal{L}_{\text{NR,int}} = \sum_{N=p,n} \sum_i c_i^{(N)'} \xi_\chi^{r',\dagger} \xi_N^{s',\dagger} \mathcal{O}_i^{\text{NR}} \xi_N^s \xi_\chi^r. \tag{2.10}$$

To construct this NR interaction Lagrangian, the set of NR operators of the theory – or building blocks as we will call them from now on – have to be determined. Relativistic operators must be Lorentz-invariant, meaning that the NR building blocks have to be Galilean-invariant. In order to construct all these Galilean-invariant building blocks for direct detection, all possible rotational- and boost-invariant operators have to be written down. These operators are built with classical kinematic variables: initial and final DM(nucleon) momentum, $\mathbf{p}(\mathbf{k})$ and $\mathbf{p}'(\mathbf{k}')$ respectively. The mass of the nucleon is denoted as m_N and the DM mass as m_χ. Momentum conservation implies that there are three independent momenta, which we choose to be:

$$\mathbf{P} = \mathbf{p} + \mathbf{p}', \qquad \mathbf{K} = \mathbf{k} + \mathbf{k}' \quad \text{and} \quad \mathbf{q} = \mathbf{p} - \mathbf{p}' = \mathbf{k}' - \mathbf{k}. \tag{2.11}$$

It is easy to see that $\mathbf{q}$ (the momentum transfer) is Galilean-invariant. To obtain another NR boost-invariant object, one needs a combination of the momenta, such that the Galilean transformation as a whole cancels. There are only two relevant independent momentum combinations,

Table 2.1: All relevant building blocks of spin-$\frac{1}{2}$ DM-nucleon interactions. The numbering of [36, 37] is maintained in this table. $\mathbf{S}_N$ ($\mathbf{S}_\chi$) is the spin of the nucleon (DM), $\mathbf{q}$ is the momentum transfer, $\mathbf{v}_{\text{el}}^\perp$ is the elastic transverse velocity, m_N (m_χ) the mass of the nucleon (DM) and $\mathbb{1}_N$ ($\mathbb{1}_\chi$) is the identity operator of the nucleon (DM) in spin-space.

$\mathcal{O}_1$	=	$\mathbb{1}_\chi \mathbb{1}_N$	$\mathcal{O}_{10}$	=	$i\mathbf{S}_N \cdot \frac{\mathbf{q}}{m_N} \mathbb{1}_\chi$
$\mathcal{O}_3$	=	$i\mathbf{S}_N \cdot \left(\frac{\mathbf{q}}{m_N} \times \mathbf{v}_{\text{el}}^\perp\right) \mathbb{1}_\chi$	$\mathcal{O}_{11}$	=	$i\mathbf{S}_\chi \cdot \frac{\mathbf{q}}{m_N} \mathbb{1}_N$
$\mathcal{O}_4$	=	$\mathbf{S}_\chi \cdot \mathbf{S}_N$	$\mathcal{O}_{12}$	=	$\mathbf{S}_\chi \cdot \left(\mathbf{S}_N \times \mathbf{v}_{\text{el}}^\perp\right)$
$\mathcal{O}_5$	=	$i\mathbf{S}_\chi \cdot \left(\frac{\mathbf{q}}{m_N} \times \mathbf{v}_{\text{el}}^\perp\right) \mathbb{1}_N$	$\mathcal{O}_{13}$	=	$i\left(\mathbf{S}_\chi \cdot \mathbf{v}_{\text{el}}^\perp\right)\left(\mathbf{S}_N \cdot \frac{\mathbf{q}}{m_N}\right)$
$\mathcal{O}_6$	=	$\left(\mathbf{S}_\chi \cdot \frac{\mathbf{q}}{m_N}\right)\left(\mathbf{S}_N \cdot \frac{\mathbf{q}}{m_N}\right)$	$\mathcal{O}_{14}$	=	$i\left(\mathbf{S}_\chi \cdot \frac{\mathbf{q}}{m_N}\right)\left(\mathbf{S}_N \cdot \mathbf{v}_{\text{el}}^\perp\right)$
$\mathcal{O}_7$	=	$\mathbf{S}_N \cdot \mathbf{v}_{\text{el}}^\perp \mathbb{1}_\chi$	$\mathcal{O}_{15}$	=	$\left[\mathbf{S}_\chi \cdot \left(\frac{\mathbf{q}}{m_N} \times \mathbf{v}_{\text{el}}^\perp\right)\right]\left(\mathbf{S}_N \cdot \frac{\mathbf{q}}{m_N}\right)$
$\mathcal{O}_8$	=	$\mathbf{S}_\chi \cdot \mathbf{v}_{\text{el}}^\perp \mathbb{1}_N$	$\mathcal{O}_{16}$	=	$\left(\mathbf{S}_\chi \cdot \mathbf{v}_{\text{el}}^\perp\right)\left(\mathbf{S}_N \cdot \mathbf{v}_{\text{el}}^\perp\right)$
$\mathcal{O}_9$	=	$i\mathbf{S}_\chi \cdot \left(\mathbf{S}_N \times \frac{\mathbf{q}}{m_N}\right)$	$\mathcal{O}_{17}$	=	$i\left[\mathbf{S}_\chi \cdot \left(\frac{\mathbf{q}}{m_N} \times \mathbf{v}_{\text{el}}^\perp\right)\right]\left(\mathbf{S}_N \cdot \mathbf{v}_{\text{el}}^\perp\right)$

since the third corresponds to an overall movement of the DM-nucleon system. For elastic scattering, this combination of momenta leads to the elastic transverse velocity [37]

$$\mathbf{v}_{\text{el}}^\perp \equiv \frac{\mathbf{P}}{2m_\chi} - \frac{\mathbf{K}}{2m_N}. \tag{2.12}$$

The momentum transfer and elastic transverse velocity are perpendicular to each other, i.e.

$$\mathbf{v}_{\text{el}}^\perp \cdot \mathbf{q} = 0. \tag{2.13}$$

The building blocks have to be hermitian on top of being Galilean-invariant. Taking the hermitian conjugate exchanges the incoming and outgoing momenta, meaning that $\mathbf{v}_{\text{el}}^\perp$ is hermitian by itself, but $\mathbf{q}$ is not. In order to make it hermitian, a factor of i is needed in front of the momentum transfer: $i\mathbf{q}$.

DM-nucleon interactions may be spin-dependent. Spin dependencies are parameterized by the identity operator $\mathbb{1}$ in spin-space and the spin operator $\mathbf{S}$, with the appropriate index for DM and nucleon. The spin operator is defined as $\mathbf{S} = \frac{\boldsymbol{\sigma}}{2}$, where $\boldsymbol{\sigma}$ is the vector of Pauli matrices. Using this we establish that there are six boost-invariant and hermitian ingredients out of which the building blocks for 2-to-2 DM-nucleon interactions can be made: $i\mathbf{q}, \mathbf{v}_{\text{el}}^\perp, \mathbb{1}_N, \mathbb{1}_\chi, \mathbf{S}_N$ and $\mathbf{S}_\chi$. In [36, 38] it was found that these ingredients create the relevant and valid building blocks given in Table 2.1. The operators in Table 2.1 can be classified in a number of different ways. Since the direct detection experiments work in the NR regime, the larger the power of velocity or momentum in the operator, the larger the NR suppression is. Hence, it is useful to classify the building blocks on their velocity dependence:

$$\begin{aligned}
&\mathcal{O}_1, \mathcal{O}_4 && \sim O(v^0),\\
&\mathcal{O}_7, \mathcal{O}_8, \mathcal{O}_9, \mathcal{O}_{10}, \mathcal{O}_{11}, \mathcal{O}_{12} && \sim O(v^1),\\
&\mathcal{O}_3, \mathcal{O}_5, \mathcal{O}_6, \mathcal{O}_{13}, \mathcal{O}_{14}, \mathcal{O}_{16} && \sim O(v^2),\\
&\mathcal{O}_{15}, \mathcal{O}_{17} && \sim O(v^3).
\end{aligned}$$

From this we see that building blocks $\mathcal{O}_1$ and $\mathcal{O}_4$ have no NR suppression, and are therefore generally favorable if other operators are not enhanced or the $O(v^0)$ operators are suppressed by some coefficient. In general, a DM-nucleon interaction generates several NR interactions, which can involve several orders in the NR expansion.

One may have noticed that one building block is missing: $\mathcal{O}_2$. In [36] this building block is defined as

$$\mathcal{O}_2 = \left(\mathbf{v}_{\rm el}^{\perp}\right)^2 \mathbb{1}_N \mathbb{1}_\chi.$$

This building block can also be seen as $\left(\mathbf{v}_{\rm el}^{\perp}\right)^2 \mathcal{O}_1$, i.e. as a coefficient of the first building block. A general interaction operator written in terms of these NR 16 building blocks is given by [37]

$$\sum_i f_i \left(|\mathbf{q}|^2, \left(\mathbf{v}_{\rm el}^{\perp}\right)^2\right) \mathcal{O}_i, \tag{2.14}$$

where the f_i's are arbitrary functions of $|\mathbf{q}|^2$, $\left(\mathbf{v}_{\rm el}^{\perp}\right)^2$ and of non-dynamical constants, such as masses. Operator $\mathcal{O}_2$ is, therefore, a redundant operator. Putting Eq. (2.9) and Eq. (2.14) together, one is able to set up an interaction Lagrangian using the building blocks in Table 2.1 for specific interactions.

Notice that the theory discussed so far is only for elastic scattering interactions, i.e. the mass of the DM particle is unchanged after the scattering. For inelastic scattering the initial mass of the DM particle is m and the final mass is $m + \delta$, where δ is the mass splitting-parameter [36, 37]. δ is positive for exothermic scattering and negative for endothermic scattering. Hence, the scattering taking place is $\chi_1 \mathcal{O}_{i,\chi} \chi_2$, where χ_1 and χ_2 have different masses. The operators can be extended to inelastic scattering for a generic mass-splitting parameter by imposing [37]

$$\mathbf{v}_{\rm inel}^{\perp} \equiv \mathbf{v}_{\rm el}^{\perp} - \frac{\delta}{|\mathbf{q}|^2}\mathbf{q}, \tag{2.15}$$

for which

$$\mathbf{v}_{\rm inel}^{\perp} \cdot \mathbf{q} = 0 \quad \text{and} \quad \mathbf{v}_{\rm el}^{\perp} \cdot \mathbf{q} = \delta \neq 0. \tag{2.16}$$

It is straightforward to see that elastic scattering is recovered when $\delta = 0$. In all building blocks in Table 2.1 $\mathbf{v}_{\rm el}^{\perp}$ can be replaced by $\mathbf{v}_{\rm inel}^{\perp}$, turning the building blocks into inelastic scattering building blocks $\mathcal{O}_i^{\rm inel}$. Using Eq. (2.15), all *inelastic* building blocks can be written in terms of *elastic* building blocks:

$$\begin{aligned}
\mathcal{O}_3^{\rm inel} &= \mathcal{O}_3, & \mathcal{O}_{13}^{\rm inel} &= \mathcal{O}_{13} - i\frac{\delta m_N}{q^2}\mathcal{O}_6,\\
\mathcal{O}_5^{\rm inel} &= \mathcal{O}_5, & \mathcal{O}_{14}^{\rm inel} &= \mathcal{O}_{14} - i\frac{\delta m_N}{q^2}\mathcal{O}_6,\\
\mathcal{O}_7^{\rm inel} &= \mathcal{O}_7 + i\frac{\delta m_N}{q^2}\mathcal{O}_{10}, & \mathcal{O}_{15}^{\rm inel} &= \mathcal{O}_{15},\\
\mathcal{O}_8^{\rm inel} &= \mathcal{O}_8 + i\frac{\delta m_N}{q^2}\mathcal{O}_{11}, & \mathcal{O}_{16}^{\rm inel} &= \mathcal{O}_{16} + \frac{\delta^2 m_N^2}{q^4}\mathcal{O}_6 + i\frac{\delta m_N}{q^2}\left(\mathcal{O}_{13} + \mathcal{O}_{14}\right),\\
\mathcal{O}_{12}^{\rm inel} &= \mathcal{O}_{12} + i\frac{\delta m_N}{q^2}\mathcal{O}_9, & \mathcal{O}_{17}^{\rm inel} &= \mathcal{O}_{17} - i\frac{\delta m_N}{q^2}\mathcal{O}_{15}.
\end{aligned} \tag{2.17}$$

Similarly, these relations can be inverted such that all *elastic* building blocks can be written in terms of *inelastic* building blocks. An easy way to do this, is by taking the hermitian conjugate of the relations in Eq. (2.17) and exchange the label 'inel' to the other side, e.g.

$$\mathcal{O}_7 = \mathcal{O}_7^{\rm inel} - i\frac{\delta m_N}{q^2}\mathcal{O}_{10}. \tag{2.18}$$

Inelastic scattering introduces an asymmetric initial and final state, meaning that the parameter δ is always accompanied by the imaginary unit. Eventhough we will focus in this thesis on elastic scattering, it is convenient to know the translation between elastic and inelastic scattering. Knowing the translation, one does not need to perform seperate calculations for elastic and inelastic scattering, one can simply perform one calculation and use the relations above to go from one to the other.

2.3 Non-Relativistic Limit of Operators

Given the building blocks in Table 2.1, we can take the NR limit of the various scattering interactions and express them in terms of these building blocks. Although this is not within the scope of this thesis, using Eq. (2.15) the results can be extended to inelastic scattering as well, allowing for more general results. We have performed all NR-limit calculations in this section and verified the results with [37].

For each type of interaction – scalar (S), vector (V), tensor (T) and their pseudo/axial counterparts – there are four combinations, leading to a total of 12 operators. In Chapter 3, we will see that Lorentz structures will appear where γ^μ is contracted with the momentum of the other particle. Since the Dirac equation cannot be used in that case, it leads to a different set of 12 operators. Each of these operators has some NR counterpart that can be expressed in terms of the building blocks. We aim to create a list of NR limits of different operators that may be needed for calculation in predicitions in the setting of direct detection experiments.

In quantum field theory, fermions are represented by spinors and interactions are characterized by certain Lorentz structures, such as scalar interactions of the form $(\bar{e}e)\,(\bar{\mu}\mu)$, where e and μ are spinors. Going to a NR regime, requires us to take the NR limit of a spinor, because the γ-matrices are independent of momentum. Following the conventions of [39], the general expression for spinors u with four-momentum p and spin-index s is given by

$$u^s(p) = \begin{pmatrix} \sqrt{p\cdot\sigma}\xi^s \\ \sqrt{p\cdot\bar{\sigma}}\xi^s \end{pmatrix}, \tag{2.19}$$

where ξ^s are the two-component spinors, $\sigma = (I_2, \boldsymbol{\sigma})$, $\bar{\sigma} = (I_2, -\boldsymbol{\sigma})$ and $\boldsymbol{\sigma}$ are the Pauli matrices, such that the normalization is

$$\bar{u}^s(p)u^s(p) = 2m\xi^{s',\dagger}\xi^s, \tag{2.20}$$

with $\xi^{s',\dagger}\xi^s = \delta_{s',s}$ and where m is the mass of the spinor. The four-momentum is the kinematic variable characterizing the spinor, which in turn relies on the mass and three-momentum. In the NR regime $\mathbf{p}/m \ll 1$, the energy of the fermion can then be expanded in $\mathbf{p}/m$. Keeping only terms up to first order in momentum, the expansion leads to the NR-limit of the spinor (see Appendix A.4):

$$u^s(p) \approx \sqrt{m}\begin{pmatrix} (1 - \mathbf{p}\cdot\boldsymbol{\sigma}/2m)\,\xi^s \\ (1 + \mathbf{p}\cdot\boldsymbol{\sigma}/2m)\,\xi^s \end{pmatrix}. \tag{2.21}$$

Having obtained the NR limit of the spinor, we now have the necessary tools to calculate the NR limit of various Lorentz structures and, subsequently, the corresponding operators.

As an illustrative example, we will demonstrate the procedure for deriving the NR limit of the scalar Lorentz structure, beginning with the relativistic expression for the scalar Lorentz structure. This involves explicitly writing the interaction in terms of spinors and γ-matrices. We then proceed to take the NR limit and write the spinors in their NR form. Following this, we

perform the necessary matrix and vector multiplications, and simplify the result:

$$\begin{aligned}\overline{u}^{s'}(p')u^{s}(p) &= u^{\dagger,s'}(p')\gamma^0 u^s(p)\\ &\overset{\text{NR}}{\approx} m\begin{pmatrix}(1-\mathbf{p}'\cdot\boldsymbol{\sigma}/2m)\,\xi^{s'}\\(1+\mathbf{p}'\cdot\boldsymbol{\sigma}/2m)\,\xi^{s'}\end{pmatrix}^{\dagger}\begin{pmatrix}0 & I_2\\ I_2 & 0\end{pmatrix}\begin{pmatrix}(1-\mathbf{p}\cdot\boldsymbol{\sigma}/2m)\,\xi^{s}\\(1+\mathbf{p}\cdot\boldsymbol{\sigma}/2m)\,\xi^{s}\end{pmatrix}\\ &= 2m\xi^{\dagger,s'}\xi^s.\end{aligned} \tag{2.22}$$

While the calculations of the NR limit of the different Lorentz structures and operators are extensive and not central to the discussion, the derivation of all 12 Lorentz structure and all 24 operators are found in Appendix A.5. The final results of the NR limit of different Lorentz structures are summarized in Table A.1. The results in the table follow the momentum convention, such that they provide the Lorentz structure for the DM part of the operator. To obtain the corresponding structures for the nucleon, one must make the substitutions $\mathbf{P}\to\mathbf{K}$ and $\mathbf{q}\to-\mathbf{q}$, consistent with the definitions of these quantities in terms of the incoming and outgoing momenta. Note that when there are open indices, the result will not be scalar like the result above, but takes the form of the object with the open indices (see Table A.1). For example, a vector Lorentz structure $(\overline{u}\gamma^\mu u)$ has an open index and will therefore not be a scalar, but it will be a four-component vector where the spatial components are grouped together, apart from the zeroth component.

With the NR limit of the Lorentz structures now derived, we are equipped to derive the various operators and express them in terms of the NR building blocks. Before presenting the results, it is crucial to highlight an important simplification regarding the tensor structure $\sigma^{\mu\nu}\gamma^5$. As one may know, this Lorentz structure is not a basis element for the 4×4 matrices, so somehow the γ^5 in this structure does not introduce a new basis of 4×4 matrices [39]. In general, such a structure may show up in some kind of interaction, but since it is not a basis matrix, it must be some linear combination of basis γ-matrices. Actually, this structure can be rewritten purely in terms of $\sigma^{\mu\nu}$, eliminating the explicit presence of γ^5 in the expression. To achieve this, we use the following two identities:

$$\gamma^\mu\gamma^\nu\gamma^\rho\gamma_\mu = 4\eta^{\nu\rho}I_4, \tag{2.23}$$

$$\gamma^\mu\gamma^\nu\gamma^\rho = \eta^{\mu\nu}\gamma^\rho + \eta^{\nu\rho}\gamma^\mu - \eta^{\mu\rho}\gamma^\nu - i\epsilon^{\sigma\mu\nu\rho}\gamma_\sigma\gamma^5. \tag{2.24}$$

To derive the relation, begin by multiplying Eq. (2.24) by γ_μ from the right. Next, use Eq. (2.23) to cancel the sole term on the right-hand side involving the Minkowski metric. Then, utilize the anti-symmetry property of $\epsilon^{\sigma\mu\nu\rho}$ to rearrange terms appropriately. Finally, multiplying both sides with γ^5 from the right gives the desired identity relating the two Lorentz structures:

$$\sigma^{\mu\nu}\gamma^5 = \frac{i}{2}\epsilon^{\sigma\rho\mu\nu}\sigma_{\sigma\rho}. \tag{2.25}$$

This relation proves particularly useful for simplifying certain calculations. For instance, in the case of the contracted tensor operator, where two $\sigma^{\mu\nu}\gamma^5$ Lorentz structures are contracted, the above identity allows us to reduce the operator to a simpler form:

$$\left(\overline{N}^{s'}(k')\sigma^{\mu\nu}\gamma^5 N^s(k)\right)\left(\overline{\chi}^{r'}(p')\sigma_{\mu\nu}\gamma^5\chi^r(p)\right) = \left(\overline{N}^{s'}(k')\sigma^{\mu\nu}N^s(k)\right)\left(\overline{\chi}^{r'}(p')\sigma_{\mu\nu}\chi^r(p)\right). \tag{2.26}$$

Similarly, the operators where only one of the particles contains the γ^5 can also be simplified:

$$\left(\overline{N}^{s'}(k')\sigma^{\mu\nu}\gamma^5 N^s(k)\right)\left(\overline{\chi}^{r'}(p')\sigma_{\mu\nu}\chi^r(p)\right) = \frac{i}{2}\epsilon^{\sigma\rho\mu\nu}\left(\overline{N}^{s'}(k')\sigma_{\sigma\rho}N^s(k)\right)\left(\overline{\chi}^{r'}(p')\sigma_{\mu\nu}\chi^r(p)\right). \tag{2.27}$$

Table 2.2: The non-relativistic limit of the operators. Here, $N^s(k)$ is the nucleon spinor with spin index s, four-momentum k and mass m_N. Similarly, $\chi^r(p)$ is the DM particle spinor with spin index r, four-momentum p and mass m_χ. $k(p)$ and $k'(p')$ are the incoming and outgoing nucleon (DM) four-momenta, respectively. Here $\langle\mathcal{O}_i\rangle = \xi_N^{\dagger,s'}\xi_\chi^{\dagger,r'}\mathcal{O}_i\xi_\chi^r\xi_N^s$ denotes the matrix element between the two-dimensional spinors associated with the initial and final state of the DM particle and the up-quark. Color-coding used: $O(v^0)$ is green, $O(v^1)$ is orange, $O(v^2)$ is blue and $O(v^3)$ is pink.

Relativistic Operators	NR-Limit
$\left(\overline{N}^{s'}(k')N^s(k)\right)\left(\overline{\chi}^{r'}(p')\chi^r(p)\right)$	$\approx 4m_N m_\chi\,[\langle\mathcal{O}_1\rangle]$
$\left(\overline{N}^{s'}(k')\gamma^5 N^s(k)\right)\left(\overline{\chi}^{r'}(p')\chi^r(p)\right)$	$\approx 4m_N m_\chi\,[i\,\langle\mathcal{O}_{10}\rangle]$
$\left(\overline{N}^{s'}(k')N^s(k)\right)\left(\overline{\chi}^{r'}(p')\gamma^5\chi^r(p)\right)$	$\approx 4m_N m_\chi\left[-\frac{im_N}{m_\chi}\,\langle\mathcal{O}_{11}\rangle\right]$
$\left(\overline{N}^{s'}(k')\gamma^5 N^s(k)\right)\left(\overline{\chi}^{r'}(p')\gamma^5\chi^r(p)\right)$	$\approx 4m_N m_\chi\left[-\frac{m_N}{m_\chi}\,\langle\mathcal{O}_6\rangle\right]$
$\left(\overline{N}^{s'}(k')\gamma_\mu N^s(k)\right)\left(\overline{\chi}^{r'}(p')\gamma^\mu\chi^r(p)\right)$	$\approx 4m_N m_\chi\,[\langle\mathcal{O}_1\rangle]$
$\left(\overline{N}^{s'}(k')\gamma_\mu\gamma^5 N^s(k)\right)\left(\overline{\chi}^{r'}(p')\gamma^\mu\chi^r(p)\right)$	$\approx 4m_N m_\chi\left[-2\,\langle\mathcal{O}_7\rangle - \frac{2m_N}{m_\chi}\,\langle\mathcal{O}_9\rangle\right]$
$\left(\overline{N}^{s'}(k')\gamma_\mu N^s(k)\right)\left(\overline{\chi}^{r'}(p')\gamma_\mu\gamma^5\chi^r(p)\right)$	$\approx 4m_N m_\chi\,[2\,\langle\mathcal{O}_8\rangle - 2\,\langle\mathcal{O}_9\rangle]$
$\left(\overline{N}^{s'}(k')\gamma_\mu\gamma^5 N^s(k)\right)\left(\overline{\chi}^{r'}(p')\gamma^\mu\gamma^5\chi^r(p)\right)$	$\approx 4m_N m_\chi\,[-4\,\langle\mathcal{O}_4\rangle]$
$\left(\overline{N}^{s'}(k')\sigma^{\mu\nu}N^s(k)\right)\left(\overline{\chi}^{r'}(p')\sigma_{\mu\nu}\chi^r(p)\right)$ $\left(\overline{N}^{s'}(k')\sigma^{\mu\nu}\gamma^5 N^s(k)\right)\left(\overline{\chi}^{r'}(p')\sigma_{\mu\nu}\gamma^5\chi^r(p)\right)$	$\approx 4m_N m_\chi\,[8\langle\mathcal{O}_4\rangle]$
$\left(\overline{N}^{s'}(k')\sigma^{\mu\nu}\gamma^5 N^s(k)\right)\left(\overline{\chi}^{r'}(p')\sigma_{\mu\nu}\chi^r(p)\right)$ $\left(\overline{N}^{s'}(k')\sigma^{\mu\nu}N^s(k)\right)\left(\overline{\chi}^{r'}(p')\sigma_{\mu\nu}\gamma^5\chi^r(p)\right)$	$\approx 4m_N m_\chi\left[-\frac{2im_N}{m_\chi}\,\langle\mathcal{O}_{10}\rangle\right.$ $\left.+2i\,\langle\mathcal{O}_{11}\rangle + 8i\,\langle\mathcal{O}_{12}\rangle\right]$

It is straightforward to see that, since the operator contains no open indices, the operator with γ^5 on the DM part is equivalent to the one where γ^5 appears on the nucleon part.

In the SM fermions possess a chirality, meaning that they can be either right- or left-handed. Similarly, DM particles could, in principle, also possess chirality. However, in this thesis we do not consider chiral interactions for the quarks or DM particles. Instead, we present the results in a non-chiral basis, because one can easily switch between the two bases. The results for the operators are summarized in Tables 2.2 and 2.3, while the explicit expressions – with the building blocks written out in full – are detailed in Tables A.3 and A.4 and the derivation is given in Appendix A.7. In both tables the relativistic normalization and the building blocks have been separated, i.e. the building blocks are all in between square brackets with the relativistic normalization given as a pre-factor. To make the NR suppression of the operators easier to identify, we use the same color-coding scheme for the building blocks as in the previous section.

The order of NR suppression of the operators is not surprising, the NR suppression is at most $O(v^1)$ for all but one operator: the pseudo-scalar–pseudo-scalar (P-P) operator. Naively,

Table 2.3: The non-relativistic limit of vector and axial-vector operators contracted with the momentum of the other particle. Here, $N^s(k)$ is the nucleon spinor with spin index s, four-momentum k and mass m_N. Similarly, $\chi^r(p)$ is the DM particle spinor with spin index r, four-momentum p and mass m_χ. $k(p)$ and $k'(p')$ are the incoming and outgoing nucleon (DM) four-momenta, respectively. Here $\langle\mathcal{O}_i\rangle = \xi_N^{\dagger,s'}\xi_\chi^{\dagger,r'}\mathcal{O}_i\xi_\chi^r\xi_N^s$ denotes the matrix element between the two-dimensional spinors associated with the initial and final state of the DM particle and the up-quark. Color-coding used: $O(v^0)$ is green, $O(v^1)$ is orange, $O(v^2)$ is blue and $O(v^3)$ is pink.

Relativistic Operators	NR-Limit
$\left(\overline{N}^{s'}(k')\not{p}N^s(k)\right)\left(\overline{\chi}^{r'}(p')\chi^r(p)\right)$	$\approx 4m_N m_\chi^2\,[\langle\mathcal{O}_1\rangle]$
$\left(\overline{N}^{s'}(k')N^s(k)\right)\left(\overline{\chi}^{r'}(p')\not{k}\chi^r(p)\right)$	$\approx 4m_N^2 m_\chi\,[\langle\mathcal{O}_1\rangle]$
$\left(\overline{N}^{s'}(k')\not{p}N^s(k)\right)\left(\overline{\chi}^{r'}(p')\not{k}\chi^r(p)\right)$	$\approx 4m_N^2 m_\chi^2\,[\langle\mathcal{O}_1\rangle]$
$\left(\overline{N}^{s'}(k')\not{p}\gamma^5N^s(k)\right)\left(\overline{\chi}^{r'}(p')\chi^r(p)\right)$	$\approx 4m_N m_\chi\,[im_N\langle\mathcal{O}_{10}\rangle - 2m_\chi\langle\mathcal{O}_7\rangle]$
$\left(\overline{N}^{s'}(k')\gamma^5N^s(k)\right)\left(\overline{\chi}^{r'}(p')\not{k}\chi^r(p)\right)$	$\approx 4m_N m_\chi\,[-im_N\langle\mathcal{O}_{10}\rangle]$
$\left(\overline{N}^{s'}(k')\not{p}\gamma^5N^s(k)\right)\left(\overline{\chi}^{r'}(p')\not{k}\chi^r(p)\right)$	$\approx 4m_N m_\chi\left[im_N^2\langle\mathcal{O}_{10}\rangle - 2m_\chi m_N\langle\mathcal{O}_7\rangle\right]$
$\left(\overline{N}^{s'}(k')\not{p}N^s(k)\right)\left(\overline{\chi}^{r'}(p')\gamma^5\chi^r(p)\right)$	$\approx 4m_N m_\chi\,[-im_N\langle\mathcal{O}_{11}\rangle]$
$\left(\overline{N}^{s'}(k')N^s(k)\right)\left(\overline{\chi}^{r'}(p')\not{k}\gamma^5\chi^r(p)\right)$	$\approx 4m_N m_\chi\,[-im_N\langle\mathcal{O}_{11}\rangle + 2m_N\langle\mathcal{O}_8\rangle]$
$\left(\overline{N}^{s'}(k')\not{p}N^s(k)\right)\left(\overline{\chi}^{r'}(p')\not{k}\gamma^5\chi^r(p)\right)$	$\approx 4m_N m_\chi\,[-im_\chi m_N\langle\mathcal{O}_{11}\rangle + 2m_\chi m_N\langle\mathcal{O}_8\rangle]$
$\left(\overline{N}^{s'}(k')\not{p}\gamma^5N^s(k)\right)\left(\overline{\chi}^{r'}(p')\gamma^5\chi^r(p)\right)$	$\approx 4m_N m_\chi\left[-\frac{m_N^2}{m_\chi}\langle\mathcal{O}_6\rangle + 2im_N\langle\mathcal{O}_{14}\rangle\right]$
$\left(\overline{N}^{s'}(k')\gamma^5N^s(k)\right)\left(\overline{\chi}^{r'}(p')\not{k}\gamma^5\chi^r(p)\right)$	$\approx 4m_N m_\chi\,[-m_N\langle\mathcal{O}_6\rangle + 2im_N\langle\mathcal{O}_{13}\rangle]$
$\left(\overline{N}^{s'}(k')\not{p}\gamma^5N^s(k)\right)\left(\overline{\chi}^{r'}(p')\not{k}\gamma^5\chi^r(p)\right)$	$\approx 4m_N m_\chi\,[-m_N^2\langle\mathcal{O}_6\rangle + 2im_N^2\langle\mathcal{O}_{13}\rangle$ $+2im_\chi m_N\langle\mathcal{O}_{14}\rangle - 4m_\chi m_N\langle\mathcal{O}_{16}\rangle]$

each pseudo-scalar structure gives a spin and momentum dependence, leading to momentum suppression. Therefore, the NR suppression order of the P-P operator in the tables is a logical consequence of its structure. Also, axial-vector, pseudo-scalar and tensor structures lead to SD DM-nucleon scattering. As noted previously, SD scattering is not coherent and it, therefore, typically has smaller scattering rate than SI scattering.

All second order terms in the calculations of the NR-limit of the Lorentz structures, operators and spinor are discarded, therefore, other building blocks that are $O(v^2)$ and $O(v^3)$ suppressed are not present. To include the second order velocity terms, the spinor has to be expanded to second order as well, ensuring all second order terms are included. This is the focus in the next section. In the next section, we will also address why the results from the second-order calculations of the operators can be used to obtain the first-order expansion of the operators.

2.4 Expansion to Second Order

As discussed in the previous section, the results presented in Table 2.2 do not contain $O(v^2)$ or higher suppressed operators – apart from the P-P operator – since all second order velocity terms have been discarded. In this section, we expand the spinors, Lorentz structures and operators to second order. Since this has not been done in the literature, we cannot compare it to results in literature.

Expanding to second order in momentum is important, because it systematically captures momentum-dependent corrections that can become significant under certain circumstances. For instance, in cases where a propagator scales as $1/q^2$, nominal second-order terms (with factors of q^2) can cancel this suppression, effectively contributing as $\mathcal{O}(v^0)$ terms. This means that higher-order corrections might not be as suppressed as expected and can influence leading-order behavior. Moreover, when interference effects or cancellations occur among lower-order terms, the second order contributions become important. Furthermore, including these corrections refines the matching between the underlying relativistic theory and its non-relativistic effective field theory, ensuring that subtle momentum-dependent effects are accurately incorporated in predictions for scattering amplitudes and cross sections.

It is important to note that expanding the spinor to second order breaks Galilean invariance. The zeroth- and first-order terms are Galilean-invariant, but the second-order terms are not. This becomes problematic when calculating the NR limit of the operators, because Galilean invariance was one of the criteria of obtaining the building blocks and the NR limit. Tables 2.2 and 2.3 provide us with useful information that we can use to predict what operators will gain higher-order terms and which will not. Zeroth- and first-order terms will immediately result in the desired operators in Tables 2.2 and 2.3, because the second-order expansion will not do anything with lower-order terms. By including also second-order terms, the operators generally gain terms that are two powers higher in momentum, i.e. first-order terms will gain third- or higher-order corrections. This means that operators that are zeroth-order in Tables 2.2 and 2.3 will gain second-order velocity terms, while the operators only containing first-order terms at first-order will not gain second-order terms. The only operator that is already second-order in momentum at first-order expansion is P-P operator. By the same reasoning, the P-P operator is already second-order in momentum at first-order expansion, and will, therefore, not gain any new terms when expanding to second order.

Because the operators at second-order expansion will not be Galilean-invariant anymore, to obtain sensible results from the second order terms that are not present at leading order expansion, a relation between $\mathbf{P}$ and $\mathbf{K}$ is required. In fact, only a relation between either the incoming momenta $\mathbf{p}, \mathbf{k}$ or outgoing momenta $\mathbf{p}', \mathbf{k}'$ is needed, because $\mathbf{q}$ relates the incoming

and outgoing momenta. Having a relation between the incoming or outgoing momenta, we are able to obtain a relation between $\mathbf{P}$ and K. One way to do this, is by assuming the particles are in the DM-nucleon center-of-mass (CM) frame. In the CM frame, the momenta possess the following relations

$$\mathbf{p} + \mathbf{k} = 0 \qquad \text{and} \qquad \mathbf{p}' + \mathbf{k}' = 0. \tag{2.28}$$

Two straightforward calculations lead to the following two relations in the CM frame

$$\mathbf{P} + \mathbf{K} = 0, \tag{2.29a}$$

$$\mathbf{v}_{\text{el}}^{\perp} = \frac{1}{2\mu}\mathbf{P}. \tag{2.29b}$$

Going over the same steps as for the first order expansion of the spinor, but now including the second-order in each step, gives (see Appendix A.4)

$$u(p) = \sqrt{m}\begin{pmatrix}\left(1 - \mathbf{p}\cdot\boldsymbol{\sigma}/2m + \mathbf{p}^2/8m^2\right)\xi \\ \left(1 + \mathbf{p}\cdot\boldsymbol{\sigma}/2m + \mathbf{p}^2/8m^2\right)\xi\end{pmatrix}. \tag{2.30}$$

Similar to the first order expansion in the previous section, we go through the calculations of all Lorentz structures and operators, but include all terms up to and including second order velocity terms. Before going to the CM frame, we can see in Appendix A.7 that some terms look similar to some building blocks in Table 2.1. However, these terms cannot be written as building blocks, because either $\mathbf{P}$ or $\mathbf{K}$ is present, while both are needed for making it a building block. So indeed, there is no way to solve this without assuming some relation between the momenta (either by being in some frame or another type of relation). The NR limit of the operators up to and including second-order velocity terms in the CM frame that have changed by going to second-order expansion, are given in Tables 2.4 and 2.5.

First, it is important to note that in the limit of small momentum transfer ($\mathbf{q} \to 0$) and negligible initial nucleon momentum ($\mathbf{k} \to 0$), the second-order corrections do not vanish. Instead, they become solely dependent on the elastic transverse velocity, $(\mathbf{v}_{\text{el}}^{\perp})^2 \overset{\mathbf{q}^2,\mathbf{k}^2\to 0}{=} |\mathbf{p}|^2/m_\chi^2$. This observation implies that even for small momentum transfers, the second order corrections can yield non-negligible contributions to the effective operators, potentially dominating the phenomenology when the leading order operators are absent or suppressed.

Second, an interesting finding is that the second-order corrections do more than modify the existing operators, but give rise to a dependence on different NR building blocks as well. These operators, which emerge at second order in the momentum expansion, are structurally distinct from the leading-order terms and can have significant phenomenological consequences. In particular, if the leading-order operators are absent or suppressed, e.g. due to cancellations, the second-order correction induced operators may become the dominant contributions. This potentially alters the amplitude and may enhance the amplitude in case of cancellation of leading-order terms.

As noted, these results hold for the DM-nucleon CM frame. So the question arises whether these results hold for arbitrary frames or not. Let us show this by expanding the spinor again, but in a frame $\tilde{p}$ Starting in a general frame with four-momenta p, p', k and k', and perform a boost to the CM frame with the desired boosting velocity $\mathbf{v}$. In momentum space one can verify that in the relativistic setting, the scalar operator remains unchanged after boosting:

$$\overline{u}^{s'}(p')u^{s}(p) = \overline{u}^{s'}(\tilde{p}')u^{s}(\tilde{p}), \tag{2.31}$$

where $\tilde{p}'$ and $\tilde{p}$ are the boosted four-momenta. Suppose that the necessary boost to go to the CM frame, must be performed in the z direction, i.e. $\mathbf{v} = v\hat{\mathbf{z}}$. The boosted momenta are then

given by

$$\tilde{p}^{\mu} = \left(\Lambda^{-1}\right)^{\mu}_{\ \nu} p^{\nu} = \begin{pmatrix} \tilde{E} \\ \tilde{\mathbf{p}} \end{pmatrix}, \tag{2.32}$$

with $\tilde{E} = m + \frac{(\mathbf{p}+m\mathbf{v})^2}{2m}$ and $\tilde{\mathbf{p}} = \mathbf{p} + m\mathbf{v}$ in the NR limit. Hence, our spinor in the NR-limit equals

$$u(\tilde{p}) = \sqrt{m}\begin{pmatrix} \left(1 + \tilde{\mathbf{p}}^2/8m^2 + (\tilde{\mathbf{p}}\cdot\boldsymbol{\sigma})/2m\right)\xi \\ \left(1 + \tilde{\mathbf{p}}^2/8m^2 - (\tilde{\mathbf{p}}\cdot\boldsymbol{\sigma})/2m\right)\xi \end{pmatrix} = \sqrt{m}\begin{pmatrix} \left(1 + [\mathbf{p}+m\mathbf{v}]^2/8m^2 + ([\mathbf{p}+m\mathbf{v}]\cdot\boldsymbol{\sigma})/2m\right)\xi \\ \left(1 + [\mathbf{p}+m\mathbf{v}]^2/8m^2 - ([\mathbf{p}+m\mathbf{v}]\cdot\boldsymbol{\sigma})/2m\right)\xi \end{pmatrix}. \tag{2.33}$$

This means that the calculations for both frames are equal and so the scalar Lorentz structure in terms of the unboosted momentum becomes

$$\overline{u}^{s'}(\tilde{p}')u^{s}(\tilde{p}) \approx 2m\left[\xi^{s',\dagger}\xi^{s} + \frac{\mathbf{q}^2}{8m^2}\xi^{\dagger,s'}\xi^{s} - \frac{i}{4m^2}\mathbf{s}_u^{s',s}\cdot(\mathbf{P}\times\mathbf{q}) - \frac{i}{4m^2}\mathbf{s}_u^{s',s}\cdot(2m\mathbf{v}\times\mathbf{q})\right] \tag{2.34}$$

To compare, the unboosted expression is given by (see Appendix A.6):

$$\overline{u}^{s'}(\tilde{p}')u^{s}(\tilde{p}) \approx 2m\left[\xi^{\dagger,s'}\xi^{s} + \frac{\mathbf{q}^2}{8m^2}\xi^{\dagger,s'}\xi^{s} - \frac{i}{4m^2}\mathbf{s}_u^{s',s}\cdot(\mathbf{P}\times\mathbf{q})\right]. \tag{2.35}$$

Comparing Eq. (2.34) and Eq. (2.35), we see that most terms coincide and that $\mathbf{P}' = \mathbf{P} + 2m\mathbf{v}$, as expected. From this it is easy to see that the extra term that depends on boosting velocity $\mathbf{v}$, introduces extra terms that will not cancel. Then, it follows that boosting the system to the CM frame, other terms are introduced in the scalar-scalar interaction and therefore, the unboosted and boosted expressions are not equal. Hence, we conclude that the results of the interactions by including the second order expansion do not hold for arbitrary frames.

Table 2.4: Non-relativistic limit of operators at second order expansion that changed, in the CM frame. Here, $N^s(k)$ is the nucleon spinor with spin index s, four-momentum k and mass m_N. Similarly, $\chi^r(p)$ is the DM particle spinor with spin index r, four-momentum p and mass m_χ. Additionally, μ is the reduced mass of the DM-nucleon system. $k(p)$ and $k'(p')$ are the incoming and outgoing nucleon (DM) four-momenta, respectively. Here, $\langle\mathcal{O}_i\rangle = \xi_N^{\dagger,s'}\xi_\chi^{\dagger,r'}\mathcal{O}_i\xi_\chi^r\xi_N^s$ denotes the matrix element between the two-dimensional spinors associated with the initial and final state of the DM particle and the up-quark. Color-coding used: $O(v^0)$ is green, $O(v^1)$ is orange, $O(v^2)$ is blue and $O(v^3)$ is pink.

$\left(\overline{N}^{s'}(k')N^s(k)\right)\left(\overline{\chi}^{r'}(p')\chi^r(p)\right)$	$\approx 4m_N m_\chi\left[\langle\mathcal{O}_1\rangle\left(1+\frac{\mathbf{q}^2(m_N^2+m_\chi^2)}{8m_N^2m_\chi^2}\right)+\frac{\mu}{2m_N}\langle\mathcal{O}_3\rangle+\frac{\mu m_N}{2m_\chi^2}\langle\mathcal{O}_5\rangle\right]$
$\left(\overline{N}^{s'}(k')\gamma_\mu N^s(k)\right)\left(\overline{\chi}^{r'}(p')\gamma^\mu\chi^r(p)\right)$	$\approx 4m_N m_\chi\left[\langle\mathcal{O}_1\rangle\left(1+\frac{1}{2}\mathbf{v}_{\mathrm{el}}^{\perp\,2}\right)-\frac{m_\chi+2m_N}{2(m_N+m_\chi)}\langle\mathcal{O}_3\rangle-\frac{\mathbf{q}^2}{m_N m_\chi}\langle\mathcal{O}_4\rangle-\frac{m_N(m_N+2m_\chi)}{2m_\chi(m_N+m_\chi)}\langle\mathcal{O}_5\rangle+\frac{m_N}{m_\chi}\langle\mathcal{O}_6\rangle\right]$
$\left(\overline{N}^{s'}(k')\gamma_\mu\gamma^5 N^s(k)\right)\left(\overline{\chi}^{r'}(p')\gamma^\mu\gamma^5\chi^r(p)\right)$	$\approx 4m_N m_\chi\left[-\langle\mathcal{O}_4\rangle\left(4+\frac{\mathbf{q}^2(m_N^2+m_\chi^2)}{2m_\chi^2m_N^2}\right)-\frac{m_N^2}{2m_\chi(m_N+m_\chi)}\langle\mathcal{O}_3\rangle-\frac{m_\chi}{2(m_N+m_\chi)}\langle\mathcal{O}_5\rangle+\frac{m_\chi^2+m_N^2}{2m_\chi^2}\langle\mathcal{O}_6\rangle-2\langle\mathcal{O}_{16}\rangle\right]$
$\left(\overline{N}^{s'}(k')\sigma^{\mu\nu}N^s(k)\right)\left(\overline{\chi}^{r'}(p')\sigma_{\mu\nu}\chi^r(p)\right)$ $\left(\overline{N}^{s'}(k')\sigma^{\mu\nu}\gamma^5 N^s(k)\right)\left(\overline{\chi}^{r'}(p')\sigma_{\mu\nu}\gamma^5\chi^r(p)\right)$	$\approx 4m_N m_\chi\left[\langle\mathcal{O}_4\rangle\left(8+4\mathbf{v}_{\mathrm{el}}^{\perp\,2}\right)-\frac{\mathbf{q}^2}{2m_N m_\chi}\langle\mathcal{O}_1\rangle-\frac{m_N(m_N+2m_\chi)}{m_\chi(m_N+m_\chi)}\langle\mathcal{O}_3\rangle-\frac{2m_N+m_\chi}{m_N+m_\chi}\langle\mathcal{O}_5\rangle-4\langle\mathcal{O}_{16}\rangle+\frac{m_N^2+m_\chi^2}{m_\chi^2}\langle\mathcal{O}_6\rangle\right]$

Table 2.5: The non-relativistic limit of vector and axial-vector operators contracted with the momentum of the other particle that have changed at second order expansion, in the CM frame. Here, $N^s(k)$ is the nucleon spinor with spin index s, four-momentum k and mass m_N. Similarly, $\chi^r(p)$ is the DM particle spinor with spin index r, four-momentum p and mass m_χ. Additionally, μ is the reduced mass of the DM-nucleon system. $k(p)$ and $k'(p')$ are the incoming and outgoing nucleon (DM) four-momenta, respectively. Here, $\langle\mathcal{O}_i\rangle = \xi_N^{\dagger,s'}\xi_\chi^{\dagger,r'}\mathcal{O}_i\xi_\chi^r\xi_N^s$ denotes the matrix element between the two-dimensional spinors associated with the initial and final state of the DM particle and the up-quark. Color-coding used: $O(v^0)$ is green, $O(v^1)$ is orange, $O(v^2)$ is blue and $O(v^3)$ is pink.

Relativistic Operators	NR-Limit
$\left(\overline{N}^{s'}(k')\not{p}N^s(k)\right)\left(\overline{\chi}^{r'}(p')\chi^r(p)\right)$	$\approx 4m_N m_\chi^2\langle\mathcal{O}_1\rangle\left(1+\frac{1}{2}\left(\mathbf{v}_{\rm el}^\perp+\frac{\mathbf{q}}{2m_\chi}\right)^2\right.$ $\left.+\frac{\mu}{2m_N}\mathbf{v}_{\rm el}^\perp\cdot\left(\frac{m_N-\mu}{m_N}\mathbf{v}_{\rm el}^\perp+\frac{\mathbf{q}}{2m_\chi}\right)+\frac{\mathbf{q}^2}{8m_\chi^2}\right)$ $-2m_\chi^2\frac{2m_N-\mu}{m_N}\langle\mathcal{O}_3\rangle+2\mu m_N^2\langle\mathcal{O}_5\rangle$
$\left(\overline{N}^{s'}(k')N^s(k)\right)\left(\overline{\chi}^{r'}(p')\not{k}\chi^r(p)\right)$	$\approx 4m_N^2 m_\chi\langle\mathcal{O}_1\rangle\left(1+\frac{1}{2}\left(\mathbf{v}_{\rm el}^\perp+\frac{\mathbf{q}}{2m_N}\right)^2\right)$ $-2im_N^3\frac{2m_\chi-\mu}{m_\chi}\langle\mathcal{O}_5\rangle+2m_\chi m_N\mu\langle\mathcal{O}_3\rangle$
$\left(\overline{N}^{s'}(k')\not{p}N^s(k)\right)\left(\overline{\chi}^{r'}(p')\not{k}\chi^r(p)\right)$	$\approx 4m_N^2 m_\chi^2\langle\mathcal{O}_1\rangle\left(1+\frac{1}{2}\left((\mathbf{v}_{\rm el}^\perp)^2+\frac{\mathbf{q}}{2m_\chi}\right)^2\right.$ $\left.+\frac{1}{2}\left((\mathbf{v}_{\rm el}^\perp)^2+\frac{\mathbf{q}}{2m_N}\right)^2\right)$ $+2m_N^3(2m_\chi-\mu)\langle\mathcal{O}_5\rangle-2m_N m_\chi^2(2m_N-\mu)\langle\mathcal{O}_3\rangle$

CHAPTER 3

ALP-Mediated Dark Matter-Nucleon Scattering

In the previous chapter we derived the non-relativistic (NR) limit of 24 different operators and expressed them in terms of NR building blocks. In the end we want to make predictions for the cross section-DM mass search space. Hence, we need to calculate the cross section for DM-nucleon scattering. To obtain a cross section, we need a theory or model to work with. In this model we know we need fermionic DM, as this is our assumption, but in order to have interactions between DM and Standard Model (SM) particles we need a mediator as well. The possible candidate mediator that we will use is the axion-like particle (ALP). In this chapter we first introduce in Section 3.1 the ALP and ALP effective field theory from literature, where we will derive the vertex factor for this model. Although scattering could be with any fermion in the SM, we are eventually interested in nucleon scattering, and will therefore use DM–up-quark scattering. Knowing the Feynman rules, we calculate the simplest scattering process in Section 3.2: scattering at tree-level. This type of scattering comes with problems and calls for going to loop-level calculations. Thus, we perform a one-loop calculation of the scattering process to find an enhanced cross section in Section 3.3. The calculation calls for the use of Passarino-Veltman reduction and, because of the long expression, for simplifications and approximations. Next, we discuss the UV-divergence of the loop integrals in Section 3.4. There are some processes discussed in the literature that help us to set bounds on the couplings and cutoff scale, that are discussed in Section 3.6. Next, in Section 3.5 we use the renormalization-group equations derived in [40] to evolve the couplings down to other scales. Lastly, in Section 3.7 we make a prediction of the cross section and compare it with experimental results, using bounds from meson experiments.

3.1 ALP Effective Field Theory

The ALP is a generalization of the QCD axion. The QCD axion was introduced to solve the strong CP problem. The strong CP problem arises from the term

$$\mathcal{L}_{\theta QCD} = \frac{\overline{\theta}\alpha_s}{4\pi} G^a_{\mu\nu} G^{a,\mu\nu}, \tag{3.1}$$

in the QCD Lagrangian, which is violating CP-symmetry. Here, θ is the CP-violating angle, α_s is the strong coupling constant and G is the gluon field strength tensor, with $\tilde{G}^{\mu\nu} = \frac{1}{2}\epsilon^{\alpha\beta\mu\nu}\tilde{G}_{\alpha\beta}$ the

dual tensor. This term is odd under CP and introduces CP-violating interactions, including the electric dipole moment (EDM) in the neutron, d_n [41]. In [42] the authors calculated the EDM in the SM to be $d_n \approx 3.6\times10^{-16}\theta\ e$ cm, while experiments constrain the EDM to $|d_n| < 3.6\times10^{-26}\ e$ cm (95% CL) [43]. Comparing the two results, we come to the conclusion that $\theta \lesssim 10^{-10}$.

If strong interactions are CP-conserving, then $\theta = 0$. The question arises: why is θ so small or why is the strong force CP-conserving? Peccei and Quinn [44, 45], Weinberg [46] and Wilczek [47] tried to solve the strong CP problem by introducing a $U(1)_{PQ}$ symmetry that is spontaneously broken. Spontaneously breaking this symmetry effectively replaces the CP-violating angle θ with a CP-conserving field, called the axion. The QCD axion is a Nambu-Goldstone boson arising from the broken $U(1)_{PQ}$ symmetry [46, 47]. Under $U(1)_{PQ}$ transformations the axion field transforms as $a \to a + \alpha f_a$, where $\Lambda = 4\pi f_a$ is the energy scale associated with breaking the $U(1)_{PQ}$ symmetry and α is a free parameter. The Lagrangian should be invariant under this transformation, and so $\overline{\theta}$ should transform like $\overline{\theta} \to \overline{\theta} - \alpha$. When the axion couples to other particles–where CP-violating angle θ is not present–the axion field should appear together with a derivative $\partial_\mu a$, if field redefinitions are not possible, such that the Lagrangian stays invariant under this shift symmetry where $\theta \to \theta + \alpha$. [40]

In the past decades, besides the WIMP, axions and ALPs have been a theoretical candidate for DM [48]. ALPs do not necessarily tied to the strong CP problem and are generic pseudo-Nambu-Goldstone bosons. ALPs are among the best-motivated candidates for new particles in beyond the SM physics [49]. By imposing fermionic DM, the question may arise how this form of DM interacts with the SM. SM particles are uncharged under the PQ-symmetry, but the effective ALP couplings to the SM fermions must exhibit the shift-symmetry and, therefore, ALP has derivative couplings to fermion currents and resembles a pseudo-scalar particle with Yukawa-like couplings [49]. Since the $U(1)_{PQ}$ symmetry is broken at scale $4\pi f_a$, the ALP couplings are naturally suppressed by decay constant f_a. For simplicity, we will refer to f_a as the cutoff scale throughout this thesis. However, we emphasize that f_a is not the scale for new physics, which is instead $\Lambda = 4\pi f_a$. This suppression provides a weakly interacting DM theory, that is needed to align with the observational evidence for DM. Couplings to the ALP are beforehand undetermined, but – as we will see – can be experimentally constrained.

Unlike the name may suggest, ALPs are particles whose couplings are not (necessarily) related to the strong CP problem. The ALP mass is not required to come from some symmetry group, unlike the QCD-axion described above. Similar to the axion, the ALP is a pseudo Nambu-Goldstone boson, a, that appears after breaking of a global symmetry and transforms as a singlet under the SM. ALPs also have a shift symmetry, such that $a \to a + c$, where c is a constant. The ALP can acquire flavor-violating couplings to quarks and leptons if the underlying symmetry is flavor-dependent. [50]

Flavor-violating couplings to the ALP open up larger sector of interactions, that would not be seen in SM-type interactions. The most general effective Lagrangian including operators of dimension up to 5 is [50]

$$\begin{aligned}\mathcal{L}_{\text{eff}}^{d\leq5} =& \frac{1}{2}\left(\partial_\mu a\right)\left(\partial^\mu a\right) - \frac{m_a^2}{2}a^2 + \frac{\partial^\mu a}{f_a}\sum_F \overline{\psi}_F \mathbf{c}_F \gamma_\mu \psi_F \\ &+ c_{GG}\frac{\alpha_s}{4\pi}\frac{a}{f_a}G^b_{\mu\nu}\tilde{G}^{b,\mu\nu} + c_{WW}\frac{\alpha_2}{4\pi}\frac{a}{f_a}W^A_{\mu\nu}\tilde{W}^{A,\mu\nu} + c_{BB}\frac{\alpha_1}{4\pi}\frac{a}{f_a}B_{\mu\nu}\tilde{B}^{\mu\nu},\end{aligned} \tag{3.2}$$

where $G^b_{\mu\nu}$ $(b = 1,\ldots,8)$,$W^A_{\mu\nu}$ $(A = 1,2,3)$ and $B_{\mu\nu}$ are the field-strength tensors of the $SU(3)_c, SU(2)_L$ and $U(1)_Y$ gauge fields, respectively, with dual field-strenth tensor defined like above. The couplings α_s, α_2 and α_1 are the SM gauge couplings for $SU(3)_c, SU(2)_L$ and $U(1)_Y$, respectively. In the first line, the sum is over chiral fermion multiplets $F \in \{U, D, E, u, d, e\}$,

where capital letters represent left-handed fermions and the small letters represent right-handed letters. The fermion couplings of the ALP, $\boldsymbol{c}_F$, are 3×3 hermitian matrices in generation space. Since the ALP couplings feature a shift symmetry, the fermions and Higgs boson have derivative couplings to the ALP, while the effect of the shifting of a can be removed by field redefinitions of the W and B fields [50].

In the ALP EFT discussion below, we follow [40, 50]. An equivalent form of the fermion part of the Lagrangian is

$$\mathcal{L}_{\text{eff}}^{\text{ferm}} = -\frac{a}{f_a}\left(\overline{Q}\phi\tilde{\boldsymbol{Y}}_d d_R + \overline{Q}\tilde{\phi}\tilde{\boldsymbol{Y}}_u u_R + \overline{L}\phi\tilde{\boldsymbol{Y}}_e e_R + \text{h.c.}\right). \tag{3.3}$$

Here,

$$\tilde{\boldsymbol{Y}}_d = i\left(\boldsymbol{Y}_d\boldsymbol{c}_d - \boldsymbol{c}_Q\boldsymbol{Y}_d\right), \quad \tilde{\boldsymbol{Y}}_u = i\left(\boldsymbol{Y}_u\boldsymbol{c}_u - \boldsymbol{c}_Q\boldsymbol{Y}_u\right) \quad \text{and} \quad \tilde{\boldsymbol{Y}}_e = i\left(\boldsymbol{Y}_e\boldsymbol{c}_e - \boldsymbol{c}_Q\boldsymbol{Y}_e\right), \tag{3.4}$$

where $\boldsymbol{Y}_f$ are the SM fermion Yukawa matrices. Using this form of the Lagrangian one can see the distinguishing feature of the shift symmetry of the ALP from any other pseudoscalar boson. The authors in [40] note that although there is no apparent reason for the complex matrices $\tilde{\boldsymbol{Y}}_f$ to have any particular structure, the shift symmetry of the ALP gives rise to the hierarchical structure of the matrices, resulting in the appearance of the SM Yukawa matrices.

The SM Yukawa matrices can be diagonalized via a bi-unitary transformation, such that

$$\boldsymbol{U}_f^\dagger\boldsymbol{Y}_f\boldsymbol{W}_f = \boldsymbol{Y}_u^{\text{diag}}, \qquad f = u, d, e. \tag{3.5}$$

By redefining the fermion field by

$$Q \to \boldsymbol{U}_u Q, \quad u_R \to \boldsymbol{W}_u u_R, \quad d_R \to \boldsymbol{W}_d d_R, \quad L \to \boldsymbol{U}_e L \quad \text{and} \quad e_R \to \boldsymbol{W}_e e_R, \tag{3.6}$$

the lepton-sector and up-sector Yukawa matrices are diagonalized, while the down-sector Yukawa matrix is transformed to $\boldsymbol{Y}_d \to \boldsymbol{V}\boldsymbol{Y}_d^{\text{diag}}$, where $\boldsymbol{V} = \boldsymbol{U}_u^\dagger\boldsymbol{U}_d$ is the CKM matrix.

To obtain the Lagrangian in the mass basis of the fermions, flavor matrices $\boldsymbol{c}_F$ must transform to new hermitian matrices under the field redefinition above. Redefining the fermion fields by means of the unitairy matrices above, gives

$$\begin{aligned} \boldsymbol{k}_U &= \boldsymbol{U}_u^\dagger\boldsymbol{c}_Q\boldsymbol{U}_u, & \boldsymbol{k}_D &= \boldsymbol{U}_d^\dagger\boldsymbol{c}_Q\boldsymbol{U}_d, & \boldsymbol{k}_E &= \boldsymbol{U}_e^\dagger\boldsymbol{c}_L\boldsymbol{U}_e, \\ \boldsymbol{k}_u &= \boldsymbol{W}_u^\dagger\boldsymbol{c}_u\boldsymbol{W}_u, & \boldsymbol{k}_d &= \boldsymbol{W}_d^\dagger\boldsymbol{c}_d\boldsymbol{W}_d, & \boldsymbol{k}_e &= \boldsymbol{W}_e^\dagger\boldsymbol{c}_e\boldsymbol{W}_e. \end{aligned} \tag{3.7}$$

It is fairly straightforward to see that the matrices $\boldsymbol{k}_U$ and $\boldsymbol{k}_D$ are related via the CKM matrix as $\boldsymbol{k}_D = \boldsymbol{V}^\dagger\boldsymbol{k}_U\boldsymbol{V}$. One can choose a basis such that all transformation matrices are the unit matrix, except for $\boldsymbol{U}_d = \boldsymbol{V}$. Similarly to [50], by choosing this basis, the two matrices $\boldsymbol{k}$ and $\boldsymbol{c}$ are related via

$$\begin{aligned} \boldsymbol{k}_U &= \boldsymbol{c}_U, & \boldsymbol{k}_D &= \boldsymbol{V}^\dagger\boldsymbol{c}_Q\boldsymbol{V}, \\ \boldsymbol{k}_E &= \boldsymbol{c}_\nu = \boldsymbol{c}_L & \boldsymbol{k}_{u,d,e} &= \boldsymbol{c}_{u,d,e}. \end{aligned}$$

Now writing the Lagrangian Eq. (3.2) in the mass basis, the fermion interaction Lagrangian becomes

$$\mathcal{L}_{\text{eff}}^{\text{int}} = \sum_{f,F}\frac{\partial^\mu a}{2f_a}\left[\overline{f}(\boldsymbol{k}_f + \boldsymbol{k}_F)\gamma_\mu f + \overline{f}(\boldsymbol{k}_f - \boldsymbol{k}_F)\gamma_\mu\gamma^5 f\right], \tag{3.8}$$

by using that the $f_{R,L} = \frac{1}{2}\left(1 \pm \gamma^5\right) f$. Now, $f \in \{u, d, e\}$ and $F \in \{U, D, E\}$. The first term in Eq. (3.8) is identified as a vector term and the second term is identified as an axial-vector term.

For each Lorentz structure there is a different combination of the matrices $\boldsymbol{k}_f$ and $\boldsymbol{k}_F$. It is then convenient to define new couplings, which are 3×3 matrices, by

$$\boldsymbol{c}^V_{ff} = \boldsymbol{k}_f + \boldsymbol{k}_F \quad \text{and} \quad \boldsymbol{c}^A_{ff} = \boldsymbol{k}_f - \boldsymbol{k}_F, \tag{3.9}$$

where the first coupling is the vector coupling and the second is the axial-vector coupling.

The ALP is a pseudo-scalar particle, and so the propagator is just the usual scalar propagator:

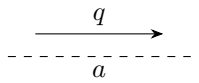

$$= \frac{i}{q^2 - m_a^2 + i\epsilon}. \tag{3.10}$$

The Feynman rules remain unchanged, such that external particle gives a spinor $u(p)$ and has propagator

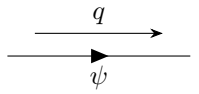

$$= \frac{i(\not{q} + m)}{q^2 - m_f^2 + i\epsilon}. \tag{3.11}$$

The vertex factor can be calculated using the Lagrangian in Eq. (3.8). Calculating the vertex factor is fairly straightforward, by going to the momentum space, after which the vertex factor can be easily read-off. Defining that particle i is the incoming particle and particle j is the outgoing particle in the vertex, the interaction Lagrangian in momentum-space is given by

$$\mathcal{L}^{\text{int}}_{\text{eff}} = \sum_f \int \frac{d^4q}{(2\pi)^4} \int \frac{d^4p}{(2\pi)^4} \int \frac{d^4p'}{(2\pi)^4} \frac{ia(q)}{2f_a} \left[c^V_{f_i f_j} \overline{f}_j(p') \not{q} f_i(p) + c^A_{f_i f_j} \overline{f}_j(p') \not{q} \gamma^5 f_i(p) \right] e^{ip' \cdot (y-z)} e^{-ip \cdot (x-z)}. \tag{3.12}$$

Here, $q = p - p'$. From this it is easy to see that the vertex factor is given by

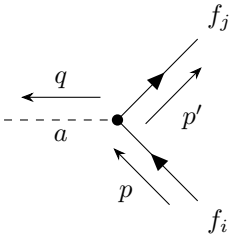

$$= \frac{1}{2f_a} \left[c^V_{f_i f_j} \not{q} + c^A_{f_i f_j} \not{q} \gamma^5 \right]. \tag{3.13}$$

Hermicity of the couplings imposes $c^{V,A}_{ij} = (c^{V,A}_{ji})^\dagger$, which means that the couplings must be real. Since the couplings in matrix form are hermitian, stating these matrices are symmetric implies that $\boldsymbol{c}^{V,A} \in \mathbb{R}$.

Notice that if the incoming and outgoing particle are on-shell, i.e. $p^2 = m^2$, both terms can be simplified by using the Dirac equation

$$\overline{f}_j(p') \not{q} f_i(p) = \overline{f}_j(p') (\not{p} - \not{p}') f_i(p) = (m_i - m_j) \overline{f}_j(p') f_i(p), \tag{3.14a}$$

$$\overline{f}_j(p') \not{q} \gamma^5 f_i(p) = \overline{f}_j(p') (-\gamma^5 \not{p} - \not{p}' \gamma^5) f_i(p) = -(m_i + m_j) \overline{f}_j(p') \gamma^5 f_i(p). \tag{3.14b}$$

Thus, the vector and axial-vector currents are for on-shell particles f_i and f_j, scalar and pseudo-scalar currents, respectively. If the particles are the same, i.e. $i = j$, the vector part is actually zero and, hence, does not contribute to the amplitude and cross section. This means that in on-shell interactions, where the vector part does not contribute, the axial-vector coupling is the

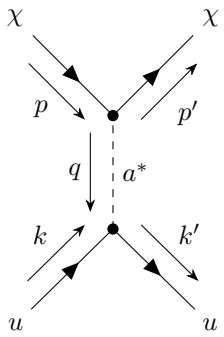

Figure 3.1: The tree-level diagram of $\chi u \to \chi u$.

only coupling of interest. It turns out that this fact will be especially useful in Sections 3.2 and 3.3 to simplify the calculations. The axial-vector part will, naively, always contribute to the amplitude, because the sum of two positive masses is never zero.

Knowing all about the axions and the ALP EFT, we can start calculating actual scattering processes.

3.2 Scattering at Tree-Level

The simplest scattering process is scattering at tree-level. Although eventually one wants scattering with a nucleon, we use that DM scatters with an up-quark. After the relevant quantities are obtained using DM–up-quark scattering, we can use some relations to go from up-quark scattering to nucleon scattering. In the ALP EFT this process is represented by the diagram in Fig. 3.1, where we have used the convention of time going from left to right.

In the previous section we used the assumption of on-shell incoming and outgoing particles to simplify the vertex factor, from (axial-)vector to (pseudo-)scalar currents. The stable external DM particles are assumed to be on-shell in this scattering process. This is a reasonable assumption for DM, since they are real particles interacting with the quarks. But, it is a little more tricky for quarks inside nucleons, because they are generally not exactly on-shell. Although one could argue that because nucleons are much heavier than the up- and down-quarks, these valence quarks are likely to be (almost) on-shell, this argument may be too simple. A commonly used and good working framework for modeling baryons is the covariant spectator framework. In this spectator framework, the baryons have a diquark pair that is on-shell and a single quark that is off-shell. When the valence quarks are close together, the on-shell diquark pair configuration changes around. [51, 52]

Using both arguments, it is reasonable to assume the valence quarks to be (approximately) on-shell. Hence, for simplicity we assume in this thesis that the incoming and outgoing up-quarks are on-shell. The ALP does not need to be on-shell.

Before writing down the amplitude, note that with the on-shell assumption the vertex factor is simplified as shown in Eqs. (3.14a) and (3.14b). The momentum transfer given in terms of the up-quark momenta has a minus-sign with respect to the definition used in Eqs. (3.14a) and (3.14b), resulting in an overall minus-sign. Using the Feynman rules from the previous section, the amplitude for this tree-level process is

$$\mathcal{M}^{\text{tree}} = \frac{-im_u m_\chi c_{uu}^A c_{\chi\chi}^A}{f_a^2} \frac{\left[\overline{\chi}(p')\gamma^5\chi(p)\right]\left[\overline{u}(k')\gamma^5 u(k)\right]}{q^2 - m_a^2}. \tag{3.15}$$

In order to make predictions, this amplitude has to be in terms of nucleon fields instead of up-quark fields. For this one must evaluate the operator matrix element $\langle N|\overline{Q}\gamma^5 Q|N\rangle$. Although the exact expression for this translation would be difficult to obtain, because one needs to account for a form factor, we can say that the amplitude would be something of the form

$$\mathcal{M}^{\text{tree, nucleon}} \propto F_{\text{SD}}(q)\frac{-im_N m_\chi c_{uu}^A c_{\chi\chi}^A}{f_a^2}\frac{\left[\overline{\chi}\gamma^5\chi\right]\left[\overline{N}\gamma^5 N\right]}{q^2-m_a^2}, \tag{3.16}$$

where N is the nucleon field and $F_{\text{SD}}(q)$ is the form factor, that in our case includes all factors that are needed to go from up-quarks to nucleons. Taking the NR-limit of the amplitude and using Table 2.2 to write the operator in terms of the building blocks, gives

$$\mathcal{M}_{\text{NR}}^{\text{tree,nucleon}} = F_{\text{SD}}(q)\frac{im_N^2 c_{uu}^A c_{\chi\chi}^A}{f_a^2}\frac{\langle\mathcal{O}_6\rangle}{-\mathbf{q}^2-m_a^2}. \tag{3.17}$$

That in turn gives the DM-nucleon cross section [7]

$$\sigma_p \propto \frac{\mu_N^2 m_N^4 m_\chi^2 (c_{uu}^A)^2 (c_{\chi\chi}^A)^2}{(\mathbf{q}^2+m_a^2)^2 f_a^4}|\langle\mathcal{O}_6\rangle|^2, \tag{3.18}$$

where the bar on top of the building block represents the average over dark fermion spins, μ_N is the reduced mass of the DM-nucleon system and m_N is the nucleon mass. There are several problems that arise from this interaction, that make this process undetectable with current experiments. In all scenarios the momentum transfer $\mathbf{q}$ is of the order $\mathbf{q}^4/f_a^4$. In the first scenario $m_a \gg \mathbf{q}$, the cross section scales with momentum transfer $\mathbf{q}^4$, making the cross section highly momentum suppressed. If that suppression could be lifted by e.g. a large mass, then it would be detectable. Although the up-quark mass is not present anymore in σ_p, the scale of the proton and neutron mass (~ 1 GeV) does not account for the large scale of the cutoff scale (~ 1 TeV).

The second scenario assumes that $m_a \ll \mathbf{q}$, then the cross section does not scale with the momentum transfer $\mathbf{q}^4$ anymore and is only dependent on the dot-product of the direction of the momentum transfer and the spin-operators. Although this is not momentum suppressed anymore, it is still heavily suppressed by the cutoff scale as it scales as m_N^4/f_a^4.

The last scenario is where $\mathbf{q}$ and m_a are on similar scales. In that case, one would obtain approximately half of the result of the second scenario, resulting in the same problems.

Not only is the diagram generally suppressed by the cutoff scale f_a and for massive ALPs also by the momentum transfer $\mathbf{q}$, experiments are generally less sensitive to spin-dependent interactions. The difference in sensitivity could be five orders of magnitude, because spin-independent interactions is coherent across all nucleons and therefore enhanced by A^2, while SD scattering involves only one nucleon inside the nucleus [29].

To overcome the suppressions and spin-dependence of the tree-level described above, we perform one-loop level calculations.

3.3 One-Loop Calculation

3.3.1 Setting Up the Problem

By going to one-loop order, we try to solve the problems that arose from the tree-level diagram. Vector and scalar interactions should arise from the one-loop diagram(s), for spin-independent scattering to take place. The diagram(s) must therefore not or not only give rise to only axial-vector or pseudo-scalar structures, causing momentum suppression. Moreover, there has to be

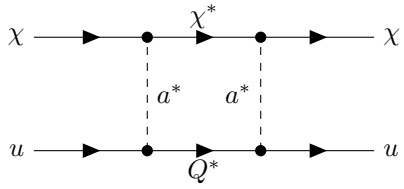

Figure 3.2

some scales or masses that counter the effect of the cutoff scale. Although the first requirement is not guaranteed, it likely gives rise to a more complex loop structure, resulting in a dependence on scalar and vector structures as well. The one-loop diagram that arises from these two requirements is given in Fig. 3.2.

As we will see, this loop diagram is not dependent on only pseudo-scalar and axial-vector structures, but contains several combinations of (axial-)vector and (pseudo-)scalar structures. In this diagram are four powers of the vertex factors, resulting in four powers of the cutoff scale in the denominator. Naively thinking, at each vertex masses are generated, because of the derivative coupling of the ALP to the fermions. The propagator for quark Q could essentially be for any quark, but since masses are generated at each vertex, a large mass would help to lift effects of f_a. Since $f_a \sim 1$ TeV, the only quark mass that comes close to this scale is that of the top-quark. The logical conclusion is to choose for Q to be the top-quark. This would lead to a dependence of $m_\chi^2 m_t^2/f_a^4$ in the integral. If it is not momentum suppressed, this could lift the scale suppression.

Since only the initial and final states of the process can be measured, the diagram in Fig. 3.2 is not the only diagram. Two of the ALP vertices can be 'exchanged', such that one obtains a diagram where the ALP propagators cross. In Fig. 3.3 both diagrams with all momenta are given, where Fig. 3.3a is the trivial diagram and Fig. 3.3b is the crossed ALP propagator diagram. The amplitude and total loop integral, is given by the sum of the two diagrams.

Particles inside the loop are off-shell at the external momenta and are denoted with an asterisk. As mentioned in Section 3.2 we assume that the external particles are on-shell.

Applying Feynman rules to diagram Fig. 3.3a, its loop integral is given by

$$\begin{aligned} I_1 = \frac{-1}{16 f_a^4} \int \frac{d^4\ell}{(2\pi)^4} & \frac{1}{\left[\ell^2 - m_a^2\right]\left[(\ell-q)^2 - m_a^2\right]\left[(\ell-p)^2 - m_\chi^2\right]\left[(\ell+k)^2 - m_t^2\right]} \\ & \times \overline{\chi}(p')\left[c_{\chi\chi}^V(\ell - \not{q}) + c_{\chi\chi}^A(\ell - \not{q})\gamma^5\right](\ell - \not{p} - m_\chi)\left[c_{\chi\chi}^V \ell + c_{\chi\chi}^A \ell\gamma^5\right]\chi(p) \\ & \times \overline{u}(k')\left[c_{tu}^V(\ell - \not{q}) + c_{tu}^A(\ell - \not{q})\gamma^5\right](\ell + \not{k} + m_t)\left[c_{tu}^V \ell + c_{tu}^A \ell\gamma^5\right] u(k), \end{aligned} \tag{3.19}$$

and diagram Fig. 3.3b gives

$$\begin{aligned} I_2 = \frac{1}{16 f_a^4} \int \frac{d^4\ell}{(2\pi)^4} & \frac{1}{\left[\ell^2 - m_a^2\right]\left[(\ell-q)^2 - m_a^2\right]\left[(\ell-p)^2 - m_\chi^2\right]\left[(\ell-k')^2 - m_t^2\right]} \\ & \times \overline{\chi}(p')\left[c_{\chi\chi}^V(\ell - \not{q}) + c_{\chi\chi}^A(\ell - \not{q})\gamma^5\right](\ell - \not{p} - m_\chi)\left[c_{\chi\chi}^V \ell + c_{\chi\chi}^A \ell\gamma^5\right]\chi(p) \\ & \times \overline{u}(k')\left[c_{tu}^V \ell + c_{tu}^A \ell\gamma^5\right](\ell - \not{k}' - m_t)\left[c_{tu}^V(\ell - \not{q}) + c_{tu}^A(\ell - \not{q})\gamma^5\right] u(k). \end{aligned} \tag{3.20}$$

The numerator contains two distinct parts: the DM and the quark part. Because the external particles are on-shell, the momenta $\not{p}, \not{p}', \not{k}$ and $\not{k}'$ can be turned into their corresponding masses using the Dirac equation. Moreover, it would help to rearrange terms such that factors in the

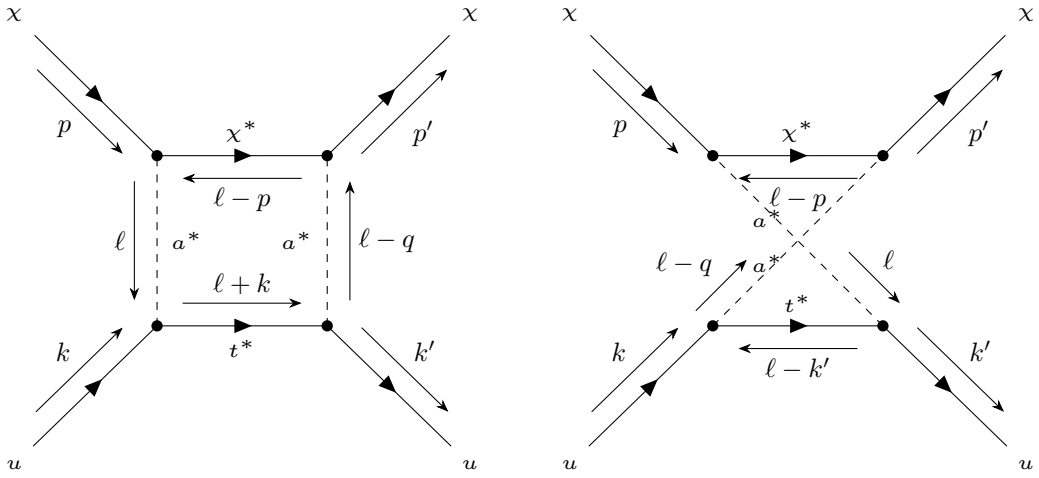

Figure 3.3: The one-loop diagrams for $\chi u \to \chi u$, with loop momentum ℓ.

denominator are cancelled. Working out each part and performing the aforementioned simplifications, one can verify that the DM part in the numerator of the integrand for both diagrams simplifies to

$$\begin{aligned}\overline{\chi}(p')\Big\{&\left(c^V_{\chi\chi}-c^A_{\chi\chi}\gamma^5\right)^2\left[(\ell-p)^2-m_\chi^2\right]\not{\ell}+2m_\chi c^A_{\chi\chi}\left(c^A_{\chi\chi}+c^V_{\chi\chi}\gamma^5\right)\left[(\ell-p)^2-m_\chi^2\right]\\&+4m_\chi^2(c^A_{\chi\chi})^2\not{\ell}\Big\}\,\chi(p).\end{aligned}\tag{3.21}$$

Going through similar steps, the quark part of the first integral, I_1, simplifies to

$$\begin{aligned}\overline{u}(k')\Big\{&\left(c^V_{tu}-c^A_{tu}\gamma^5\right)^2\left[(\ell+k)^2-m_t^2\right]\not{\ell}+m_t^2\left(c^V_{tu}-c^A_{tu}\gamma^5\right)^2\not{\ell}\\&-2m_tm_u\left((c^V_{tu})^2-(c^A_{tu})^2\right)\not{\ell}+m_t(m_t^2-m_u^2)\left((c^V_{tu})^2-(c^A_{tu})^2\right)\\&+m_t\left((c^V_{tu})^2-(c^A_{tu})^2\right)\left[(\ell+k)^2-m_t^2\right]-m_u\left(c^V_{tu}+c^A_{tu}\gamma^5\right)^2\left[(\ell+k)^2-m_t^2\right]\\&-m_u(m_t^2-m_u^2)\left(c^V_{tu}+c^A_{tu}\gamma^5\right)^2+m_u^2\left(c^V_{tu}+c^A_{tu}\gamma^5\right)^2\not{\ell}\Big\}\,u(k),\end{aligned}\tag{3.22}$$

and of the second integral, I_2, to

$$\begin{aligned}\overline{u}(k')\Big\{&\left(c^V_{tu}-c^A_{tu}\gamma^5\right)^2\left[(\ell-k')^2-m_t^2\right]\not{\ell}+m_t^2\left(c^V_{tu}-c^A_{tu}\gamma^5\right)^2\not{\ell}\\&-2m_tm_u\left((c^V_{tu})^2-(c^A_{tu})^2\right)\not{\ell}-m_t\left((c^V_{tu})^2-(c^A_{tu})^2\right)\left[(\ell-k')^2-m_t^2\right]\\&-m_t(m_t^2-m_u^2)\left((c^V_{tu})^2-(c^A_{tu})^2\right)+m_u\left(c^V_{tu}-c^A_{tu}\gamma^5\right)^2\left[(\ell-k)'^2-m_t^2\right]\\&+m_u(m_t^2-m_u^2)\left(c^V_{tu}-c^A_{tu}\gamma^5\right)^2+m_u^2\left(c^V_{tu}+c^A_{tu}\gamma^5\right)^2\not{\ell}\Big\}\,u(k).\end{aligned}\tag{3.23}$$

By multiplying the DM and quark parts, the integrals I_1 and I_2 are obtained. Summing I_1 and I_2 gives the total one-loop integral of the process $\chi u \to \chi u$. Because of factors of the loop-momenta in the numerator, one can see that the integrals I_1 and I_2 are tensor integrals, which are generally difficult to integrate and obtain analytical expressions of. Since the analytic expressions for the

scalar integrals are known, the tensor integrals must be reduced to scalar integrals. This is where we will need to use Passarino-Veltman reduction of one-loop integrals. In the next section we will introduce the theory and describe the procedure to go from tensor to scalar integals.

3.3.2 Passarino-Veltman Reduction

As loops become more complicated, the integrals become harder to calculate. One method to reduce tensor loop integrals to scalar integrals was introduced by Passarino and Veltman in [53]. This technique is now known as Passarino-Veltman (PV) reduction. Like every method, the PV-reduction scheme has drawbacks. The main drawback is the appearance of Gram determinants in the denominator, which are numerically unstable if they are small. Alternative procedures have been devised to fix the instabilities, e.g. [54]. The other drawback is that as the rank of the tensor integral increases, the computational complexity rapidly increases [55]. Although it has these drawbacks it is still a powerful technique to reduce tensor to scalar integrals.

In this thesis we follow the conventions from [56]. One-loop N-point tensor integrals in D dimensions, with N propagator factors and P integration momenta in the numerator, generally have the form

$$T^N_{\mu_1\mu_2\cdots\mu_P}(p_1,\ldots,p_{N-1},m_0,\ldots,m_{N-1}) = \frac{(2\pi\mu)^{4-D}}{i\pi^2}\int d^D\ell \frac{\ell_{\mu_1}\cdots\ell_{\mu_P}}{D_0D_1\cdots D_{N-1}}, \tag{3.24}$$

where the denominator factors are

$$D_0 = \ell^2 - m_0^2, \qquad D_i = (\ell + p_i) - m_i^2 + i\epsilon, \quad i = 1,2,\ldots,N-1 \tag{3.25}$$

and originate from the propagators in the loop. The parameter μ has mass-dimension and serves to keep the mass-dimension fixed for varying D. If the power of integration momenta in the numerator exceeds the power of integration momenta in the denominator, i.e. $P + D - 2N \geq 0$, the integral is generally UV-divergent. These divergences are regularized by calculating the integral in $D \neq 4$. The diagramatic form of Eq. (3.24) is given in Fig. 3.4. Every N-point integral T^N is denoted by the $(N-1)$th letter of the alphabet: $T^1 \equiv A, T^2 \equiv B, \ldots$. If there are no integration momenta in the numerator, $P = 0$, the integral is scalar and caries the lower-index 0.

A rank-P N-point function is symmetric in all its indices μ_i, meaning that switching two indices μ_i, μ_j does not affect the integral:

$$T^N_{\mu_1\cdots\mu_i\cdots\mu_j\cdots\mu_P}(p_1,\ldots,p_{N-1},m_0,\ldots,m_{N-1}) = T^N_{\mu_1\cdots\mu_j\cdots\mu_i\cdots\mu_P}(p_1,\ldots,p_{N-1},m_0,\ldots,m_{N-1}). \tag{3.26}$$

Note that switching either two momenta or two masses *does* change the integral:

$$\begin{aligned} &T^N_{\mu_1\mu_2\cdots\mu_P}(p_1,\ldots,p_i,\ldots,p_j,\ldots,p_{N-1},m_0,\ldots,m_i,\ldots,m_j,\ldots,m_{N-1}) \\ &\qquad \neq T^N_{\mu_1\mu_2\cdots\mu_P}(p_1,\ldots,p_j,\ldots,p_i,\ldots,p_{N-1},m_0,\ldots,m_i,\ldots,m_j,\ldots,m_{N-1}), \end{aligned} \tag{3.27}$$

but it is invariant under changing the momenta p_i, p_j and masses m_i, m_j simultaneously, such that the momenta and masses with the same index are paired up again.

Lorentz covariance allows every tensor integral to be decomposed into tensors, constructed by the external momenta and the metric tensor $g_{\mu\nu}$. The explicit Lorentz decomposition for rank-one and rank-two N-point integrals reads [56]

$$T_\mu = \sum_{i=1}^{N-1} p_{i\mu} T_i, \tag{3.28a}$$

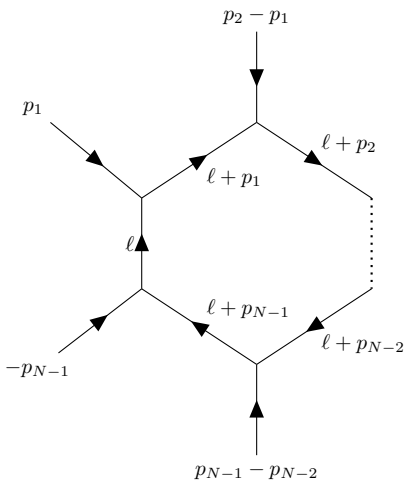

Figure 3.4: N-point integral convention.

$$T_{\mu\nu} = g_{\mu\nu} T_{00} + \sum_{i,j=1}^{N-1} p_{i\mu} p_{j\nu} T_{ij}. \tag{3.28b}$$

The goal is to reduce the tensor integrals to scalar integrals, but the reduction above does not provide an explicit decomposition in terms of T_0-type integrals. Let us go through the simplest example for PV-reduction, which is reducing the integral B_μ to scalar form. This integral is defined as

$$B_\mu(p, m_1, m_2) = \frac{(2\pi\mu)^{4-D}}{i\pi^2} \int d^D\ell \frac{\ell_\mu}{[\ell^2 - m_1^2]\,[(\ell+p)^2 - m_2^2]}. \tag{3.29}$$

Eq. (3.28a) suggests that this integral is decomposed by $B_\mu = p_\mu B_1$, i.e. it is projected onto momentum p_μ. Using this decomposition, we contract the integral with p_μ and divide by p^2, resulting in

$$B_1(p; m_1, m_2) = \frac{1}{p^2} \frac{(2\pi\mu)^{4-D}}{i\pi^2} \int d^D\ell \frac{p \cdot \ell}{[\ell^2 - m_1^2]\,[(\ell+p)^2 - m_2^2]}. \tag{3.30}$$

The numerator can also be written as $\frac{1}{2}\left((\ell+p)^2 - p^2 - \ell^2\right)$. Adding and subtracting masses to cancel terms in the denominator, gives

$$B_1(p; m_1, m_2) = \frac{1}{2p^2} \frac{(2\pi\mu)^{4-D}}{i\pi^2} \int d^D\ell \frac{(\ell+p)^2 - m_2^2 - \ell^2 + m_1^2 - p^2 - m_1^2 + m_2^2}{[\ell^2 - m_1^2]\,[(\ell+p)^2 - m_2^2]}. \tag{3.31}$$

By simplifying this expression and rewriting the simplified integrand as scalar integrals, we obtain the definition of B_1 in terms of scalar integrals

$$B_1(p; m_1, m_2) = \frac{1}{2p^2}\left[A_0(m_1) - A_0(m_2) - \left(p^2 + m_1^2 - m_2^2\right) B_0(p, m_1, m_2)\right]. \tag{3.32}$$

Now we know B_1, we also know B_μ, because of the decomposition of Eq. (3.28a). It is computationally expensive to decompose every tensor integral by hand, especially for integrals with a higher rank or higher-order N integrals. Packages like `FeynCalc` [57–60] in Mathematica do this decomposition for you. In this thesis we used `FeynCalc` to decompose some integrals presented in Section 3.3.3.

Knowing the general procedure of tensor integral reduction, the last thing that is needed is the analytical form of the scalar N-point functions. The one- and two-point integrals have the simplest expressions, where the analytic expression of the two-point function is most relevant in this work. The scalar one-point function is given by [56]

$$A_0(m_0) = m_0^2 \left(\Delta - \log \frac{m_0^2}{\mu^2} + 1 \right), \tag{3.33}$$

where

$$\Delta = \frac{2}{4-D} - \gamma_E + \log 4\pi, \tag{3.34}$$

is the UV-divergence and the γ_E is Euler's constant. Here, the factor μ appears in the logarithm and is an artificial energy scale. The analytic expression of the scalar two-point function is [56]

$$B_0(p, m_0, m_1) = \Delta + 2 - \log \frac{m_0 m_1}{\mu^2} + \frac{m_0^2 - m_1^2}{p^2 + i\epsilon} \log \frac{m_1}{m_0} - \frac{m_0 m_1}{p^2 + i\epsilon} \left(\frac{1}{r_{01}} - r_{01} \right) \log r_{01}, \tag{3.35}$$

where r and $\frac{1}{r}$ are determined from

$$x^2 + \frac{m_0^2 + m_1^2 - p^2 - i\epsilon}{m_0 m_1} x + 1 = (x + r_{01}) \left(x + \frac{1}{r_{01}} \right). \tag{3.36}$$

The solution for r then reads

$$r_{01} = \frac{m_0^2 + m_1^2 - p^2 - i\epsilon \pm \sqrt{(m_0^2 + m_1^2 - p^2 - i\epsilon)^2 - 4m_0^2 m_1^2}}{2m_0 m_1}. \tag{3.37}$$

Even though both the positive and negative sign solution are equal in the combination $\left(\frac{1}{r} - r\right) \log r$, throughout this thesis we only use the positive sign.

Although Eq. (3.35) seems to be singular when $p^2 = 0$, one can show that the limit as $p^2 \to 0$ does exist. Instead of taking a limit, it is easier to look at the integral representation to derive expressions in this limit. First assume the masses are not equal, then using partial fractions

$$\begin{aligned} B_0(0, m_0, m_1) &= \frac{(2\pi\mu)^{4-D}}{i\pi^2} \int d^D\ell \frac{1}{[\ell^2 - m_0^2][\ell^2 - m_1^2]} \\ &= \frac{1}{m_1^2 - m_0^2} \frac{(2\pi\mu)^{4-D}}{i\pi^2} \int d^D\ell \left[\frac{1}{\ell^2 - m_1^2} - \frac{1}{\ell^2 - m_0^2} \right] \\ &= \frac{A_0(m_1) - A_0(m_0)}{m_1^2 - m_0^2}. \end{aligned} \tag{3.38}$$

When the masses are equal we notice that taking the derivative of the scalar one-point function with respect to m^2 gives back the scalar two-point function:

$$\begin{aligned} \frac{d}{dm^2} A_0(m) &= \frac{(2\pi\mu)^{4-D}}{i\pi^2} \int d^D\ell \frac{d}{dm^2} \frac{1}{\ell^2 - m^2} \\ &= \frac{(2\pi\mu)^{4-D}}{i\pi^2} \int d^D\ell \frac{1}{[\ell^2 - m^2]^2} \\ &= B_0(0, m, m). \end{aligned} \tag{3.39}$$

The same techniques can be used to go from a scalar three-point function with one or both momenta equal to zero, to scalar one- and two-point functions. Without spoiling too much of

the end result, we will see that the scalar three-point function where one momentum is zero and two masses are equal, $C_0(0, p, m, m, M)$, can be reduced to an expression dependent on only the two-point function. Using the above reasoning, this scalar three-point function has the following relation to the scalar two-point function:

$$C_0(0, p, m, m, M) = \frac{d}{dm^2} B_0(p, m, M). \tag{3.40}$$

It is important to note that the momentum p appears together with mass M, *not* mass m. If it appears together with mass m this does not hold anymore. Taking the derivative of the two-point function can easily be done, given the anayltic expression in Eq. (3.35). Assuming that $p^2 = M^2$, the derivative then is

$$\begin{aligned} m^2 \frac{d}{dm^2} B_0(M, m, M) = \frac{1}{2} \Bigg[-1 + \frac{2m^2}{M^2} \log \frac{M}{m} - \frac{m^2 - M^2}{M^2} - \frac{m}{M} \left(\frac{1}{r} - r \right) \log r \\ - \frac{m^2}{M} \left(\frac{1 - \log r}{r^2} - 1 - \log r \right) \frac{dr}{dm} \Bigg], \end{aligned} \tag{3.41}$$

where we have multiplied the derivative by m^2 to obtain a result that has no mass dimension, like the scalar two-point function itself. Here we have used that

$$r = \frac{m^2 - i\epsilon + \sqrt{(m^2 - i\epsilon)^2 - 4m^2 M^2}}{2mM} \tag{3.42a}$$

$$\frac{dr}{dm} = -\frac{r}{m} + \frac{2m \left(r - \frac{M}{m} \right)}{\sqrt{(m^2 - i\epsilon)^2 - 4m^2 M^2}}. \tag{3.42b}$$

Last, the rank-p N-point functions may contain divergent parts. For example, the scalar two-point function given in Eq. (3.35) has a divergent part of $\frac{-2}{D-4}$. It is useful to know what the UV-divergent parts are of the tensor integrals. Below we listed the UV-divergent parts of different tensor integrals that appear in the loop integral, where all divergent parts are given as a product of $D - 4$ and the integral itself [56]:

$$(D-4)A_0(m) = -2m^2, \tag{3.43a}$$

$$(D-4)B_0(p, m_0, m_1) = -2, \tag{3.43b}$$

$$(D-4)B_1(p, m_0, m_1) = 1, \tag{3.43c}$$

$$(D-4)B_{00}(p, m_0, m_1) = \frac{1}{6} \left(p^2 - 3m_0^2 - 3m_1^2 \right), \tag{3.43d}$$

$$(D-4)B_{11}(p, m_0, m_1) = -\frac{2}{3}, \tag{3.43e}$$

$$(D-4)C_{00}(p_1, p_2, m_0, m_1, m_2) = -\frac{1}{2}. \tag{3.43f}$$

For the integrals where the divergent part is independent of masses and momenta, i.e. constant, the difference of two of the same integral-type results in canceling the divergent part. As an example, the rank-two three-point integral has a constant UV-divergent part of $-\frac{1}{2}$. If there is another rank-two three-point function that is subtracted from the first one, the divergences cancel.

After this intermezzo of PV-reduction, we can go back to our problem: the one-loop integral(s).

3.3.3 Simplifications, Approximations and Final Result

After multiplying the DM and quark parts in Eqs. (3.21) to (3.23), symplifying the expressions, writing them in terms of the Passarino-Veltman integral functions, and adding up I_1 and I_2, we obtain the total loop integral $\mathcal{I}$ in Eq. (B.4). $\mathcal{I}$ is a long expression, and reducing a tensor integral like the rank-two four-point integral $D_{\mu\nu}$ is complex and computationally expensive. If the full expression of $\mathcal{I}$ is reduced, the result would be very long. Not all terms in $\mathcal{I}$ have the same order of magnitude. Some terms may be negligible compared to other terms in the integral. In order to make predictions we need to simplify the integral and do some well-motivated approximations.

The first simplifications that can be done is by utilizing the properties of the two- and three-point functions. First, if the B_μ integral functions depend only on momentum transfer q, the reduction of $B_\mu(q, m_0, m_1)$ is $q_\mu B_1(q, m_0, m_1)$ and therefore gives a factor of q_μ. Then, when contracted with a vector Lorentz structure, this term will be zero (see Eq. (3.14a)) and when contracted with an axial-vector structure, it results in twice the mass times the pseudo-scalar structure (see Eq. (3.14b)).

Next, by utilizing the momentum transfer dependence of the three-point functions, the integration variable can be shifted by q. A three-point function dependent on momentum k' can then be expressed in terms of three-point functions dependent on momentum k only. Because most three-point functions appear as a sum or difference of two three-point functions, where one carries momentum k and the other k', these terms can be heavily simplified by also using the knowledge of what happens when one contracts with (axial-)vector structures. In Section B.2.1 we showed the following relations:

$$\begin{aligned} C_{\mu\nu}(k,-q,m_a,m_t,m_a) - C_{\mu\nu}(-k',-q,m_a,m_t,m_a) = \; & q_\mu C_\nu(k,-q,m_a,m_t,m_a) \\ & + q_\nu C_\mu(k,-q,m_a,m_t,m_a) \\ & - q_\nu q_\mu C_0(k,-q,m_a,m_t,m_a), \end{aligned} \tag{3.44a}$$

$$\begin{aligned} C_\mu(k,-q,m_a,m_t,m_a) - C_\mu(-k',-q,m_a,m_t,m_a) = \; & 2C_\mu(k,-q,m_a,m_t,m_a) \\ & - q_\mu C_0(k,-q,m_a,m_t,m_a), \\ C_\mu(k,-q,m_a,m_t,m_a) + C_\mu(-k',-q,m_a,m_t,m_a) \; & = q_\mu C_0(k,-q,m_a,m_t,m_a), \end{aligned} \tag{3.44b}$$

$$\begin{aligned} C_\nu(k,-q,m_a,m_t,m_a) - C_\nu(-k',-q,m_a,m_t,m_a) = \; & 2C_\nu(k,-q,m_a,m_t,m_a) \\ & - q_\nu C_0(k,-q,m_a,m_t,m_a), \end{aligned} \tag{3.44c}$$

$$C_0(k,-q,m_a,m_t,m_a) + C_0(-k',-q,m_a,m_t,m_a) = 2C_0(k,-q,m_a,m_t,m_a), \tag{3.44d}$$

$$C_0(k,-q,m_a,m_t,m_a) - C_0(-k',-q,m_a,m_t,m_a) = 0. \tag{3.44e}$$

Now, one can see that a lot of terms are zero when the momentum transfer is contracted with vector structures, and axial-vector become pseudo-scalar structures. Unfortunately, the same cannot be done for the four-point function. Performing a similar trick allows one to change the $-k'$ to a k, but then $-p$ changes to p'. The four-point function terms therefore stay in their full form.

Most up-masses appear together with the top-mass, i.e. $m_t \pm m_u$. The mass of the top-quark is about 172.57 GeV/c^2, which is much larger than the mass of the up-quark (a few MeV) [61]. Hence, all up-masses that appear together with a top-mass are neglected.

The simplifications and mass approximation above already reduces the integral to a more compact expression.

$$64i\pi^2 f_a^4 \mathcal{I} = 64i\pi^2 f_a^4 (I_1 + I_2)$$

$$
\begin{aligned}
&= 2m_\chi m_t^2 m_u (c^A_{\chi\chi})^2 c^V_{tu} c^A_{tu} \left[\overline{\chi}(p')\chi(p)\right] \left[\overline{u}(k')\gamma^5 u(k)\right] C_0(k,-q,m_a,m_t,m_a) \\
&+ 2m_\chi m_t^2 (c^A_{\chi\chi})^2 c^V_{tu} c^A_{tu} \left[\overline{\chi}(p')\chi(p)\right] \left[\overline{u}(k')\gamma^5\gamma^\nu u(k)\right] C_\nu(k,-q,m_a,m_t,m_a) \\
&+ 2m_\chi^2 m_t^2 (c^A_{\chi\chi})^2 c^V_{tu} c^A_{tu} \left[\overline{\chi}(p')\gamma^\mu\chi(p)\right] \left[\overline{u}(k')\gamma^5\gamma^\nu u(k)\right] \\
&\times \left[D_{\mu\nu}(k,-q,-p,m_a,m_t,m_a,m_\chi) - D_{\mu\nu}(-k',-q,-p,m_a,m_t,m_a,m_\chi)\right] \\
&+ 2m_\chi^2 m_t^2 m_u (c^A_{\chi\chi})^2 c^V_{tu} c^A_{tu} \left[\overline{\chi}(p')\gamma^\mu\chi(p)\right] \left[\overline{u}(k')\gamma^5 u(k)\right] \\
&\times \left[D_{\mu}(k,-q,-p,m_a,m_t,m_a,m_\chi) - D_{\mu}(-k',-q,-p,m_a,m_t,m_a,m_\chi)\right] \\
&\\
&- m_\chi m_t (c^A_{\chi\chi})^2 \left((c^V_{tu})^2 - (c^A_{tu})^2\right) \left[\overline{\chi}(p')\chi(p)\right] \left[\overline{u}(k')u(k)\right] \left[B_0(-q,m_a,m_a) + m_t^2 C_0(k,-q,m_a,m_t,m_a)\right] \\
&- m_\chi^2 m_t (c^A_{\chi\chi})^2 \left((c^V_{tu})^2 - (c^A_{tu})^2\right) \left[\overline{\chi}(p')\gamma^\mu\chi(p)\right] \left[\overline{u}(k')u(k)\right] \left[-2C_\mu(q,p,m_a,m_a,m_\chi)\right. \\
&\left.+ m_t^2 D_\mu(k,-q,-p,m_a,m_t,m_a,m_\chi) + m_t^2 D_\mu(-k',-q,-p,m_a,m_t,m_a,m_\chi)\right] \\
&- m_\chi m_t^2 (c^A_{\chi\chi})^2 \left((c^V_{tu})^2 + (c^A_{tu})^2\right) \left[\overline{\chi}(p')\chi(p)\right] \left[\overline{u}(k')\gamma^\nu u(k)\right] C_\nu(k,-q,m_a,m_t,m_a) \\
&- m_\chi^2 m_t^2 (c^A_{\chi\chi})^2 \left((c^V_{tu})^2 + (c^A_{tu})^2\right) \left[\overline{\chi}(p')\gamma^\mu\chi(p)\right] \left[\overline{u}(k')\gamma^\nu u(k)\right] \\
&\times \left[D_{\mu\nu}(k,-q,-p,m_a,m_t,m_a,m_\chi) - D_{\mu\nu}(-k',-q,-p,m_a,m_t,m_a,m_\chi)\right].
\end{aligned}
\tag{3.45}
$$

If a term has an axial-vector or pseudo-scalar Lorentz structure, it means the term contains both a vector and an axial-vector fermion coupling to the ALP. In order to explain this, note that in the vertex factor the vector-coupling term does not contain a γ^5-factor and that each axial-vector term contains a factor of γ^5. Because both the DM and quark part have two vertices, two factors of γ^5 can be brought together, that results in I_4. This only occurs with two axial-vector couplings. If there is a mix of an axial-vector and vector coupling, there is only one factor of γ^5, and we cannot use the identity $(\gamma^5)^2 = I_4$. Only when the axial-vector and vector coupling of the quark-part are non-zero, axial-vector and pseudo-scalar structures appear.

Note that the DM part is only dependent on the axial-vector coupling, even though no assumptions have been made on the DM vector coupling. We have introduced only one type of DM particle, hence, the DM-ALP vector coupling has to be absent for the shift symmetry to be fulfilled. Another way to look at it is, that at each vertex a difference of the masses is generated for the vector coupling, because of the derivative coupling. Since the DM particle in the propagator has the same mass as the incoming and outgoing DM particles, the vector term will not be present after performing the simplifications of shifting the three-point functions momenta and using the reduction of the rank-one two-point function. The integral is now highlu dependent on the axial-vector DM-ALP coupling. If $c^A_{\chi\chi}$ is zero, this whole scattering interaction is impossible. So either the axial-vector coupling cannot be zero or, similar to the quark-part, a different particle is needed in the propagator with mass that differs from m_χ. The other thing to note, before futher simplifying any further, is that if the coupling strength of the vector and axial-vector up-top-ALP couplings are equal, the integral is not UV-divergent anymore.

In dark matter direct detection experiments the momentum transfer and all external momenta are small, meaning that axial-vector and pseudo-scalar currents are momentum suppressed, as seen in Sections 2.3 and 3.2. Compared to the leading-order scalar and vector currents, the axial-vector and pseudo-scalar currents are negligible for small momenta. We can, therefore, discard all terms dependent on axial-vector and pseudo-scalar type structures. The simplified and approximated expression of the loop integral then reads

$$
\begin{aligned}
-64i\pi^2 f_a^4 \mathcal{I} = {} & m_\chi^2 m_t^2 (c^A_{\chi\chi})^2 \left((c^V_{tu})^2 + (c^A_{tu})^2\right) \left[\overline{\chi}(p')\gamma^\mu\chi(p)\right] \left[\overline{u}(k')\gamma^\nu u(k)\right] \\
&\times \left[D_{\mu\nu}(k,-q,-p,m_a,m_t,m_a,m_\chi) - D_{\mu\nu}(-k',-q,-p,m_a,m_t,m_a,m_\chi)\right]
\end{aligned}
$$

$$
\begin{aligned}
&+ m_\chi^2 m_t (c_{\chi\chi}^A)^2 \left((c_{tu}^V)^2 - (c_{tu}^A)^2\right) [\overline{\chi}(p')\gamma^\mu \chi(p)] [\overline{u}(k')u(k)] [-2C_\mu(q,p,m_a,m_a,m_\chi) \\
&+ m_t^2 D_\mu(k,-q,-p,m_a,m_t,m_a,m_\chi) + m_t^2 D_\mu(-k',-q,-p,m_a,m_t,m_a,m_\chi)] \\
&+ m_\chi m_t^2 (c_{\chi\chi}^A)^2 \left((c_{tu}^V)^2 + (c_{tu}^A)^2\right) [\overline{\chi}(p')\chi(p)] [\overline{u}(k')\gamma^\nu u(k)] C_\nu(k,-q,m_a,m_t,m_a) \\
&+ m_\chi m_t (c_{\chi\chi}^A)^2 \left((c_{tu}^V)^2 - (c_{tu}^A)^2\right) [\overline{\chi}(p')\chi(p)] [\overline{u}(k')u(k)] [B_0(q,m_a,m_a) \\
&+ m_t^2 C_0(k,-q,m_a,m_t,m_a)] \,. \qquad (3.46)
\end{aligned}
$$

Even though there are only four terms left, reducing the rank-two and rank-one four-point functions give long and complex expressions. It would, therefore, be good to rank and at the same time approximate each term, and eventually only using the dominant terms. We know that $k^2 \ll m_t^2$, so the propagator-factor $\left[(\ell+k)^2 - m_t^2\right]$ can be expanded in k^2/m_t^2:

$$
\frac{1}{(\ell+k)^2 - m_t^2} = \frac{1}{\ell^2 - m_t^2} \frac{1}{1 + \frac{2k\cdot\ell + k^2}{\ell^2 - m_t^2}} \approx \frac{1}{\ell^2 - m_t^2} \left[1 - \frac{k^2 + 2k\cdot\ell}{\ell^2 - m_t^2} + \cdots\right], \qquad (3.47)
$$

and similarly for the propagator involving k'.

In Section B.2.2 we have gone through the procedure for each term in Eq. (3.46) that is dependent on k, k'. The first term in Eq. (3.46) involving the rank-two four-point functions is proportional to the up-quark momenta. Hence, this term is suppressed by the momenta k and k'. Using packages like `FeynCalc` one can verify that the pre-factor of this term, $m_\chi^2 m_t^2$, is cancelled by the denominator after reducing the four-point tensor integrals.

The second term in Eq. (3.46) is not proportional to any small masses or momenta after performing the approximation. Together with its pre-factor in the integral, this term's pre-factor scales with $m_\chi m_t$ and the scalar N-point functions are not suppressed by any momentum or mass.

The third term in Eq. (3.46) is small and at leading-order in $\frac{m_t}{m_u}$, it is zero, because after performing the approximation (i.e. the expansion of the top propagator in Eq. (3.47)) the rank-one three-point function is proportional to q_ν. After contracting with the DM vector-current it gives $[\overline{u}\not{q}u]$, which is shown to be zero.

The last term in the integral has the prefactor $m_\chi m_t$ and the expansion of the propagator does not gain or lose any power of m_χ or m_t, meaning that the order in mass dimension remains the same.

To summarize, the second and last term in Eq. (3.46) are of the same order in DM-mass and top-mass, while the third term's contribution is zero in leading-order approximation and the first term is suppressed by the up-quark momenta. Hence, the second and fourth term are at leading order the leading terms in Eq. (3.46) and the other terms can be discarded.

With the same reasoning as for discarding the axial-vector and pseudo-scalar structure, we can approximate our integral by setting the momentum transfer to zero. This is only justifyable if $m_a^2 \not\ll q^2$, which is alright since Kaon decays strongly constrain the light ALPs with FCNC. This is the last approximation that we do, which makes the resulting approximation of the one-loop integral only dependent on the DM momentum. The highest order and only N-point function that our integral is dependent on, is then the two-point function and its derivative with respect to m_a^2. Since the scalar two-point function is dependent on only the square of the momentum (see Eq. (3.35)), the DM-momentum can be replaced by the DM-mass, because of the on-shell assumption.

After these approximations, the reduction of the integrals and contraction of momenta, the final form of our one-loop integral is (using the expansions derived in Section B.2.2)

$$\begin{aligned}\mathcal{I} \approx & \frac{im_\chi m_t}{64\pi^2(m_t^2-m_a^2)^2 f_a^4}(c_{\chi\chi}^A)^2\left((c_{tu}^V)^2-(c_{tu}^A)^2\right)[\overline{\chi}(p')\chi(p)]\,[\overline{u}(k')u(k)] \\ & \times\Big[m_a^2\left(m_a^2-2m_t^2\right)B_0(m_\chi,m_a,m_\chi)+m_t^4 B_0(m_\chi,m_t,m_\chi) \\ & -m_a^4(m_t^2-m_a^2)\frac{d}{dm_a^2}B_0(m_\chi,m_a,m_\chi)\Big]\,.\end{aligned} \tag{3.48}$$

With this result, we now have an analytical expression of the dominant parts of the loop integral of the diagrams in Fig. 3.3, where the analytical expressions of the scalar two-point function and its derivative with respect to m_a^2 are given by Eqs. (3.35) and (3.41), respectively.

Note that when $(c_{tu}^V)^2=(c_{tu}^A)^2$, this approximation of the integral is zero. If the couplings are equal, the first and third terms in Eq. (3.46) are the leading order terms, which are momentum suppressed and zero at leading order, respectively. In that case, the diagrams in Fig. 3.3 are heavily suppressed by the up-mass and the up-quark momenta k, k'.

3.3.4 Limiting Cases

It is good to look at the behavior of the integral in some limiting cases. In Eq. (3.48) the expression is divided by $(m_t^2-m_a^2)^2$, which means it has a potential pole where $m_a=m_t$. If there is a pole at the top-mass, this would prove there is no such interaction taking place, because the cross section would also diverge and experments would have already seen such an interaction in their detectors. Although the original expression of the integrals in Eqs. (3.19) and (3.20) did not give any reason to have a pole where the top quark and ALP-masses are equal, it is good to check that no artificial pole is created after the PV-reduction. All together the limiting cases that are studied are the heavy ALP and DM limits, massless ALP and DM limits, and the $m_a=m_t$ limit. In Appendix B.3 the limiting cases have been derived more thoroughly, in this subsection we will go through the procedure, results and their implications.

In the massless ALP limit we expect there not to be any problems, because the ALP-mass is only present in the denominator of Eqs. (3.19) and (3.20). A massless ALP-mediator would also not cause the integral to be zero, i.e. no interaction. It suffices to show that no extra divergences arise in the ALP-mass dependent two-point functions when the ALP is massless, because then these terms are zero due to the pre-factor m_a^2. The factor $r_{a\chi}$ is finite and nonzero when $m_a\to 0$, so the logarithm is finite and so is $1/r_{a\chi}$. Substituting this into the expression of the two-point function $B_0(m_\chi,m_a,m_\chi)$, this function remains finite, meaning that when multiplied by m_a^2 the whole term is zero. Using that $r_{a\chi}$ remains finite and is nonzero, then taking the limit of $m_a^2\frac{d}{m_a^2}B_0(m_\chi,m_a,m_\chi)$ shows that it remains finite in the massless ALP limit. Since the ALP-mass dependent terms are zero, the only term that remains is the ALP-mass independent two-point function $B_0(m_\chi,m_t,m_\chi)$. Although it is enough to know the behavior, we have an exact expression for this limit:

$$\lim_{m_a\to 0}\mathcal{I}=\frac{im_\chi m_t}{64\pi^2 f_a^4}(c_{\chi\chi}^A)^2\left((c_{tu}^V)^2-(c_{tu}^A)^2\right)[\overline{\chi}(p')\chi(p)]\,[\overline{u}(k')u(k)]\,B_0(m_\chi,m_t,m_\chi). \tag{3.49}$$

From this we can conclude that for low ALP-masses or massless ALPs the integral (and also the cross section) is nonzero and constant as a function of the ALP-mass.

To study the behavior of the integral when ALPs are heavy, requires us to take the limit $m_a\to\infty$, i.e. the ALP is heavier than all other scales in $\mathcal{I}$. In this limit $r_{a\chi}=m_a/m_\chi$ and $m_a\frac{dr_{a\chi}}{dm_a}=m_a/m_\chi$. The ALP-mass independent two-point function is constant, and because of

the pre-factor of m_a^{-4}, this term is zero in the heavy ALP limit. This factor of m_a^{-4} cancels with the pre-factor of the ALP-mass dependent two-point function terms and partially cancels the pre-factor of its derivative, where a factor of m_a^2 remains. Now dependencies are substituted in the expression of the two-point function and its derivative and the limits then are:

$$\lim_{m_a\to\infty} B_0(m_\chi, m_a, m_\chi) \propto -\log\frac{m_a^2}{\mu^2}, \tag{3.50}$$

$$\lim_{m_a\to\infty} m_a^2 \frac{d}{dm_a^2} B_0(m_\chi, m_a, m_\chi) = -1. \tag{3.51}$$

Since $\log m_a$ is much larger in the limit than $-\frac{1}{2}$, this constant can be neglected as an overall dependence. Hence, the proportionality of the integral in the heavy ALP limit is $\mathcal{I} \propto -\log m_a$ and is thus log-divergent. Eventually $\mathcal{I}$ only appears squared, and therefore the minus-sign is not important for the cross section.

It turns out the supposed pole at $m_a = m_t$ is not a real pole, since the diverging denominator is cancelled by the PV-part of $\mathcal{I}$. To see this, first note that at first $\mathcal{I}$ takes the form $\frac{0}{0}$ in the limit. Then using L'Hôpital's rule to evaluate the limit and simplifying, gives

$$\begin{aligned}\lim_{m_a\to m_t} \mathcal{I} \approx \lim_{m_a\to m_t} \frac{im_\chi m_t}{64\pi^2 f_a^4}(c_{\chi\chi}^A)^2 \left((c_{tu}^V)^2 - (c_{tu}^A)^2\right) [\overline{\chi}(p')\chi(p)]\,[\overline{u}(k')u(k)] \\ \times \left[B_0(m_\chi, m_a, m_\chi) + 2m_a^2\frac{d}{m_a^2}B_0(m_\chi, m_a, m_\chi) + \frac{1}{2}m_t^4\frac{d^2}{d(m_a^2)^2}B_0(m_\chi, m_a, m_\chi)\right].\end{aligned} \tag{3.52}$$

All terms in this expression are finite when $m_a = m_t$. Hence, the integral does not diverge where the ALP-mass is equal to the top-mass.

Going through similar steps for heavy and massless DM, gives the following limiting behavior:

$$\lim_{m_\chi\to 0} \mathcal{I} = m_\chi \to 0 \tag{3.53}$$

$$\lim_{m_\chi\to\infty} \mathcal{I} \propto m_\chi \log\frac{m_\chi^2}{\mu^2} \tag{3.54}$$

Hence, no interaction takes place when the DM particle is massless, as expected. If the DM-mass is very small, the cross section is proportional to $m_\chi^2 \log\frac{(m_\chi)^2}{\mu^2}^2$. This means that for small DM-masses the cross section decreases even faster. Heavy DM seems, therefore, more favorable, since the cross section would be large enough measure scattering events. In the heavy ALP limit the same proportionality is obtained as for the massless DM limit. This shows that the cross section grows faster with the DM-mass than the ALP-mass.

Although heavy ALPs and DM particles seem to be favorable, but purely guided by proportionality it is more favorable to have heavy DM. It is favorable, because then the cross section would be much larger than for light masses. For the ALP there is a lower limit on the magnitude of $\mathcal{I}$, since it is constant and nonzero when in the massless ALP limit. In the worst case the ALP is massless, but for heavy DM it still grows with $m_\chi \log m_\chi$. If DM has a low mass, then $\mathcal{I}$ becomes very small, but even for heavy ALPs it only grows with $\log m_a$, which may not be enough to 'cancel' the low mass effect of DM.

3.4 UV-Divergences

The one-loop integrals in Eqs. (3.19) and (3.20) have at most six powers of integration momentum in the numerator ($P = 6$), and these integrals both have four propagator-factors in the numerator

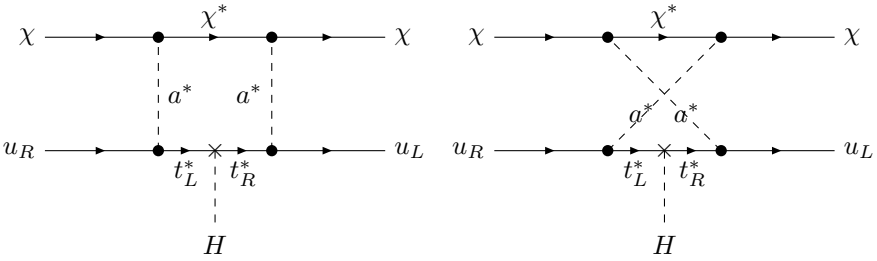

Figure 3.5: Diagrams that renormalizes the UV-divergence of the loop-diagrams in Fig. 3.3, where H is the Higgs boson.

($N = 4$). In four dimensions ($D = 4$), the equation from Section 3.3.2 tells us that this integral is UV-divergent: $P + D - 2N = 2 \geq 0$. A quick look at Eqs. (3.48) and (B.4) tells us already that the integral *is* divergent. Although most divergences cancel, e.g. the divergences of the $C_{\mu\nu}$ integrals, there is one divergence that does not cancel: the divergent part of the scalar two-point function B_0. From Section 3.3.2 we see–from either Eq. (3.35) or Eq. (3.43b)–that the divergent part of the scalar two-point function is $\frac{-2}{D-4}$. Then the divergent part of the total loop integral is

$$\frac{D-4}{2}\mathcal{I}^{\text{UV-div}} = \frac{-i}{64\pi^2 f_a^4} m_\chi (c^A_{\chi\chi})^2 \left((m_t - m_u)(c^V_{tu})^2 - (m_t + m_u)(c^A_{tu})^2\right) [\overline{\chi}(p')\chi(p)] \, [\overline{u}(k')u(k)] \,. \tag{3.55}$$

On the quark part in Fig. 3.3, the chirality has to flip from left to right or vice versa. It is more obvious looking at Eq. (3.3), and we see that the Higgs causes a flip in chirality for the quarks. The operator that will renormalize our amplitude is $(\overline{\chi}\chi)\left(\overline{Q}\boldsymbol{C}\boldsymbol{Y}_u\boldsymbol{C}\tilde{\phi}u_R\right)$, for some couplings $\boldsymbol{C}$ and up-type Yukwawa matrices $\boldsymbol{Y}_u$. In our diagrams the only couplings are $\boldsymbol{C}_{31}$ and $\boldsymbol{C}_{13}$, that results in having $\boldsymbol{Y}_{33}$, which is the top-Yukawa coupling. Having the top-Yukawa coupling in the operator means that the Higgs couples to the top. Hence, the Higgs is inserted in the top-propagator and we set the reference scale $\mu = m_t$. The resulting diagrams are given in Fig. 3.5.

3.5 Evolution of the Couplings

At this moment the couplings are evaluated at the scale Λ, which we set to be 4π TeV. The goal is to obtain a cross section in the NR regime, which is at the energy scale of the momentum transfer $|\mathbf{q}| \ll \Lambda$. There are several scales in our diagrams that have to be taken into account. In Fig. 3.6 these different energy scales and the valid diagram at each scale is shown for a particular mass hierarchy. Between these scales, the amplitude for χ-u scattering can be calculated using the diagrams in Fig. 3.3. The difference between the diagrams at the two scales is the value of the couplings and can be seen in Fig. 3.6. As we will see, the couplings are dependent on the energy scale they are evaluated at. So at the cutoff scale the couplings are $c^{A,V}_{tu}(\Lambda)$, while at the top-mass the couplings are different, namely $c^{A,V}_{tu}(m_t)$. Below the top-mass the top-quark is integrated out of the theory and the top-propagator is pinched to a point, i.e. no longer present in the diagram.

If we follow the mass hierarchy in Fig. 3.6, the DM particle is integrated out next. Between the DM-mass and top-mass scales, the second diagram from above in Fig. 3.6 is our new diagram.

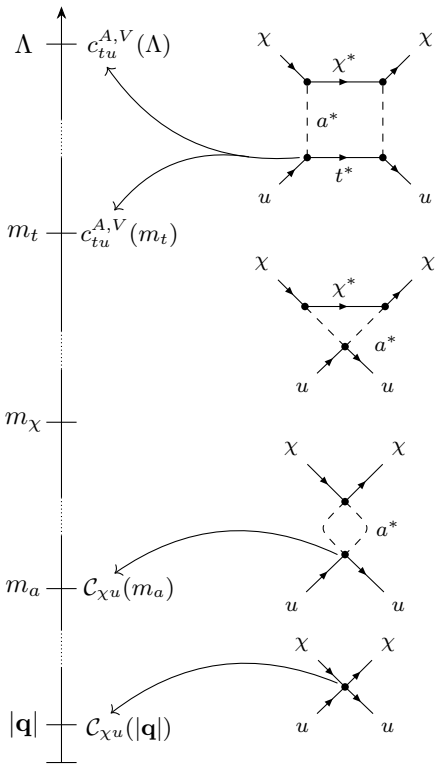

Figure 3.6: Example of separation of energy scales for the renormalization-group equations and the diagrams that correspond to this energy scale.

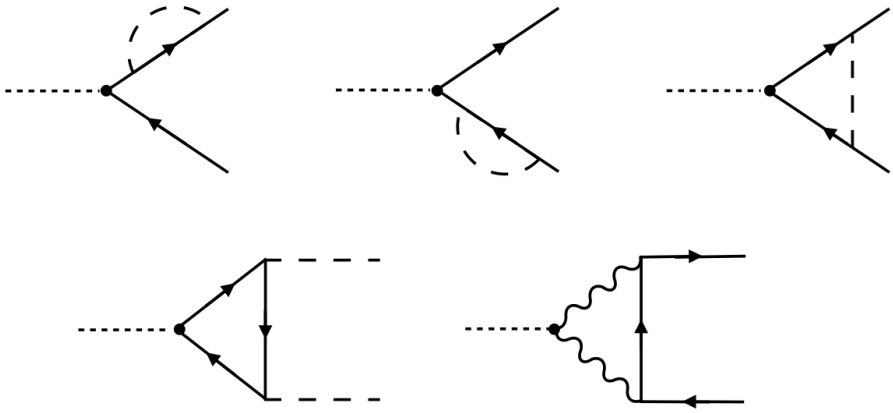

Figure 3.7: One-loop diagrams accounting for operator mixing through Yukawa and gauge interactions, contributing to the RGEs. [40]

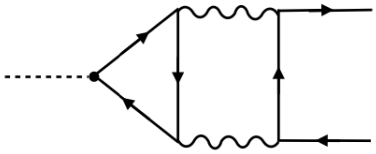

Figure 3.8: Two-loop diagram contributing to the RGEs. [40]

When χ is integrated out, we are in the region between m_a and m_χ, where the third diagram in Fig. 3.6 is the new valid diagram. At the scale of m_a, the effective coupling $C_{\chi u}(m_a)$ is dependent on our original couplings $c_{tu}^{A,V}$ and on the energy scale it is evaluated at.

To go down to the energy scale of the momentum transfer, that is on the keV scale, it is the ALP's turn to be integrated out. The diagram that is left is a vertex connecting four external lines, that has an effective coupling $\mathcal{C}_{\chi u}(|\mathbf{q}|)$, as can be seen in Fig. 3.6. This is the effective coupling that is measured by experiments.

Using the renormalization-group equations (RGEs) the couplings can be evolved from the cutoff down to top-mass scale, and furhter down to lower energy scales. Apart from assuming the ALP is massive, we also assume that the m_a is of order m_t or less, but let us not assume anything about m_χ. The Wilson coefficients (i.e. couplings) and operators in the effective Lagrangian can be evolved down to the top-mass by solving the RGEs.

Let us start with the evolution from the cutoff scale to the top-quark mass scale. This procedure has been derived in [40]. We will go through the steps from [40] below, and we then derive the evolution of the vector and axial-vector couplings used in our calculations.

At one-loop order there are contributions to the running of the fermion Wilson coefficients from Yukawa interactions. These diagrams are given in Fig. 3.7. In general the multiplicative renormalization effects from the first two diagrams are not diagonal in generation space. The third diagram leads to mixing of $SU(2)_L$ singlet and doublet coefficients $\boldsymbol{c}_Q$ and $\boldsymbol{c}_{u,d}$. In addition, the last diagram shows that there is also mixing between the Wilson coefficients of the ALP-boson interactions, c_{VV} and the coefficients $\boldsymbol{c}_F$. These terms *are* diagonal in generation space.

There are additional generation-independent contributions to the RGEs at two-loop order in gauge interactions that are proportional to the ALP-fermion couplings. Corrections from this type are shown in Fig. 3.8 and are diagonal in generation space. Altogether, this gives rise to the following evolution equations of the singlet and doublet Wilson coefficients for the quarks, respectively,

$$\begin{aligned}\frac{d}{d\ln\mu}\boldsymbol{c}_Q(\mu) =& \frac{1}{32\pi^2}\left\{\boldsymbol{Y}_u\boldsymbol{Y}_u^\dagger + \boldsymbol{Y}_d\boldsymbol{Y}_d^\dagger, \boldsymbol{c}_Q\right\} - \frac{1}{16\pi^2}\left(\boldsymbol{Y}_u\boldsymbol{c}_u\boldsymbol{Y}_u^\dagger + \boldsymbol{Y}_d\boldsymbol{c}_d\boldsymbol{Y}_d\right)\\ &+ \left[\frac{\beta_Q}{8\pi^2}X - \frac{3\alpha_s^2}{4\pi^2}C_F^{(3)}\tilde{c}_{GG} - \frac{3\alpha_2^2}{4\pi^2}C_F^{(3)}\tilde{c}_{WW} - \frac{3\alpha_1^2}{4\pi^2}\mathcal{Y}_q^2\tilde{c}_{BB}\right]\mathbb{1},\end{aligned} \tag{3.56}$$

$$\begin{aligned}\frac{d}{d\ln\mu}\boldsymbol{c}_q(\mu) =& \frac{1}{16\pi^2}\left\{\boldsymbol{Y}_q\boldsymbol{Y}_q^\dagger, \boldsymbol{c}_q\right\} - \frac{1}{8\pi^2}\boldsymbol{Y}_q^\dagger\boldsymbol{c}_Q\boldsymbol{Y}_q + \left[\frac{\beta_q}{8\pi^2}X + \frac{3\alpha_s^2}{4\pi^2}C_F^{(3)}\tilde{c}_{GG}\right.\\ &\left.+\frac{3\alpha_1^2}{4\pi^2}\mathcal{Y}_q^2\tilde{c}_{BB}\right]\mathbb{1},\end{aligned} \tag{3.57}$$

where $C_F^{(N)} = \frac{N^2-1}{2N}$ is the eigenvalue of the quadratic Casimir operator in the fundamental representation of $SU(N)$, $\mathcal{Y}_q$ denotes the hypercharge of the SM quarks, and

$$X = \mathrm{Tr}\left[3\boldsymbol{c}_Q\left(\boldsymbol{Y}_u\boldsymbol{Y}_u^\dagger - \boldsymbol{Y}_d\boldsymbol{Y}_d^\dagger\right) - 3\boldsymbol{c}_u\boldsymbol{Y}_u^\dagger\boldsymbol{Y}_u + 3\boldsymbol{c}_d\boldsymbol{Y}_d^\dagger\boldsymbol{Y}_d - 3\boldsymbol{c}_L\boldsymbol{Y}_e\boldsymbol{Y}_e^\dagger + 3\boldsymbol{c}_e\boldsymbol{Y}_e^\dagger\boldsymbol{Y}_e\right]. \tag{3.58}$$

Eqs. (3.56) to (3.58) are a set of coupled differential equations, that can be simplified by means of bi-unitary transformations. The SM Yukawa matrices are diagonalized as follows,

$$\boldsymbol{U}_u^\dagger\boldsymbol{Y}_u\boldsymbol{W}_u = \boldsymbol{Y}_u^{\mathrm{diag}} = \mathrm{diag}\left(y_u, y_c, y_t\right), \tag{3.59a}$$

$$\boldsymbol{U}_d^\dagger\boldsymbol{Y}_d\boldsymbol{W}_d = \boldsymbol{Y}_d^{\mathrm{diag}} = \mathrm{diag}\left(y_d, y_s, y_b\right). \tag{3.59b}$$

When we redefine the fermion field by

$$Q \to \boldsymbol{U}_u Q, \quad u_R \to \boldsymbol{W}_u u_R \quad \text{and} \quad d_R \to \boldsymbol{W}_d, \tag{3.60}$$

the up Yukawa matrix is diagonalized, while the down Yukawa matrix is transformed into

$$\boldsymbol{Y}_d \to \boldsymbol{U}_u^\dagger\boldsymbol{Y}_d\boldsymbol{W}_d = \boldsymbol{V}\boldsymbol{Y}_d^{\mathrm{diag}}. \tag{3.61}$$

Here, $\boldsymbol{V} = \boldsymbol{U}_u^\dagger\boldsymbol{U}_d$ is the CKM matrix. The top-quark is much heavier than other SM particles, so it is a good approximation to neglect all Yukawa couplings other than y_t. For our purpose, we only look at the off-diagonal couplings. After field redefinitions, the RGE for off-diagonal couplings, with $(i \neq j)$, is

$$\frac{d}{d\ln\mu}\left[c_Q(\mu)\right]_{ij} = \frac{y_t^2}{32\pi^2}\left(\delta_{i3} + \delta_{j3}\right)\left[c_Q\right]_{ij}, \tag{3.62}$$

$$\frac{d}{d\ln\mu}\left[c_u(\mu)\right]_{ij} = \frac{y_t^2}{16\pi^2}\left(\delta_{i3} + \delta_{j3}\right)\left[c_u\right]_{ij}. \tag{3.63}$$

$$\tag{3.64}$$

These equations are not coupled anymore and can be solved quite easily. The general solution to the evolution equations of the off-diagonal up-type quark-ALP couplings down to the top-mass are given by

$$\left[c_Q(m_t)\right]_{ij} = e^{-(\delta_{i3}+\delta_{j3})U(m_t,f_a)}\left[c_Q(\Lambda)\right]_{ij}, \tag{3.65}$$

$$[c_u(m_t)]_{ij} = e^{-2(\delta_{i3}+\delta_{j3})U(m_t,f_a)}\,[c_u(\Lambda)]_{ij}\,, \tag{3.66}$$

where

$$U(\mu,\Lambda) = -\int_\Lambda^\mu \frac{d\mu'}{\mu}\frac{\alpha_t^2(\mu')}{8\pi}, \tag{3.67}$$

with $\alpha_t = y_t^2/(4\pi)$. The top-quark Yukawa and the strong coupling follow a set of coupled differential equations

$$\frac{d\alpha_s(\mu)}{d\ln\mu} = -\frac{7\alpha_s^2(\mu)}{2\pi} \quad \text{and} \quad \frac{d\alpha_t(\mu)}{d\ln\mu} = \frac{\alpha_t(\mu)}{2\pi}\left[\frac{9}{2}\alpha_t(\mu) - 8\alpha_s(\mu)\right]. \tag{3.68}$$

Here, small effects from the weak interaction are ignored. In the solution of this set of coupled diffeential equations, the running of $\alpha_t(\mu)$ tracks the running of $\alpha_s(\mu)$. With reference scale μ_0, one finds

$$\frac{\alpha_t(\mu)}{\alpha_t(\mu_0)} = \left(\frac{\alpha_s(\mu)}{\alpha_s(\mu_0)}\right)^{8/7}\left[1+\frac{9}{2}\frac{\alpha_t(\mu_0)}{\alpha_s(\mu_0)}\left[\left(\frac{\alpha_s(\mu)}{\alpha_s(\mu_0)}\right)^{1/7}-1\right]\right]^{-1}. \tag{3.69}$$

Using the exact expression for the top-quark Yukawa coupling, the integral solution to the integral in Eq. (3.67) can be solved and gives

$$U(\mu,\Lambda) = -\frac{1}{18}\log\left(1-\frac{9}{2}\frac{\alpha_t(\mu)}{\alpha_s(\mu)}\left[1-\left(\frac{\alpha_s(\Lambda)}{\alpha_s(\mu)}\right)^{1/7}\right]\right). \tag{3.70}$$

In our calculations we are not working with these flavor couplings $\boldsymbol{c}_F$. Rather, we work with a vector and an axial-vector coupling, which in turn depend on couplings from the Lagrangian in the mass basis, $\boldsymbol{k}_F$, as in [50]. The transformation relating $\boldsymbol{c}_F$ and $\boldsymbol{k}_F$ given in Section 3.1, makes that the evolution for the up-type quark couplings $\boldsymbol{c}_F$ and $\boldsymbol{k}_F$ is equal. Using our definitions in Eq. (3.9) and the solutions to the RGEs, one finds the evolution of the vector and axial-vector couplings to be

$$c_{tu}^V(\mu) = \xi(\mu)\left(\xi(\mu)\,[k_u(\Lambda)]_{tu} + [k_U(\Lambda)]_{tu}\right), \tag{3.71}$$

$$c_{tu}^A(\mu) = \xi(\mu)\left(\xi(\mu)\,[k_u(\Lambda)]_{tu} - [k_U(\Lambda)]_{tu}\right), \tag{3.72}$$

with

$$\xi(\mu) = \left(1-\frac{9}{2}\frac{\alpha_t(\mu)}{\alpha_s(\mu)}\left[1-\left(\frac{\alpha_s(\Lambda)}{\alpha_s(\mu)}\right)^{1/7}\right]\right)^{\frac{1}{18}}. \tag{3.73}$$

In the loop integral the couplings are in the combination $(c_{tu}^V)^2 - (c_{tu}^A)^2$, which means that

$$\left(c_{tu}^V(\mu) - c_{tu}^A(\mu)\right)\left(c_{tu}^V(\mu) + c_{tu}^A(\mu)\right) = 4\xi^3(\mu)\,[k_u(\Lambda)]_{tu}\,[k_U(\Lambda)]_{tu}\,. \tag{3.74}$$

For convenience, we take $(c_{tu}^V)^2 - (c_{tu}^A)^2 = 1$ at Λ. Assuming $c_{tu}^A = a$, gives $c_{tu}^V = \pm\sqrt{a^2+1}$. At Λ we obtain that $[k_u(\Lambda)]_{tu} = \frac{a\pm\sqrt{a^2+1}}{2}$ and $[k_U(\Lambda)]_{tu} = -\frac{a\mp\sqrt{a^2+1}}{2}$, from which follows that

$$(c_{tu}^V(\mu))^2 - (c_{tu}^A(\mu))^2 = \xi^3(\mu). \tag{3.75}$$

For simplicity, we will neglect the RGE below the top-mass.

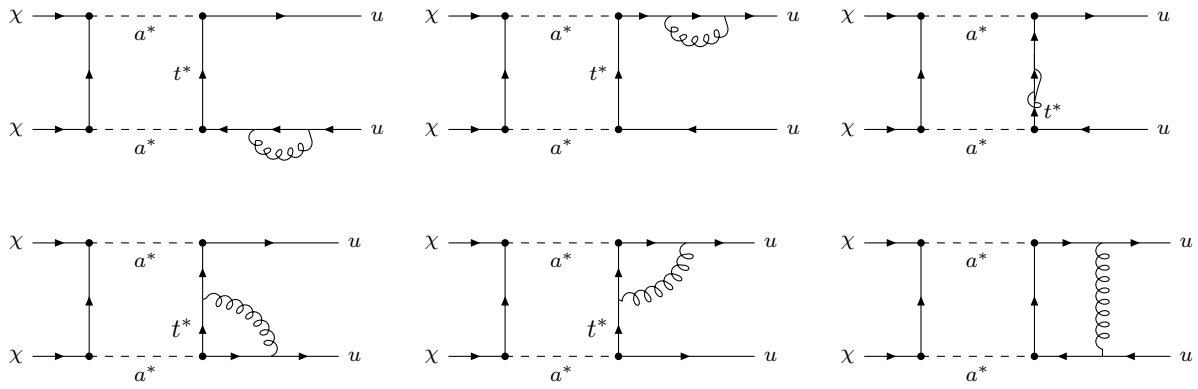

Figure 3.9: Two-loop diagrams contributing the RGEs.

3.6 Bounds on the Couplings

Up until now the couplings have (to some extent) arbitrary values. For cross section predictions and comparison to experimental results and projections, it would be good to try to constrain the couplings as much as we can. An upper bound for the couplings will in turn give an upper bound for the cross section. These upper bounds will give more realistic predictions to compare to experiments, but also help to make modeling choices. Namely, if the bounds are too large or strong for certain ALP-masses, detecting scattering events for these masses may be impossible with current detectors.

It was found in [62] that stringent bounds on the top couplings to the ALP are obtained from virtual corrections in low-energy observables. Radiative Yukawa corrections from the top-ALP coupling at the cutoff scale Λ give sizable contributions to flavor-changing down-quark couplings as well, because of the large mass of the top-quark. Assuming diagonal couplings are zero and only including the top-up coupling, the radiative corrections to the coupling $c^V_{d_i d_j}$ are [62]

$$\Delta c^V_{d_i d_j}(\mu) = -\frac{y_t^2}{64\pi^2}\log\frac{f_a}{\mu}\left[V^*_{ud_i}V_{td_j} + V^*_{td_i}V_{ud_j}\right]\left(c^V_{tu}(\Lambda) - c^A_{tu}(\Lambda)\right). \tag{3.76}$$

The total coupling at energy scale μ is $c_{ij}(\mu) = \Delta c_{ij}(\mu) + c_{ij}(\Lambda)$. Stringent constraints on c_{tu} are obtained by assuming that $\Delta c_{d_i d_j}(\mu) \gg c_{d_i d_j}(\Lambda)$. If this cannot be assumed, it means that the coupling $c_{ij}(\Lambda)$ is on the same order or larger than the radiative corrections. Thus, the constraints on c_{tu} due to radiative corrections $\Delta c_{d_i d_j}$ are not stringent constraints since there could be accidental cancellation between $\Delta c_{d_i d_j}$ and $c_{d_i d_j}(\Lambda)$, but depending on the size of the corrections it may be stringent enough to exclude or include regions for different ALP-masses. Let us define $F^{V,A}_{ij} = 2f_a/c_{ij}$, such that

$$\frac{2f_a}{c^V_{tu}(\Lambda) - c^A_{tu}(\Lambda)} = -\frac{y_t^2}{64\pi^2}\log\frac{\Lambda}{\mu}\left[V^*_{ud_i}V_{td_j} + V^*_{td_i}V_{ud_j}\right]F^V_{d_i d_j}(\mu). \tag{3.77}$$

The couplings appear in Eq. (3.48) as $((c^V_{tu})^2 - (c^A_{tu})^2)/f_a^2$, so the equation above gives part of this expression. By multiplying by $2f_a/(c^V_{tu}(\Lambda) + c^A_{tu}(\Lambda))$, the couplings appear in the right form. Constraining the difference of the couplings, also constrains the sum of the coulings to some extent.

To constrain the top-up-ALP couplings, $F^V_{d_i d_j}$ must be constrained first. For this we will discuss three meson decay processes: $B^\pm \to K^\pm a$, $B^\pm \to \pi^\pm a$ and $K^\pm \to \pi^\pm a$. B-decays are

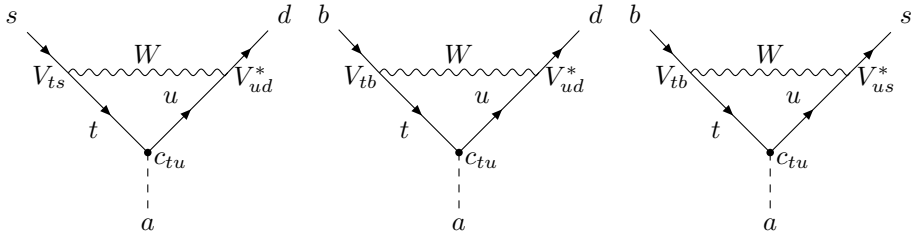

Figure 3.10: Decay processes of $K^\pm \to \pi^\pm a$ (left), $B^\pm \to \pi^\pm a$ (middle) and $B^\pm \to K^\pm a$ (right). The corresponding CKM matrix elements and the up-top-ALP coupling, c_{tu}, are written down at each vertex.

valid for ALP-masses up to about 5 GeV/c^2 and Kaon-decay is valid up to about 250 MeV/c^2. The diagrams corresponding to these decays are given in Fig. 3.10, where one can see how the coupling c_{tu} is connected to these decays. Since the CKM matrix elements $V_{tb}, V_{ud} \sim 1$, $B^\pm \to \pi^\pm a$ is expected to give a more stringent constraint than $B^\pm \to K^\pm a$, which was–as far as we could find–first noticed by one of my supervisors Ahn Vu Phan. The production rate for an ALP from $B^\pm \to h^\pm a$ is [63]

$$\Gamma_{B^\pm \to h^\pm a} = \frac{m_B}{16\pi} \frac{1}{F_{d_j b}^2} \left(1 - \frac{m_h^2}{m_B^2}\right)^2 f_{0,B}^2(m_a^2) \lambda^{1/2}(m_B^2, m_h^2, m_a^2), \tag{3.78}$$

where $\lambda(x,y,z) = x^2 + y^2 + z^2 - 2(xy + xz + yz)$ is the kinematic function, and $h^\pm = K^\pm, \pi^\pm$ and $d_j = s, d$, respectively. The scalar form factor for the B-meson evaluated at the momentum transfer equal to the ALP-mass, $f_{0,B}(m_a)$, parameterizes hadronic effects in the decay of $B \to K$. Particle Data Group (PDG) provides the upper bound of the branching ratio $\mathcal{B}\left(B^\pm \to h^\pm X^0\right) < 4.9 \times 10^{-5}$, where X^0 is some uncharged unkown particle [61]. This data was obtained by the CLEO II experiment. Relating the production rate to the branching ratio by $\Gamma_{B^\pm \to h^\pm a} = \Gamma_{\text{tot},B} \mathcal{B}\left(B^\pm \to h^\pm X^0\right)$, we obtain an expression for $F_{d_j b}$

$$F_{d_j b} = \sqrt{\frac{m_B}{16\pi} \frac{f_{0,B}^2(m_a^2)}{\mathcal{B}(B^\pm \to h^\pm a)\Gamma_{\text{tot},B}} \left(1 - \frac{m_h^2}{m_B^2}\right)^2 \lambda^{1/2}(m_B^2, m_h^2, m_a^2)}. \tag{3.79}$$

Similarly, for the Kaon decay

$$F_{sd} = \sqrt{\frac{m_K}{16\pi} \frac{f_{0,K}^2(m_a^2)}{\mathcal{B}(K^\pm \to \pi^\pm a)\Gamma_{\text{tot},K}} \left(1 - \frac{m_\pi^2}{m_K^2}\right)^2 \lambda^{1/2}(m_K^2, m_\pi^2, m_a^2)}. \tag{3.80}$$

The NA62 collaboration has obtained estimates for an upper bound on the branching ratio for $K^\pm \to \pi^\pm X^0$. If we assume the ALP to have a long lifetime ($> 5ns$) the strongest limit on the branching ratio for ALP-masses of $150 - 250$ MeV/c^2 is $\mathcal{B}(K^\pm \to \pi^\pm a) < 5 \times 10^{-11}$ and for ALP-masses of $0 - 110$ MeV/c^2 is $\mathcal{B}(K^\pm \to \pi^\pm a) < 7 \times 10^{-11}$ [64]. For the mass range $110 - 150$ MeV/c^2, the SM background makes it hard to estimate an upper bound. Nevertheless, experiments have found an upper bound for the branching ratio of $K^\pm \to \pi^\pm \pi^0 \to \pi^\pm + \text{inv}$: $\mathcal{B}(K^\pm \to \pi^\pm \pi^0 \to \pi^\pm + \text{inv}) < 8.8 \times 10^{-10}$ [61].

The form factor of the Kaon is [65]

$$f_{0,K}(q^2) = f_+(0) \left(1 + \lambda_0' \frac{q^2}{m_\pi^2} + \frac{1}{2}\lambda_0'' \left(\frac{q^2}{m_\pi^2}\right)^2 + \frac{1}{6}\lambda_0''' \left(\frac{q^2}{m_\pi^2}\right)^3\right), \tag{3.81}$$

with $\lambda_0' = \frac{m_\pi^2}{q_{CT}^2}[\log C - 0.0398]$, $\lambda_0'' = (\lambda_0')^2 + 4.16\cdot 10^{-4}$, $\lambda_0''' = (\lambda_0')^3 + 4.16\cdot 10^{-4}\cdot(3\lambda_0') + 2.72\cdot 10^{-5}$ and $f_+(0) = 0.9709$. In these definitions $\log C = 0.1998$ and $q_{CT}^2 = m_K^2 - m_\pi^2$. Similarly, the form factor of the B-meson is [66]

$$f_{0,B}(q^2) = \frac{1}{1 - q^2/m_R^2} \sum_{k=0}^{2} \alpha \left(z\left(q^2\right) - z\left(0\right)\right)^k , \tag{3.82}$$

where $m_R = 5.540$ GeV/c^2 for $d_j = d$ and $m_R = 5.630$ GeV/c^2 is the resonance mass, $\alpha_0 = 0.21$,

$$\begin{aligned} z(t) &= \frac{\sqrt{t_+ - t} - \sqrt{t_+ - t_0}}{\sqrt{t_+ - t} + \sqrt{t_+ - t_0}}, \\ t_\pm &= \left(m_B \pm m_h\right)^2 , \\ t_0 &= t_+ \left(1 - \sqrt{1 - t_-/t_+}\right), \end{aligned} \tag{3.83}$$

and $q^2 \leq 5$ GeV^2. Then the bounds with $f_a = 1$ TeV and $\mu = m_t$ (we will see why in the next section), are

$K^\pm \to \pi^\pm a$: $\frac{2f_a}{c_{tu}^V(\Lambda) - c_{tu}^A(\Lambda)} > 1.5 \times 10^5$ TeV using F_{sd} for $m_a < 250$ MeV/c^2,

$B^\pm \to \pi^\pm a$: $\frac{2f_a}{c_{tu}^V(\Lambda) - c_{tu}^A(\Lambda)} > 3.8 \times 10^3$ TeV using F_{bd} for $m_a < 5$ GeV/c^2,

$B^\pm \to K^\pm a$: $\frac{2f_a}{c_{tu}^V(\Lambda) - c_{tu}^A(\Lambda)} > 0.8 \times 10^3$ TeV using F_{sb} for $m_a < 5$ GeV/c^2.

The implications of these strong bounds will be discussed in Section 3.7.

3.7 The Cross Section

Up to this point we have calculated the loop integral and simplified and approximated it as much as possible to obtain the leading order contributions to the integral, and we calculated bounds on the couplings and evolved the couplings from the cutoff scale Λ down to the scale of the top-mass. This gives us the tools to calculate the cross section. Our effective Lagrangian is of the following form

$$\mathcal{L}_{\text{eff}} = c_S(\mu)\overline{\chi}\chi\overline{u}u. \tag{3.84}$$

Here,

$$\begin{aligned} ic_S(\mu) = \frac{im_\chi m_t \xi^3(\mu)}{64\pi^2(m_t^2 - m_a^2)^2 f_a^4} (c_{\chi\chi}^A)^2 \Big[& m_a^2(m_a^2 - 2m_t^2) B_0(m_\chi, m_a, m_\chi) \\ & + m_t^4 B_0(m_\chi, m_t, m_\chi) - m_a^4(m_t^2 - m_a^2)\frac{d}{dm_a^2} B_0(m_\chi, m_a, m_\chi)\Big], \end{aligned} \tag{3.85}$$

is the Wilson coefficient of the scalar operator. Following the notation of [7], the scattering amplitude for nuclei with atomic number Z and mass number A, is

$$\mathcal{M} = [Zf_p + (A - Z)f_n]\,\overline{\chi}\chi\overline{n}nF(q), \tag{3.86}$$

where $F(q^2)$ is the nuclear form factor, n are the nucleus fields and $f_p(f_n)$ is the coupling of DM to the proton(neutron)

$$f_p = c_S \frac{m_p}{m_u} f_{T_u}^p \quad \text{and} \quad f_n = c_S \frac{m_n}{m_u} f_{T_u}^n . \tag{3.87}$$

The constants $f^p_{T_u} = 0.0149$ and $f^n_{T_u} = 0.0117$ [67], are the up-quark content of the proton and neutron, respectively. Taking the NR limit of the amplitude and dropping the relativistic normalization factors $2m_\chi$ and $2m_u$, we can now use Table 2.2 to write the amplitude in terms of the building blocks:

$$\mathcal{M}_{\text{NR}} = [Z f_p + (A - Z) f_n]\, F(q)\, \langle \mathcal{O}_1 \rangle \,. \tag{3.88}$$

Given the relation in Eq. (2.6), we obtain the DM-nucleon cross section:

$$\sigma_p = \frac{\mu_p^2}{\pi} \left[\frac{m_p}{m_u} \frac{Z}{A} f^p_{T_u} + \frac{m_n}{m_u} \left(1 - \frac{Z}{A}\right) f^n_{T_u} \right]^2 |c_S(q)|^2, \tag{3.89}$$

where we take $c_S(q) = c_S(m_t)$. This gives the tools to plot the cross section as a function of the ALP-mass and the DM-mass. The experiments we will include use Xenon, where a veriety of isotopes are inside the liquid Xenon. Because there is not only one isotope of Xenon, the abundances of the different isotopes has to be taken into account. For more details on this, see [68] around Eq. (40). Although it is more accurate to take into account the different abundances of the isotopes, we use $Z = 54$ and $A = 131.29$, for simplicity. We assume that $f_a = 1$ TeV and take $c^A_{\chi\chi} = 1$. In $\xi(m_t)$ the values for α_s are obtained and extrapolated from [69], and the Yukawa coupling of the top-quark is $y_t = 1.16$ [70].

Before looking at the cross section as a function of the DM-mass, let us take a look at the cross section versus the ALP-mass in Fig. 3.11. The cross section as a function of the ALP-mass is shown for a DM-mass of 40 GeV/c^2, because LZ is most sensitive in this region [71]. Here we see that for low ALP-masses, the cross section is deep inside the neutrino fog, because of the bounds presented in Section 3.6. Hence, it is far outside the measurable region of the search-space in current experiments. For masses above 5 GeV/c^2 there are no bounds yet on the couplings, so the couplings just take the form of $\xi^3(m_t)$ with $f_a = 1$ TeV. ALP-masses up to 70 GeV/c^2 and above 145 GeV/c^2 are excluded for this particular coupling strength, because the cross section lies withtin the excluded region of current results from LZ. When $c^A_{\chi\chi}, f_a$ and $c^{V,A}_{tu}$ are left constant, only by decreasing the DM-mass the cross section would be lowered for all ALP masses.

At a mass of approximately 108 GeV/c^2 the cross section becomes zero, because of an interplay between the scale μ, m_a and m_χ in the B_0-functions. When the scale μ is lowered appropriately, by using the RGEs from the top-mass down to the scale of the momentum $|\mathbf{q}|$, we expect the sharp dip to become narrower, until it vanishes and the curve is smooth. This means that also these masses are excluded by current experiments. Of course, the cutoff scale could be larger than 4π TeV or the couplings could be smaller than 1 at Λ, in turn lowering the curve and potentially not excluding some masses anymore. For example, if f_a would be twice as large, the cross section is 16 times smaller. Then, ALP-mediated DM is not excluded for a DM mass of 40 GeV/c^2.

The important knowledge to take away from Fig. 3.11, is that plots with results for ALP-masses around 100 GeV/c^2 are not reliable, but that the results will likely be on the same order as for masses further away from 100 GeV/c^2. Moreover, the bounds on the couplings lower the cross section by a lot, where the cross section is far outside the measurable regime and deep inside the neutrino fog.

Next we discuss the curves in Figs. 3.12 and 3.13, where we examine the behavior of the cutoff scale. In Fig. 3.12 the cross section is fixed at 5×10^{-48} cm^2 and $\frac{f_a^2}{c_{\chi\chi}\sqrt{(c^V_{tu})^2 - (c^A_{tu})^2}}$ is plotted as a function of the dark matter mass, for different values of the ALP-mass: 10, 50 and 150 GeV/c^2, Overall, as the DM-mass m_χ increases, the cutoff scale can also be larger or the couplings smaller. Changing the ALP-mass does not influence the size of the cutoff scale by

much, as they are all within one order of magnitude for different ALP-masses. If the couplings are approximately $\frac{f_a^2}{c_{\chi\chi}\sqrt{(c_{tu}^V)^2-(c_{tu}^A)^2}} = 1$ TeV^2, changing the ALP-mass only changes the cutoff scale by a maximum factor of $\sqrt{10}$ TeV.

Depending on the ALP-mass, there are points for some DM-mass where the cutoff scale could mathematically be zero and the cross section would remain the same. In a physical setting, having the cutoff scale at zero, does not make a lot of sense. Even though this makes mathematical sense, because if one rearranges terms in Eq. (3.89) one obtains

$$\begin{aligned}\sigma_p \left(\frac{f_a^4}{(c_{\chi\chi}^A)^2 \left((c_{tu}^V(m_t))^2 - (c_{tu}^A(m_t))^2 \right)} \right)^2 &= \frac{\mu_p^2}{\pi} \left[\frac{m_p}{m_u} \frac{Z}{A} f_{T_u}^p + \frac{m_n}{m_u} \left(1 - \frac{Z}{A} \right) f_{T_u}^n \right]^2 \\ &\times \Big| \frac{m_\chi m_t}{64\pi^2 (m_t^2 - m_a^2)^2} \Big[m_a^2 (m_a^2 - 2m_t^2) B_0(m_\chi, m_a, m_\chi) \\ &+ m_t^4 B_0(m_\chi, m_t, m_\chi) - m_a^4 (m_t^2 - m_a^2) \frac{d}{dm_a^2} B_0(m_\chi, m_a, m_\chi) \Big] \Big|^2 .\end{aligned} \tag{3.90}$$

If the right-hand side is zero, then so must the left-hand side. For these curves the same holds as for the curve in Fig. 3.11: we expect the dip to become narrower until the curve is smooth.

In Fig. 3.13 – instead of fixing the cross section and ALP-mass, and varying the DM-mass – we varied the cutoff scale and fixed the ALP and DM-masses. It is easy to verify if the behavior of the curve is correct when we look at the dependence of σ_p on f_a. A quick look at the figure tells us the cross section scales with f_a^{-8}, which we know to be correct. The range of the cross section is set to the region where our prediction is not excluded. If one needs a larger cutoff scale or smaller couplings, Fig. 3.13 favors heavy ALPs or heavy DM. At the same cutoff scale, the cross section for heavy DM ($\sim 100\text{GeV}/c^2$) is approximately one order of magnitude larger than for smaller DM masses (~ 40 GeV$/c^2$). Although the cross sections below $\sim 10^{-49}$ cm^2 are in the neutrino fog, for most regions of the search-space, one can still detect signals of DM with sufficient statistics.

Now, we finally look at the most important figure in this entire thesis: the spin-independent cross section–DM-mass search-space in Fig. 3.14. The DM-mass is unkown, so in order to decrease the size of the search-space it is important to rule out DM-masses in combination with a certain cross section. In Fig. 3.14 the current sensitivity results of the DarkSide-50, PandaX-4T, XENONnT and LZ are shown, as well as the projected sensitivity of LZ and XENONnT. Since no signal of DM has been detected in these experiments, this region of the search-space has been ruled out and is shaded gray. The neutrino fog is shaded blue and on top of the neutrino fog we added gray line that shows the boundary of the neutrino fog. The projected sensitivity of LZ already seems to be in the neutrino fog, but in a light-blue region where sufficient statistics help to decrease the background. The red lines show our prediction of the cross section from Eq. (3.89) for ALP-masses $m_a = 10, 50, 150$ GeV$/c^2$. For these curves we expect, similar to the other curves, when the couplings are evolved more properly down to $|\mathbf{q}|$, the dips to also become narrower, until the curves become smooth. Fig. 3.14 shows that for ALP-masses between $10 - 150$ GeV$/c^2$, all DM-masses above ≈ 20 GeV$/c^2$ are excluded by current results of LZ and XENONnT. Also, the cross section for DM-masses below 10 GeV$/c^2$ are all inside the neutrino fog, making it more difficult to detect, but this does not exclude these masses. The most promising region of the search-space for our prediction is where 10 GeV$/c^2 \leq m_\chi \leq 20$ GeV$/c^2$. If one would want to discover DM with a mass below 10 GeV$/c^2$ one would need to increase the sensitivity of current experiments by four or more orders of magnitude.

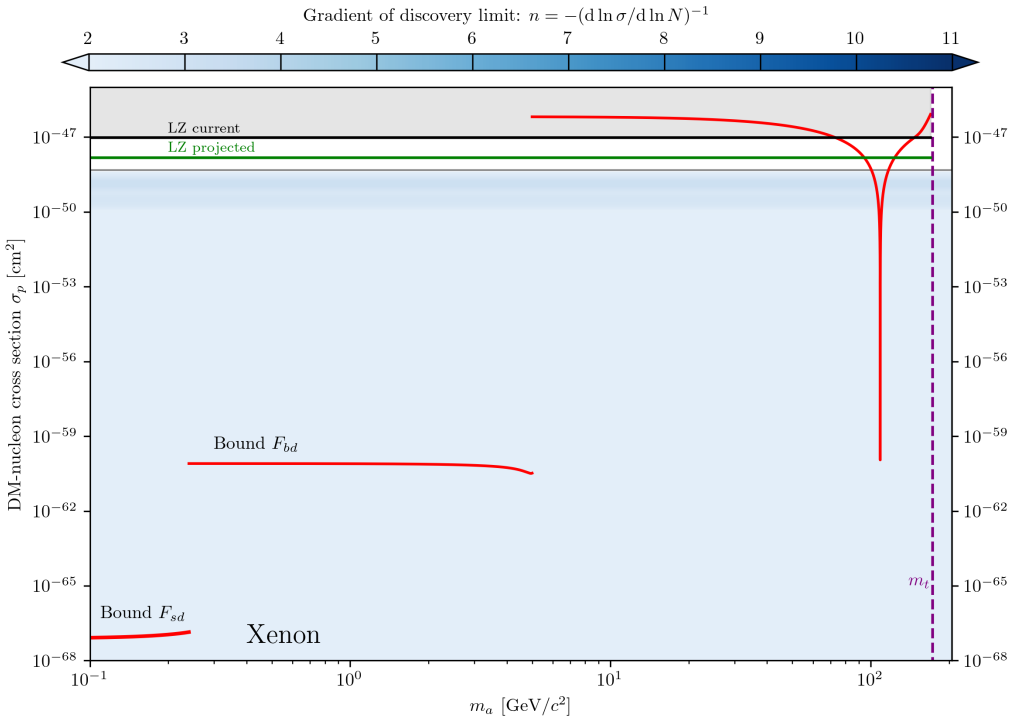

Figure 3.11: Nucleon cross section σ_p as a function of the ALP-mass (red) at $m_\chi = 40$ GeV/c^2. The region that is shaded gray is the excluded by the LZ experiment, which has the highest sensitivity of the experiments that are used in this work (see Fig. 3.14). The measured sensitivity [29] and projected sensitivity [71] at $m_\chi = 40$ GeV/c^2 are given in green and black, respectively. The purple dashed line is where the ALP-mass is equal to the top-mass m_t. The region shaded blue is the neutrino fog at $m_\chi = 40$ GeV/c^2.

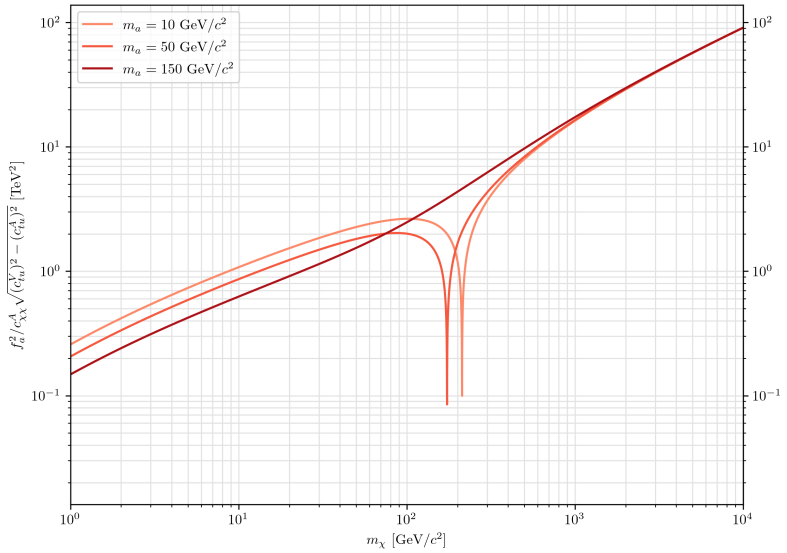

Figure 3.12: The cutoff scale and coupplings $f_a^2/c_{\chi\chi}^A\sqrt{(c_{tu}^V)^2-(c_{tu}^A)^2}$ at $\sigma_p = 5\times10^{-48}$ cm^2 as a function of the DM-mass m_χ, for different values of the ALP-mass.

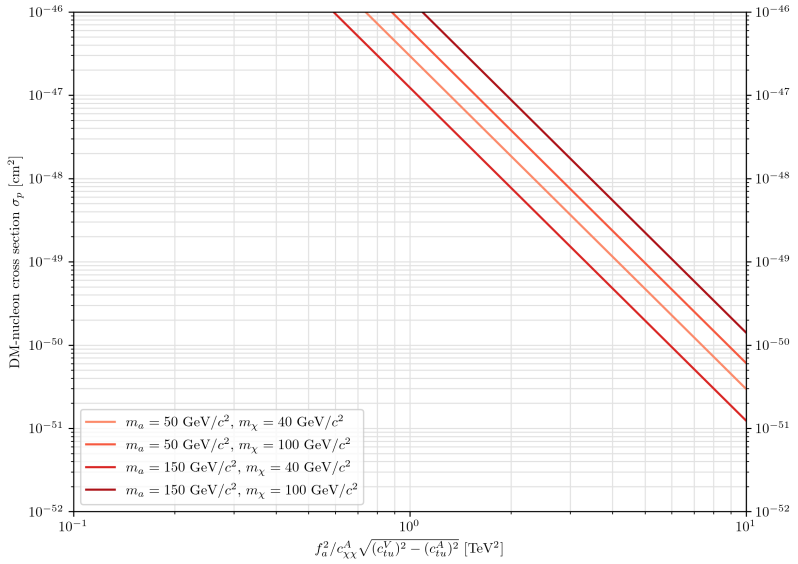

Figure 3.13: Nucleon cross section σ_p as a function of the cutoff scale and couplings $f_a^2/c_{\chi\chi}^A\sqrt{(c_{tu}^V)^2-(c_{tu}^A)^2}$ for different ALP and DM-masses. In this plot, regions of σ_p that are either excluded by experiments or too small to measure with current detectors or detectors in the near future for these DM-masses, are not shown.

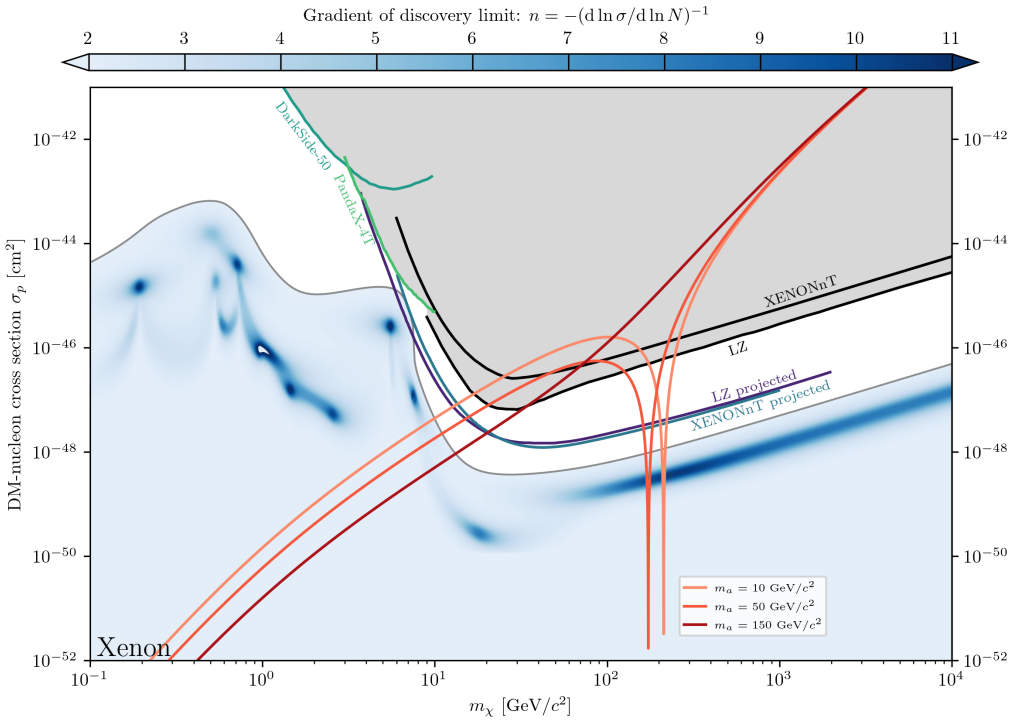

Figure 3.14: Nucleon cross section σ_p as a function of the DM-mass (red). The region that is shaded gray is the region excluded by current experiments. The blue-colored region is the region of the neutrino fog and the gray line at the top of this region is the border where the neutrino fog starts ($n > 2$). The data of DarkSide-50 measured sensitivity is taken from [27], LZ measured sensitivity from [29], LZ projected sensitivity from [71], XENONnT measured sensitivity from [72], XENONnT projected sensitivity from [73] and PandaX-4T sensitivity from [28].

CHAPTER 4

Summary, Conclusion & Discussion

In Chapter 1 we discussed several prominent pieces of evidence for DM, and established that DM should have some kind of interactions with the Standard Model to explain the relic abundance of DM. Although observational evidence exists, there is no direct evidence for DM. Observations and models (like ΛCDM) suggest DM is NR. Hence, direct detection experiments that aim to detect DM operate in the NR regime.

EFT is used to describe DM scattering with nucleons. In Chapter 2 we identified 24 relativistic operators and took the NR limit of all 24 operators, resulting in Tables 2.2 and 2.3. In these tables one can observe that only seven out of 24 operators are not momentum or velocity suppressed. We observed that, generally, pseudo-scalar and axial-vector structures, and tensor structures with one γ^5 in the operator give rise to momentum suppressed behavior, except when both the DM and SM part carry γ^5 in their Lorentz structure.

By going to second-order in the NR limit, the only operators that gain higher-order terms are operators that at first-order are not momentum or velocity suppressed. The second-order expansion is important in case lower-order terms cancel or are in some way suppressed. The second-order expansion does not add only corrections to the pre-factor of the existing building block, but generates new building blocks in the operator. One downside is, that by going to second order Galilean invariance is broken for second-order terms. Then, the building blocks can only be generated by assuming some relation between the momenta. We have established our relations in Tables 2.4 and 2.5 by assuming the center-of-mass frame. Hence, our second-order expansion results are only valid in the center-of-mass frame.

In Chapter 3 we discussed ALP EFT from literature, and we derived the vertex factor for the ALP Lagrangian. Before going to DM-nucleon scattering, we first used scattering between DM and up-quarks. The simplest scattering process, scattering at tree-level, is cutoff scale and momentum suppressed and only conntributes to SD scattering, to which experiments are less sensitive. To resolve the suppression, we calculated the loop-integrals corresponding to the one-loop diagrams in Fig. 3.3. Because of the derivative coupling of the ALP, a top-quark in the loop enhances the cross section, such that the effects of extra factors of the cutoff scale are cancelled to some extent by the top mass.

The pseudo-scalar and axial-vector-type structures lead (except when both the DM and SM Lorentz structures carry a factor of γ^5), in the NR limit, to spatial momentum-suppressed terms,

making their contribution to direct detection negligible. Taking this into account allows us to simplify the loop function and focus on the dominant interactions that influence experimental observability. Together with neglecting the up-mass and expanding the top-propagator, this leads to the expression of the leading contribution to the integral, that is given by Eq. (3.48). This expression tells us that the loop-integral is UV-diverent. In Section 3.4 we identified the operator and diagrams that renormalize our loop-integral.

Kaon ($K \to \pi a$) and B-meson ($B \to Ka, B \to \pi a$) decays provide the tools to set bounds on the c_{tu} couplings (see Fig. 3.10). The lower bounds on the quantity $2f_a/(c_{tu}^V - c_{tu}^A)$ for low ALP masses, $m_a < 250$ GeV/c^2 for Kaon decays and $m_a < 5$ GeV/c^2 for B-meson decays, are 1.5×10^5 TeV and 3.8×10^3 TeV, respectively.

Bounds could not be set for larger ALP-masses by the use of meson-decays. Top-decays could be useful to set bounds on large ALP-masses, but top-decay comes with multi-jet plus neutrino signatures. This makes setting stringent bound on the couplings hard. With more data, from e.g. the LHC, bounds on couplings for large ALP masses below the top-mass could be set, that would make our prediction more reliable. But the branching ratio for this exotic top decay is already very small.

Evolving the couplings down from the cutoff scale Λ to m_t leads to Eq. (3.75), with constraint $(c_{tu}^V)^2 - (c_{tu}^A)^2 = 1$ at Λ. In the instance for calculating DM-nucleon scattering, the ALP must have a smaller mass than m_t. To go down from the top-mass to lower scales, the diagrams in Fig. 3.6 become important. Because the top-quark is inside the loop, the two-loop diagrams must be calculated, since the RGE effects may be non-trivial. Calculating these diagrams is outside the scope of this thesis, but we can predict what properly following the RGEs down to the scale of the momentum transfer would possibly do to our cross section.

One may disagree with the chosen value of the couplings at Λ and cutoff scale. The couplings could take a different value at scale Λ, e.g. $(c_{tu}^V)^2 - (c_{tu}^A)^2 = \delta$. At $\mu = m_t$ and lower energy scales, the value of the couplings would be scaled by δ. Increasing the value of f_a with a factor η would generally scale the cross section down by η^8. Hence, increasing the cutoff scale or decreasing the couplings is quite straightforward to implement, because the cross section is dependent on only the ratio between the cutoff scale and couplings.

Fig. 3.11 shows the DM-nucleon scattering cross section as a function of the ALP-mass, with $m_\chi = 40$ GeV/c^2. Properly evolving the couplings would most likely smoothen the curve and the dip vanishes. Together with Figs. 3.12 and 3.13 we observe that the ALP-mass does not have a large influence on the cross section, because – at a fixed DM-mass – the difference for the cross section and the cutoff scale (Fig. 3.12) are within one order of magnitude.

Finally, the main result of this thesis is given in Fig. 3.14. Similar to the curves in Fig. 3.11, the curves in the σ_p-DM plot that have a dip would be smoothened as well. After smoothening, the mass range of DM that we predict to be promising for ALPs with masses between 5−172 GeV/c^2 is 10 Gev/$c^2 \leq m_\chi \lesssim 30$ Gev/c^2. In this mass-range the cross section is for some ALP-masses above the neutrino fog, which make it likely that current and future experiments may detect scattering events. The cross section corresponding to this mass-range is 5×10^{-49} cm$^2 \lesssim \sigma_p \lesssim 10^{-47}$ cm^2. The cross section for DM-masses smaller than 10 GeV/c^2 are inside the neutrino fog, but are within the region of the neutrino fog where sufficient statistics decrease the neutrino background.

In this thesis we primarily focused on GeV-scale DM. If one would want to focus on MeV-scale DM-masses ($0.1-10^3$ MeV/c^2), DM-electron scattering is generally better than DM-nucleon scattering. The cross section for the same type of loop-induced scattering as in Fig. 3.3, where the up-quark is replaced by the electron and the top-quark is replaced by the tau, has a maximum value of 10^{-54} cm^2 with a maximum ALP-mass of 1 GeV/c^2. This small cross section is because $m_\tau/f_a \ll m_t/f_a$ and DM-electron scattering does not have the A^2 enhancement from coherent scattering with nucleons. This is 20 orders of magnitude smaller than experiments like SENSEI

can currently measure [74]. Similar to CEνNS, experiments become sensitive to electron-neutrino scattering below some cross section. A cross section of $\sim 10^{-54}$ cm^2, using liquid Xenon, is well into the neutrino fog for electron scattering [75].

To conclude, this study demonstrates that ALP-mediated DM-nucleon scattering, particularly through loop-induced top-quark interactions, provides a viable mechanism for direct DM detection. The predicted cross-section falls within experimentally accessible ranges, making this an important direction for future searches. Further work, including precise coupling evolution and experimental refinements, will be crucial for validating these predictions.

APPENDIX A

Direct Detection & Operator Calculations

A.1 Differential Cross Section

We start with the following definition of the differential cross section

$$d\sigma = \frac{\left\langle |\mathcal{M}(\chi N \to \chi N)|^2 \right\rangle}{4|E_{\mathbf{k}_N}\mathbf{p} - E_{\mathbf{p}}\mathbf{k}_N|} d\Pi_2, \tag{A.1}$$

where $\left\langle |\mathcal{M}|^2 \right\rangle$ is the squared amplitude and averaged over the initial spins, $E_{\mathbf{k}_N}$ ($E_{\mathbf{p}}$) is the energy of the nucleus (DM) and $d\Pi_2$ is the two-body phase-space element of the final state momenta [39]:

$$d\Pi_2 = \frac{d^3\mathbf{p}'}{(2\pi)^3}\frac{1}{2E_{\mathbf{p}'}}\frac{d^3\mathbf{k}'_N}{(2\pi)^3}\frac{1}{2E_{\mathbf{k}'_N}}(2\pi)^4\delta^{(4)}(p + k_N - p' - k'_N), \tag{A.2}$$

where k_N (k'_N) is the incoming (outgoing) four-momentum of the nucleus, p (p') the incoming (outgoing) dark matter four-momentum and $\mathbf{q}$ is the spatial-part of the transfer momentum. Here we have taken the final state to be a DM particle and a nucleus and assumed that the nucleus was initially at rest, and therefore obtained a final momentum of $\mathbf{q}$. Since the direct detection experiments work in the non-relativistic (NR) regime, we would like the NR limit of the cross-section. Taking this limit, we obtain

$$d\sigma = \frac{\left\langle |\mathcal{M}_{\mathrm{NR}}(\chi N \to \chi N)|^2 \right\rangle}{(4m_N m_\chi)^2 v}\frac{d^3\mathbf{p}'}{(2\pi)^3}\frac{d^3\mathbf{q}}{(2\pi)^3}(2\pi)^4\delta^{(3)}(\mathbf{p} - \mathbf{p}' + \mathbf{k}_N - \mathbf{k}'_N)\delta(E_{\mathbf{p}} - E_{\mathbf{p}'} + E_{\mathbf{k}_N} - E_{\mathbf{k}'_N}). \tag{A.3}$$

Integrating over $\mathbf{p}'$ to get rid of the Dirac delta-function involving the momenta gives

$$d\sigma = \frac{\left\langle |\mathcal{M}_{\mathrm{NR}}(\chi N \to \chi N)|^2 \right\rangle}{(4m_N m_\chi)^2 v}\frac{d^3\mathbf{q}}{(2\pi)^2}\delta\left(v|\mathbf{q}|\cos\theta - \frac{|\mathbf{q}|^2}{2\mu_{\chi N}}\right), \tag{A.4}$$

where $\cos\theta = \hat{\mathbf{q}}\cdot\hat{\mathbf{p}}$ and $\mu_{\chi N}$ is the reduced mass of the DM and nucleus. From this we see we need to go to spherical coordinates. Going to spherical coordinates and integrating over ϕ and

change variables from $|\mathbf{q}|$ to $|\mathbf{q}|^2$, we obtain

$$d\sigma = \frac{\left\langle |\mathcal{M}_{\rm NR}(\chi N \to \chi N)|^2 \right\rangle}{4\pi v^2} \frac{1}{(4m_N m_\chi)^2} \delta\left(\cos\theta - \frac{|\mathbf{q}|}{2\mu_{\chi N} v}\right) \, d|\mathbf{q}|^2 \, d\cos\theta. \tag{A.5}$$

We need to have an expression which includes the recoil energy, which has the following relation to momentum transfer $\mathbf{q}$

$$E_R = \frac{|\mathbf{q}|^2}{2m_N}. \tag{A.6}$$

Substituting this into Eq. (A.5) and integrating over $\cos\theta$, gives

$$\frac{d\sigma}{dE_R} = \frac{m_N \left\langle |\mathcal{M}_{\rm NR}(\chi N \to \chi N)|^2 \right\rangle}{2\pi v^2} \frac{1}{(4m_\chi m_N)^2}. \tag{A.7}$$

The factor $(4m_\chi m_N)^{-2}$ is the relativistic normalization, which we can drop – but we have to make sure to also drop the normalization inside the amplitude when taking the NR limit – doing that, the results of the cross section are given by

$$\frac{d\sigma}{dE_R} = \frac{m_N \left\langle |\mathcal{M}_{\rm NR}(\chi N \to \chi N)|^2 \right\rangle}{2\pi v^2}. \tag{A.8}$$

A.2 Results for Lorentz Structure and Operator Calculations

Below one finds the non-relativistic limit of the spinors to first-order in Table A.1 and to second-order in Table A.2. In Tables A.3 and 2.3 the results are given for the non-relativistic limit of the relativistic operators.

Table A.1: Non-relativistic limit of different Lorentz structures, which have been verified with [37]. Here m_u is the mass of the spinor, $s(s')$ is the spin index of the spinor, $\mathbf{P} = \mathbf{p} + \mathbf{p}'$ is the sum of initial and final momentum respectively, $\mathbf{q} = \mathbf{p} - \mathbf{p}'$ is the momentum transfer and $\mathbf{s}_u^{s',s} = \xi^{s'} \mathbf{S}_u \xi^s$ is the expectation value of the spin operator. In the last row γ^μ is contracted with momentum k_μ of another fermion with mass m_k. See Appendix A.5 for the derivations.

Lorentz structure	NR-Limit
$\overline{u}^{s'}(p')u^s(p)$	$\approx 2m_u \xi^{\dagger,s'}\xi^s$
$\overline{u}^{s'}(p')\gamma^5 u^s(p)$	$\approx 2\mathbf{q}\cdot\mathbf{s}_u^{s',s}$
$\overline{u}^{s'}(p')\gamma^\mu u^s(p)$	$\approx \begin{pmatrix} 2m_u\xi^{\dagger,s'}\xi^s \\ \mathbf{P}\xi^{\dagger,s'}\xi^s + 2i\mathbf{q}\times\mathbf{s}_u^{s',s} \end{pmatrix}$
$\overline{u}^{s'}(p')\gamma^\mu\gamma^5 u^s(p)$	$\approx \begin{pmatrix} 2\mathbf{P}\cdot\mathbf{s}_u^{s',s} \\ 4m_u\mathbf{s}_u^{s',s} \end{pmatrix}$
$\overline{u}^{s'}(p')\sigma^{\mu\nu} u^s(p)$	$\approx \begin{pmatrix} 0 & i\mathbf{q}\xi^{\dagger,s'}\xi^s - 2\mathbf{P}\times\mathbf{s}_u^{s',s} \\ -i\mathbf{q}\xi^{\dagger,s'}\xi^s + 2\mathbf{P}\times\mathbf{s}_u^{s',s} & 4m_u\epsilon_{jkl}s_u^{l,s',s} \end{pmatrix}$
$\overline{u}(p')\sigma^{\mu\nu}\gamma^5 u^s(p)$	$\approx \begin{pmatrix} 0 & 4im_u\mathbf{s}_u^{s',s} \\ -4im_u\mathbf{s}_u^{s',s} & \epsilon_{jkl}\mathbf{q}^l\xi^{\dagger,s'}\xi^s + 2i\epsilon_{jkl}\left(\mathbf{P}\times\mathbf{s}_u^{s',s}\right)^l \end{pmatrix}$
$\overline{u}^{s'}(p')\not{k}u^s(p)$	$\approx 2m_u m_k \xi^{\dagger,s'}\xi^s$

Table A.2: Non-relativistic limit of Lorentz structures expanded to second order in velocity. Here m_u is the mass of the spinor, $s(s')$ is the spin index of the spinor, $\mathbf{P} = \mathbf{p} + \mathbf{p}'$ is the sum of initial and final momentum respectively, $\mathbf{q} = \mathbf{p} - \mathbf{p}'$ is the momentum transfer and $\mathbf{s}_u^{s',s} = \xi^{s'} \mathbf{S}_u \xi^s$ is the expectation value of the spin operator. In the last row γ^μ is contracted with momentum k_μ of another fermion with mass m_k. See Appendix A.6 for the derivations.

Lorentz structure	NR-Limit
$\overline{u}^{s'}(p')u^s(p)$	$\approx 2m_u \xi^{\dagger,s'}\xi^s + \frac{\mathbf{q}^2}{4m_u}\xi^{\dagger,s'}\xi^s - \frac{i}{2m_u}\mathbf{s}_u^{s',s}\cdot(\mathbf{P}\times\mathbf{q})$
$\overline{u}^{s'}(p')\gamma^5 u^s(p)$	$\approx 2\mathbf{q}\cdot\mathbf{s}_u^{s',s}$
$\overline{u}^{s'}(p')\gamma^\mu u^s(p)$	$\approx \begin{pmatrix} 2m_u\xi^{\dagger,s'}\xi^s + \mathbf{P}^2\xi^{\dagger,s'}\xi^s/4m_u + i\mathbf{s}_u^{s',s}\cdot(\mathbf{P}\times\mathbf{q})/2m_u \\ \mathbf{P}\xi^{\dagger,s'}\xi^s + 2i\mathbf{q}\times\mathbf{s}_u^{s',s} \end{pmatrix}$
$\overline{u}^{s'}(p')\gamma^\mu\gamma^5 u^s(p)$	$\approx \begin{pmatrix} 2\mathbf{P}\cdot\mathbf{s}_u^{s',s} \\ A \end{pmatrix}$
$\overline{u}^{s'}(p')\sigma^{\mu\nu}u^s(p)$	$\approx \begin{pmatrix} 0 & i\mathbf{q}\xi^{\dagger,s'}\xi^s - 2\mathbf{P}\times\mathbf{s}_u^{s',s} \\ -i\mathbf{q}\xi^{\dagger,s'}\xi^s + 2\mathbf{P}\times\mathbf{s}_u^{s',s} & B \end{pmatrix}$
$\overline{u}^{s'}(p')\not{k}u^s(p)$	$\approx 2m_u m_k \xi^{\dagger,s'}\xi^s\left(1 + \frac{\mathbf{k}^2}{2m_k^2} + \frac{\mathbf{P}^2}{8m_u^2} - \frac{\mathbf{k}\cdot\mathbf{P}}{4m_u m_k}\right) + m_k i\mathbf{s}_u^{s',s}\cdot\left(\frac{\mathbf{P}}{2m_u}\times\mathbf{q}\right)$ $-2i\mathbf{k}\cdot\left(\mathbf{q}\times\mathbf{s}_u^{s',s}\right)$

$$A = 4m_u\mathbf{s}_u^{s',s} + \mathbf{s}_u^{s',s}\frac{\mathbf{q}^2}{2m_u} - \frac{1}{2m_u}\left(\mathbf{q}\cdot\mathbf{s}_u^{s',s}\right)\mathbf{q} + \frac{1}{2m_u}\left(\mathbf{P}\cdot\mathbf{s}_u^{s',s}\right)\mathbf{P} + \frac{i}{4m_u}\mathbf{q}\times\mathbf{P}\xi^{\dagger,s'}\xi^s \quad \text{(A.9a)}$$

$$B = \epsilon_{ijk}\left[4m_u\mathbf{s}_u^{s',s} + \frac{\mathbf{P}^2}{2m_u}\mathbf{s}_u^{s',s} + \frac{i}{4m_u}\mathbf{P}\times\mathbf{q}\xi^{\dagger,s'}\xi^s + \mathbf{q}\frac{\mathbf{q}\cdot\mathbf{s}_u^{s',s}}{2m_u} - \mathbf{P}\frac{\mathbf{P}\cdot\mathbf{s}_u^{s',s}}{2m_u}\right]^k \quad \text{(A.9b)}$$

Table A.3: Non-relativistic limit of operators written out with momentum transfer $\mathbf{q}$, transverse velocity $\mathbf{v}_{\rm el}^{\perp}$, the expectation value of the spin operator $\mathbf{s}_N^{s',s}$ and $\mathbf{s}_\chi^{r',r}$ for the nucleon and DM particle, respectively. The expectation value of the unit operator in spin-space is given by the Kronecker delta, i.e. $\delta_{s',s}$ for the nucleon and $\delta_{r',r}$ for the DM particle. The mass of the nucleon (DM) is denoted by $m_N(m_\chi)$. Green, orange and blue are $O(v^0), O(v^1)$ and $O(v^2)$ NR suppressed, respectively. See Appendix A.7 for the derivation.

Relativistic Operators	NR-Limit
$\left(\overline{N}^{s'}(k')N^s(k)\right)\left(\overline{\chi}^{r'}(p')\chi^r(p)\right)$	$\approx 4m_N m_\chi\left[\delta_{s',s}\delta_{r',r}\right]$
$\left(\overline{N}^{s'}(k')\gamma^5 N^s(k)\right)\left(\overline{\chi}^{r'}(p')\chi^r(p)\right)$	$\approx 4m_N m_\chi\left[-\delta_{r',r}\left(\mathbf{s}_N^{s',s}\cdot\frac{\mathbf{q}}{m_N}\right)\right]$
$\left(\overline{N}^{s'}(k')N^s(k)\right)\left(\overline{\chi}^{r'}(p')\gamma^5\chi^r(p)\right)$	$\approx 4m_N m_\chi\left[\frac{m_N}{m_\chi}\delta_{s',s}\left(\mathbf{s}_\chi^{r',r}\cdot\frac{\mathbf{q}}{m_N}\right)\right]$
$\left(\overline{N}^{s'}(k')\gamma^5 N^s(k)\right)\left(\overline{\chi}^{r'}(p')\gamma^5\chi^r(p)\right)$	$\approx 4m_N m_\chi\left[-\frac{m_N}{m_\chi}\left(\mathbf{s}_\chi^{r',r}\cdot\frac{\mathbf{q}}{m_N}\right)\left(\mathbf{s}_N^{s',s}\cdot\frac{\mathbf{q}}{m_N}\right)\right]$
$\left(\overline{N}^{s'}(k')\gamma_\mu N^s(k)\right)\left(\overline{\chi}^{r'}(p')\gamma^\mu\chi^r(p)\right)$	$\approx 4m_N m_\chi\left[\delta_{s',s}\delta_{r',r}\right]$
$\left(\overline{N}^{s'}(k')\gamma_\mu\gamma^5 N^s(k)\right)\left(\overline{\chi}^{r'}(p')\gamma^\mu\chi^r(p)\right)$	$\approx 4m_N m_\chi\left[-2\delta_{r',r}\left(\mathbf{s}_N^{s',s}\cdot\mathbf{v}_{\rm el}^{\perp}\right)\right.$ $\left.-\frac{2im_N}{m_\chi}\mathbf{s}_\chi^{r',r}\cdot\left(\mathbf{s}_N^{s',s}\times\frac{\mathbf{q}}{m_N}\right)\right]$
$\left(\overline{N}^{s'}(k')\gamma_\mu N^s(k)\right)\left(\overline{\chi}^{r'}(p')\gamma_\mu\gamma^5\chi^r(p)\right)$	$\approx 4m_N m_\chi\left[2\delta_{s',s}\left(\mathbf{s}_\chi^{r',r}\cdot\mathbf{v}_{\rm el}^{\perp}\right)\right.$ $\left.-2i\mathbf{s}_\chi^{r',r}\cdot\left(\mathbf{s}_N^{s',s}\times\frac{\mathbf{q}}{m_N}\right)\right]$
$\left(\overline{N}^{s'}(k')\gamma_\mu\gamma^5 N^s(k)\right)\left(\overline{\chi}^{r'}(p')\gamma^\mu\gamma^5\chi^r(p)\right)$	$\approx 4m_N m_\chi\left[-4\mathbf{s}_\chi^{r',r}\cdot\mathbf{s}_N^{s',s}\right]$
$\left(\overline{N}^{s'}(k')\sigma^{\mu\nu}N^s(k)\right)\left(\overline{\chi}^{r'}(p')\sigma_{\mu\nu}\chi^r(p)\right)$ $\left(\overline{N}^{s'}(k')\sigma^{\mu\nu}\gamma^5 N^s(k)\right)\left(\overline{\chi}^{r'}(p')\sigma_{\mu\nu}\gamma^5\chi^r(p)\right)$	$\approx 4m_N m_\chi\left[8\mathbf{s}_\chi^{r',r}\cdot\mathbf{s}_N^{s',s}\right]$
$\left(\overline{N}^{s'}(k')\sigma^{\mu\nu}\gamma^5 N^s(k)\right)\left(\overline{\chi}^{r'}(p')\sigma_{\mu\nu}\chi^r(p)\right)$ $\left(\overline{N}^{s'}(k')\sigma^{\mu\nu}N^s(k)\right)\left(\overline{\chi}^{r'}(p')\sigma_{\mu\nu}\gamma^5\chi^r(p)\right)$	$\approx 4m_N m_\chi\left[\frac{2m_N}{m_\chi}\delta_{r',r}\left(\mathbf{s}_N^{s',s}\cdot\frac{\mathbf{q}}{m_N}\right)\right.$ $\left.-2\delta_{s',s}\left(\mathbf{s}_\chi^{r',r}\cdot\frac{\mathbf{q}}{m_N}\right)+8i\mathbf{s}_\chi^{r',r}\cdot\left(\mathbf{s}_N^{s',s}\times\mathbf{v}_{\rm el}^{\perp}\right)\right]$

Table A.4: The non-relativistic limit of vector and axial-vector operators contracted with the momentum of the other particle. Here $N^s(k)$ is the nucleon spinor with spin index s, four-momentum k and mass m_N. Similarly, $\chi^r(p)$ is the DM particle spinor with spin index r, four-momentum p and mass m_χ. $k(p)$ and $k'(p')$ are the incoming and outgoing quark/nucleon (DM) four-momenta, respectively. Here $\langle \mathcal{O}_i \rangle = \xi_N^{\dagger,s'} \xi_\chi^{\dagger,r'} \mathcal{O}_i \xi_\chi^r \xi_N^s$ denotes the matrix element between the two-dimensional spinors associated with the initial and final state of the DM particle and the up-quark. Color-coding used: $O(v^0)$ is green, $O(v^1)$ is orange, $O(v^2)$ is blue and $O(v^3)$ is pink.

Relativistic Operators	NR-Limit
$\left(\overline{N}^{s'}(k')\not{p}N^s(k)\right)\left(\overline{\chi}^{r'}(p')\chi^r(p)\right)$	$\approx 4m_N m_\chi^2 \left[\delta_{s',s}\delta_{r',r}\right]$
$\left(\overline{N}^{s'}(k')N^s(k)\right)\left(\overline{\chi}^{r'}(p')\not{k}\chi^r(p)\right)$	$\approx 4m_N^2 m_\chi \left[\delta_{s',s}\delta_{r',r}\right]$
$\left(\overline{N}^{s'}(k')\not{p}N^s(k)\right)\left(\overline{\chi}^{r'}(p')\not{k}\chi^r(p)\right)$	$\approx 4m_N^2 m_\chi^2 \left[\delta_{s',s}\delta_{r',r}\right]$
$\left(\overline{N}^{s'}(k')\not{p}\gamma^5 N^s(k)\right)\left(\overline{\chi}^{r'}(p')\chi^r(p)\right)$	$\approx 4m_N m_\chi \left[-\left(\mathbf{s}_N^{s',s}\cdot\mathbf{q}\right)\delta_{r',r} - 2m_\chi \mathbf{s}_N^{s',s}\cdot\mathbf{v}_{\rm el}^\perp \delta_{r',r}\right]$
$\left(\overline{N}^{s'}(k')\gamma^5 N^s(k)\right)\left(\overline{\chi}^{r'}(p')\not{k}\chi^r(p)\right)$	$\approx 4m_N m_\chi \left[-\left(\mathbf{s}_N^{s',s}\cdot\mathbf{q}\right)\delta_{r',r}\right]$
$\left(\overline{N}^{s'}(k')\not{p}\gamma^5 N^s(k)\right)\left(\overline{\chi}^{r'}(p')\not{k}\chi^r(p)\right)$	$\approx 4m_N m_\chi \left[-m_N\left(\mathbf{s}_N^{s',s}\cdot\mathbf{q}\right)\delta_{r',r} - 2m_\chi m_N\left(\mathbf{s}_N^{s',s}\cdot\mathbf{v}_{\rm el}^\perp\right)\delta_{r',r}\right]$
$\left(\overline{N}^{s'}(k')\not{p}N^s(k)\right)\left(\overline{\chi}^{r'}(p')\gamma^5\chi^r(p)\right)$	$\approx 4m_N m_\chi \left[\left(\mathbf{s}_\chi^{r',r}\cdot\mathbf{q}\right)\delta_{s',s}\right]$
$\left(\overline{N}^{s'}(k')N^s(k)\right)\left(\overline{\chi}^{r'}(p')\not{k}\gamma^5\chi^r(p)\right)$	$\approx 4m_N m_\chi \left[\left(\mathbf{s}_\chi^{r',r}\cdot\mathbf{q}\right)\delta_{s',s} + 2m_N\left(\mathbf{s}_\chi^{r',r}\cdot\mathbf{v}_{\rm el}^\perp\right)\delta_{s',s}\right]$
$\left(\overline{N}^{s'}(k')\not{p}N^s(k)\right)\left(\overline{\chi}^{r'}(p')\not{k}\gamma^5\chi^r(p)\right)$	$\approx 4m_N m_\chi \left[m_\chi\left(\mathbf{s}_\chi^{r',r}\cdot\mathbf{q}\right)\delta_{s',s} + 2m_\chi m_N\left(\mathbf{s}_\chi^{r',r}\cdot\mathbf{v}_{\rm el}^\perp\right)\delta_{s',s}\right]$
$\left(\overline{N}^{s'}(k')\not{p}\gamma^5 N^s(k)\right)\left(\overline{\chi}^{r'}(p')\gamma^5\chi^r(p)\right)$	$\approx 4m_N m_\chi \left[-m_N\left(\mathbf{s}_N^{s',s}\cdot\frac{\mathbf{q}}{m_N}\right)\left(\mathbf{s}_\chi^{r',r}\cdot\frac{\mathbf{q}}{m_N}\right) -2\left(\mathbf{s}_\chi^{r',r}\cdot\mathbf{q}\right)\left(\mathbf{s}_N^{s',s}\cdot\mathbf{v}_{\rm el}^\perp\right)\right]$
$\left(\overline{N}^{s'}(k')\gamma^5 N^s(k)\right)\left(\overline{\chi}^{r'}(p')\not{k}\gamma^5\chi^r(p)\right)$	$\approx 4m_N m_\chi \left[-m_N\left(\mathbf{s}_N^{s',s}\cdot\frac{\mathbf{q}}{m_N}\right)\left(\mathbf{s}_\chi^{r',r}\cdot\frac{\mathbf{q}}{m_N}\right) -2\left(\mathbf{s}_\chi^{r',r}\cdot\mathbf{v}_{\rm el}^\perp\right)\left(\mathbf{s}_N^{s',s}\cdot\mathbf{q}\right)\right]$
$\left(\overline{N}^{s'}(k')\not{p}\gamma^5 N^s(k)\right)\left(\overline{\chi}^{r'}(p')\not{k}\gamma^5\chi^r(p)\right)$	$\approx 4m_N m_\chi \left[-\left(\mathbf{s}_N^{s',s}\cdot\mathbf{q}\right)\left(\mathbf{s}_\chi^{r',r}\cdot\mathbf{q}\right) -2m_N\left(\mathbf{s}_\chi^{r',r}\cdot\mathbf{v}_{\rm el}^\perp\right)\left(\mathbf{s}_N^{r',r}\cdot\mathbf{q}\right) -2m_\chi\left(\mathbf{s}_\chi^{r',r}\cdot\mathbf{q}\right)\left(\mathbf{s}_N^{s',s}\cdot\mathbf{v}_{\rm el}^\perp\right) -4m_\chi m_N\left(\mathbf{s}_\chi^{r',r}\cdot\mathbf{v}_{\rm el}^\perp\right)\left(\mathbf{s}_N^{s',s}\cdot\mathbf{v}_{\rm el}^\perp\right)\right]$

A.3 Useful Relations for Derivations

The general procedure for taking the NR-limit of different Lorentz structures is to first write out the expression, then take the NR-limit of the spinors and multiplying out all vectors and matrices. In some cases (e.g. the scalar structure) it is fairly straightforward to simplify the expression, in other cases we need to use one or more of the following kinematic relations and

identities:

$$\mathbf{P}^2 + \mathbf{q}^2 = 2\left(\mathbf{p}^2 + \mathbf{p}'^2\right) \tag{A.10a}$$
$$\mathbf{P}^2 - \mathbf{q}^2 = 4\mathbf{p}\cdot\mathbf{p}' \tag{A.10b}$$
$$2\mathbf{p}'\times\mathbf{p} = \mathbf{P}\times\mathbf{q} \tag{A.10c}$$
$$2\mathbf{k}\times\mathbf{k}' = \mathbf{K}\times\mathbf{q} \tag{A.10d}$$
$$(\boldsymbol{\sigma}\cdot\mathbf{p})(\boldsymbol{\sigma}\cdot\mathbf{p}') = \mathbf{p}\cdot\mathbf{p}' + i\boldsymbol{\sigma}\cdot(\mathbf{p}\times\mathbf{p}') \tag{A.10e}$$
$$(\mathbf{p}'\cdot\boldsymbol{\sigma})\,\sigma^i\,(\mathbf{p}\cdot\boldsymbol{\sigma}) = (\mathbf{P}\cdot\mathbf{S}_u)\,\mathbf{P}^i - \mathbf{q}^i(\mathbf{S}_u\cdot\mathbf{q}) + \frac{i}{2}(\mathbf{q}\times\mathbf{P})^i - \frac{S_u^i}{2}(\mathbf{P}^2-\mathbf{q}^2) \tag{A.10f}$$
$$\sigma^j\sigma^k = i\epsilon_{jkl}\sigma^l \qquad \text{for } j\neq k \tag{A.10g}$$

The following vector identities are also good to remember when taking the NR-limit:

$$\mathbf{a}\cdot(\mathbf{b}\times\mathbf{c}) = \mathbf{b}\cdot(\mathbf{c}\times\mathbf{a}) = \mathbf{c}\cdot(\mathbf{a}\times\mathbf{b}) \tag{A.11a}$$
$$(\mathbf{a}\times\mathbf{b})\cdot(\mathbf{c}\times\mathbf{d}) = (\mathbf{a}\cdot\mathbf{c})(\mathbf{b}\cdot\mathbf{d}) - (\mathbf{a}\cdot\mathbf{d})(\mathbf{b}\cdot\mathbf{c}) \tag{A.11b}$$
$$(\mathbf{a}\times\mathbf{b})\times\mathbf{c} = \mathbf{b}(\mathbf{c}\cdot\mathbf{a}) - \mathbf{a}(\mathbf{b}\cdot\mathbf{c}) \tag{A.11c}$$

Let us define the spin-operator as $\mathbf{S} = \frac{\boldsymbol{\sigma}}{2}$, where $\boldsymbol{\sigma}$ is the vector of Pauli matrices, and let $\hat{\mathbf{x}}_i$ be the unit vector in the ith direction. We use the Weyl representation of the γ-matrices:

$$\gamma^0 = \begin{pmatrix} 0 & I_2 \\ I_2 & 0 \end{pmatrix}, \quad \gamma^i = \begin{pmatrix} 0 & \sigma^i \\ -\sigma^i & 0 \end{pmatrix}, \quad \text{and} \quad \gamma^5 = i\gamma^0\gamma^1\gamma^2\gamma^3 = \begin{pmatrix} -I_2 & 0 \\ 0 & I_2 \end{pmatrix}. \tag{A.12}$$

A.4 NR-Limit of Spinor

Writing out the definition of the spinors in Eq. (2.19) gives

$$u^s(p) = \begin{pmatrix} \sqrt{E-\mathbf{p}\cdot\boldsymbol{\sigma}}\xi^s \\ \sqrt{E+\mathbf{p}\cdot\boldsymbol{\sigma}}\xi^s \end{pmatrix} \tag{A.13}$$

In the NR-limit the relativistic energy is

$$E = \sqrt{m^2+\mathbf{p}^2} = m\sqrt{1+\mathbf{p}^2/m^2} \approx m\left(1+\frac{\mathbf{p}^2}{2m^2}\right) \approx m. \tag{A.14}$$

We assumed that $\mathbf{p}/m \ll 1$, so we are allowed to only include the zeroth and first order term in the expansion. Substituting the above expression for the energy and doing a similar expansion we obtain

$$\begin{aligned} u^s(p) &\approx \sqrt{m}\begin{pmatrix} \sqrt{1-\mathbf{p}\cdot\boldsymbol{\sigma}/m}\xi^s \\ \sqrt{1+\mathbf{p}\cdot\boldsymbol{\sigma}/m}\xi^s \end{pmatrix} \\ &\approx \sqrt{m}\begin{pmatrix} (1-\mathbf{p}\cdot\boldsymbol{\sigma}/2m)\,\xi^s \\ (1+\mathbf{p}\cdot\boldsymbol{\sigma}/2m)\,\xi^s \end{pmatrix} \end{aligned} \tag{A.15}$$

Where the last line is the expression we use for the first order expansion NR-limit of the spinors. Doing the expansion to second order gives:

$$\begin{aligned}
u(p) &= \begin{pmatrix} \sqrt{p\cdot\sigma}\xi \\ \sqrt{p\cdot\overline{\sigma}}\xi \end{pmatrix} \\
&= \sqrt{E}\begin{pmatrix} \sqrt{I_2 - \mathbf{p}\cdot\boldsymbol{\sigma}/E}\xi \\ \sqrt{I_2 + \mathbf{p}\cdot\boldsymbol{\sigma}/E}\xi \end{pmatrix} \\
&\approx \sqrt{m}\left(1+\frac{\mathbf{p}^2}{4m^2}\right)\begin{pmatrix} \left(1-\mathbf{p}\cdot\boldsymbol{\sigma}/2E - \mathbf{p}^2/8E^2\right)\xi \\ \left(1+\mathbf{p}\cdot\boldsymbol{\sigma}/2E - \mathbf{p}^2/8E^2\right)\xi \end{pmatrix} \\
&\approx \sqrt{m}\left(1+\frac{\mathbf{p}^2}{4m^2}\right)\begin{pmatrix} \left(1-\left(1-\frac{\mathbf{p}^2}{2m^2}\right)\mathbf{p}\cdot\boldsymbol{\sigma}/2m - \left(1-\frac{\mathbf{p}^2}{m^2}\right)\mathbf{p}^2/8m^2\right)\xi \\ \left(1+\left(1-\frac{\mathbf{p}^2}{2m^2}\right)\mathbf{p}\cdot\boldsymbol{\sigma}/2m - \left(1-\frac{\mathbf{p}^2}{m^2}\right)\mathbf{p}^2/8m^2\right)\xi \end{pmatrix} \\
&\approx \sqrt{m}\begin{pmatrix} \left(1-\mathbf{p}\cdot\boldsymbol{\sigma}/2m + \mathbf{p}^2/8m^2\right)\xi \\ \left(1+\mathbf{p}\cdot\boldsymbol{\sigma}/2m + \mathbf{p}^2/8m^2\right)\xi \end{pmatrix}
\end{aligned} \tag{A.16}$$

To go from the third to the fourth line, we used that $\frac{1}{\sqrt{1+x}} \approx 1 - \frac{x}{2}$ for small x and that $1/E$ can be approximated like this.

A.5 First Order NR-Limit of Lorentz Structures

The procedure to calculate the limit of different Lorentz structures is very straightforward, because we have calculated the NR limit of the spinor already in Appendix A.4. Given some structure, go through the following steps:

1. Write out the term such that all components (spinors and γ-matrices) are separated.
2. If necessary, simplify the γ-matrices using different identities.
3. Take the NR limit of the spinors and write out the γ-matrices in terms of their matrix representation. Taking the NR limit of the spinor is in this section the same as substituting the expression for the spinor derived in Appendix A.4.
4. Multiply the spinors and γ-matrices and discard all second order and higher order momentum terms.
5. Separate the relativistic normalization pre-factor from the rest of the expression (not necessary).

A.5.1 (Pseudo-)Scalar

Scalar:

$$\begin{aligned}
\overline{u}^{\lambda'}(p')u^{\lambda}(p) &= u^{\dagger,\lambda'}(p')\gamma^0 u^{\lambda}(p) \\
&\approx m\begin{pmatrix} \left(1-\mathbf{p}'\cdot\boldsymbol{\sigma}/2m\right)\xi^{\lambda'} \\ \left(1+\mathbf{p}'\cdot\boldsymbol{\sigma}/2m\right)\xi^{\lambda'} \end{pmatrix}^{\dagger}\begin{pmatrix} 0 & I_2 \\ I_2 & 0 \end{pmatrix}\begin{pmatrix} \left(1-\mathbf{p}\cdot\boldsymbol{\sigma}/2m\right)\xi^{\lambda} \\ \left(1+\mathbf{p}\cdot\boldsymbol{\sigma}/2m\right)\xi^{\lambda} \end{pmatrix} \\
&\approx 2m\xi^{\dagger,\lambda'}\xi^{\lambda}
\end{aligned} \tag{A.17}$$

Pseudo-scalar:

$$\begin{aligned}\overline{u}^{\lambda'}(p')\gamma^5 u^{\lambda}(p) &= u^{\dagger,\lambda'}(p')\gamma^0\gamma^5 u^{\lambda}(p)\\ &\approx m\begin{pmatrix}(1-\mathbf{p}'\cdot\boldsymbol{\sigma}/2m)\,\xi^{\lambda'}\\(1+\mathbf{p}'\cdot\boldsymbol{\sigma}/2m)\,\xi^{\lambda'}\end{pmatrix}^{\dagger}\begin{pmatrix}0 & I_2\\ I_2 & 0\end{pmatrix}\begin{pmatrix}-I_2 & 0\\ 0 & I_2\end{pmatrix}\begin{pmatrix}(1-\mathbf{p}\cdot\boldsymbol{\sigma}/2m)\,\xi^{\lambda}\\(1+\mathbf{p}\cdot\boldsymbol{\sigma}/2m)\,\xi^{\lambda}\end{pmatrix}\\ &\approx 2m\left[\frac{\mathbf{q}}{m}\cdot\mathbf{s}_u^{\lambda',\lambda}\right]\end{aligned} \tag{A.18}$$

A.5.2 (Axial-)Vector

The vector structure has four components, because there are 4 different γ-matrices. The zeroth γ-matrix is different from the other three, because the latter all contain Pauli matrices and the former does not. We therefore split the calculation in two, where we first take the NR-limit with index $\mu = 0$ and in the second we do the same for $\mu = 1, 2, 3$ simultaneously. First starting with the zeroth γ-matrix:

$$\begin{aligned}\overline{u}^{\lambda'}(p')\gamma^0 u^{\lambda}(p) &= u^{\dagger,\lambda'}(p')\gamma^0\gamma^0 u^{\lambda}(p)\\ &\approx m\begin{pmatrix}(1-\mathbf{p}'\cdot\boldsymbol{\sigma}/2m)\,\xi^{\lambda'}\\(1+\mathbf{p}'\cdot\boldsymbol{\sigma}/2m)\,\xi^{\lambda'}\end{pmatrix}^{\dagger}\begin{pmatrix}(1-\mathbf{p}\cdot\boldsymbol{\sigma}/2m)\,\xi^{\lambda}\\(1+\mathbf{p}\cdot\boldsymbol{\sigma}/2m)\,\xi^{\lambda}\end{pmatrix}\\ &\approx 2m\xi^{\dagger,\lambda'}\xi^{\lambda}\end{aligned} \tag{A.19}$$

Now taking the $i = 1, 2, 3$ γ-matrix:

$$\begin{aligned}\overline{u}^{\lambda'}(p')\gamma^i u^{\lambda}(p) &= u^{\dagger,\lambda'}(p')\gamma^0\gamma^i u^{\lambda'}(p)\\ &\approx m\begin{pmatrix}(1-\mathbf{p}'\cdot\boldsymbol{\sigma}/2m)\,\xi^{\lambda'}\\(1+\mathbf{p}'\cdot\boldsymbol{\sigma}/2m)\,\xi^{\lambda'}\end{pmatrix}^{\dagger}\begin{pmatrix}0 & I_2\\ I_2 & 0\end{pmatrix}\begin{pmatrix}0 & \sigma^i\\ -\sigma^i & 0\end{pmatrix}\begin{pmatrix}(1-\mathbf{p}\cdot\boldsymbol{\sigma}/2m)\,\xi^{\lambda}\\(1+\mathbf{p}\cdot\boldsymbol{\sigma}/2m)\,\xi^{\lambda}\end{pmatrix}\\ &\approx 2m\xi^{\dagger,\lambda'}\left[\sigma^i\frac{\mathbf{p}\cdot\boldsymbol{\sigma}}{2m}+\frac{\mathbf{p}'\cdot\boldsymbol{\sigma}}{2m}\sigma^i\right]\xi^{\lambda}\\ &= \xi^{\dagger,\lambda'}\left[\mathbf{p}\cdot\hat{\mathbf{x}}_i + i\boldsymbol{\sigma}\cdot(\hat{\mathbf{x}}_i\times\mathbf{p}) + \mathbf{p}'\cdot\hat{\mathbf{x}}_i + i\boldsymbol{\sigma}\cdot(\mathbf{p}'\times\hat{\mathbf{x}}_i)\right]\xi^{\lambda}\\ &= 2m\left[\left(\frac{\mathbf{P}}{2m}\right)^i\xi^{\dagger,\lambda'}\xi^{\lambda} + \left(\frac{i\mathbf{q}}{m}\times\mathbf{s}_u^{\lambda',\lambda}\right)^i\right]\end{aligned} \tag{A.20}$$

Similar to the vector structure, the axial vector structure has four components. Hence, we take the same approach as for the vector structure: separate calculations for the zeroth and $i = 1, 2, 3$ components. First the zeroth component:

$$\begin{aligned}\overline{u}^{\lambda'}(p')\gamma^0\gamma^5 u^{\lambda}(p) &= u^{\dagger,\lambda'}(p')\gamma^5 u^{\lambda}(p)\\ &\approx m\begin{pmatrix}(1-\mathbf{p}'\cdot\boldsymbol{\sigma}/2m)\,\xi^{\lambda'}\\(1+\mathbf{p}'\cdot\boldsymbol{\sigma}/2m)\,\xi^{\lambda'}\end{pmatrix}^{\dagger}\begin{pmatrix}-I_2 & 0\\ 0 & I_2\end{pmatrix}\begin{pmatrix}(1-\mathbf{p}\cdot\boldsymbol{\sigma}/2m)\,\xi^{\lambda}\\(1+\mathbf{p}\cdot\boldsymbol{\sigma}/2m)\,\xi^{\lambda}\end{pmatrix}\\ &\approx 2m\left[\frac{\mathbf{P}}{m}\cdot\mathbf{s}_u^{\lambda',\lambda}\right]\end{aligned} \tag{A.21}$$

using the identity $(\gamma^0)^2 = I_4$. Then below the $i = 1, 2, 3$ components:

$$\begin{aligned}\overline{u}^{\lambda'}(p')\gamma^i\gamma^5 u^{\lambda'}(p) &= u^{\dagger,\lambda'}(p')\gamma^0\gamma^i\gamma^5 u^{\lambda}(p) \\ &\approx m \begin{pmatrix}(1 - \mathbf{p}'\cdot\boldsymbol{\sigma}/2m)\,\xi^{\lambda'} \\ (1 + \mathbf{p}'\cdot\boldsymbol{\sigma}/2m)\,\xi^{\lambda'}\end{pmatrix}^\dagger \begin{pmatrix}\sigma^i & 0 \\ 0 & \sigma^i\end{pmatrix} \begin{pmatrix}(1 - \mathbf{p}\cdot\boldsymbol{\sigma}/2m)\,\xi^{\lambda} \\ (1 + \mathbf{p}\cdot\boldsymbol{\sigma}/2m)\,\xi^{\lambda}\end{pmatrix} \\ &\approx 2m\left[2\left(\mathbf{s}_u^{\lambda',\lambda}\right)^i\right]\end{aligned} \tag{A.22}$$

A.5.3 Tensor

Before calculating every component, there are two observations we can make. Note that

$$\sigma^{\mu\nu} = \frac{i}{2}\left[\gamma^\mu, \gamma^\nu\right]. \tag{A.23}$$

This means that all components for which $\mu = \nu$ are zero:

$$\overline{u}^{\lambda'}(p')\sigma^{00}u^{\lambda}(p) = 0 \tag{A.24}$$

$$\overline{u}^{\lambda'}(p')\sigma^{ii}u^{\lambda}(p) = 0. \tag{A.25}$$

Because $\sigma^{\mu\nu}$ is the commutator of γ-matrices, the tensor is anti-symmetric. Hence, we only need to calculate the NR-limit for the off-diagonal components σ^{i0} and σ^{jk} $(j \neq k, j, k = 1, 2, 3)$:

$$\begin{aligned}\overline{u}^{\lambda'}(p')\sigma^{i0}u^{\lambda}(p) &= \frac{i}{2}\overline{u}^{\lambda'}(p')\left[\gamma^i, \gamma^0\right]u^{\lambda}(p) \\ &= -iu^{\dagger,\lambda'}(p')\gamma^i u^{\lambda}(p) \\ &\approx -im \begin{pmatrix}(1 - \mathbf{p}'\cdot\boldsymbol{\sigma}/2m)\,\xi^{\lambda'} \\ (1 + \mathbf{p}'\cdot\boldsymbol{\sigma}/2m)\,\xi^{\lambda'}\end{pmatrix}^\dagger \begin{pmatrix}0 & \sigma^i \\ -\sigma^i & 0\end{pmatrix} \begin{pmatrix}(1 - \mathbf{p}\cdot\boldsymbol{\sigma}/2m)\,\xi^{\lambda} \\ (1 + \mathbf{p}\cdot\boldsymbol{\sigma}/2m)\,\xi^{\lambda}\end{pmatrix} \\ &\approx -i\xi^{\dagger,\lambda'}\left[\sigma^i\left(\mathbf{p}\cdot\boldsymbol{\sigma}\right) - \left(\mathbf{p}'\cdot\boldsymbol{\sigma}\right)\sigma^i\right]\xi^{\lambda} \\ &= -i\xi^{\dagger,\lambda'}\left[\mathbf{p}\cdot\hat{\mathbf{x}}_i + i\boldsymbol{\sigma}\cdot(\hat{\mathbf{x}}_i\times\mathbf{p}) - \mathbf{p}'\cdot\hat{\mathbf{x}}_i - i\boldsymbol{\sigma}\cdot(\mathbf{p}'\times\hat{\mathbf{x}}_i)\right]\xi^{\lambda} \\ &= 2m\left[-\left(\frac{i\mathbf{q}}{2m}\right)^i\xi^{\dagger,\lambda'}\xi^{\lambda} + \left(\frac{\mathbf{P}}{m}\times\mathbf{s}_u^{\lambda',\lambda}\right)^i\right]\end{aligned} \tag{A.26}$$

$$\begin{aligned}\overline{u}^{\lambda'}(p')\sigma^{jk}u^{\lambda}(p) &= iu^{\dagger,\lambda'}(p')\gamma^0\gamma^j\gamma^k u^{\lambda}(p) \qquad j \neq k \\ &\approx -im \begin{pmatrix}(1 - \mathbf{p}'\cdot\boldsymbol{\sigma}/2m)\,\xi^{\lambda'} \\ (1 + \mathbf{p}'\cdot\boldsymbol{\sigma}/2m)\,\xi^{\lambda'}\end{pmatrix}^\dagger \begin{pmatrix}0 & i\epsilon_{jkl}\sigma^l \\ i\epsilon_{jkl}\sigma^l & 0\end{pmatrix} \begin{pmatrix}(1 - \mathbf{p}\cdot\boldsymbol{\sigma}/2m)\,\xi^{\lambda} \\ (1 + \mathbf{p}\cdot\boldsymbol{\sigma}/2m)\,\xi^{\lambda}\end{pmatrix} \\ &\approx 2m\left[2\epsilon_{jkl}\left(\mathbf{s}_u^{\lambda',\lambda}\right)^l\right]\end{aligned} \tag{A.27}$$

Similar to the previous tensor structure, the diagonal components are zero and – using the asymmetry of $\sigma^{\mu\nu}$ – we only need to calculate the off-diagonal components σ^{0i} and σ^{jk} $(j \neq k, j, k = 1, 2, 3)$:

$$\overline{u}^{\lambda'}(p')\sigma^{00}\gamma^5 u^{\lambda}(p) = 0 \tag{A.28}$$

$$\overline{u}^{\lambda'}(p')\sigma^{ii}\gamma^5 u^{\lambda}(p) = 0. \tag{A.29}$$

$$\begin{aligned}
\overline{u}^{\lambda'}(p')\sigma^{i0}\gamma^5 u^{\lambda}(p) &= \frac{i}{2}\overline{u}^{\lambda'}(p')\left[\gamma^i,\gamma^0\right]\gamma^5 u^{\lambda}(p) \\
&= -iu^{\dagger,\lambda'}(p')\gamma^i\gamma^5 u^{\lambda}(p) \\
&\approx -im\begin{pmatrix}(1-\mathbf{p}'\cdot\boldsymbol{\sigma}/2m)\,\xi^{\lambda'}\\(1+\mathbf{p}'\cdot\boldsymbol{\sigma}/2m)\,\xi^{\lambda'}\end{pmatrix}^{\dagger}\begin{pmatrix}0 & \sigma^i\\-\sigma^i & 0\end{pmatrix}\begin{pmatrix}-I_2 & 0\\0 & I_2\end{pmatrix}\begin{pmatrix}(1-\mathbf{p}\cdot\boldsymbol{\sigma}/2m)\,\xi^{\lambda}\\(1+\mathbf{p}\cdot\boldsymbol{\sigma}/2m)\,\xi^{\lambda}\end{pmatrix} \\
&\approx 2m\left[-2i\left(\mathbf{s}_u^{\lambda',\lambda}\right)_i\right]
\end{aligned} \tag{A.30}$$

$$\begin{aligned}
\overline{u}^{\lambda'}(p')\sigma^{jk}\gamma^5 u^{\lambda}(p) &= iu^{\dagger,\lambda'}(p')\gamma^0\gamma^i\gamma^k\gamma^5 u^{\lambda}(p) \qquad j\neq k \\
&\approx -im\begin{pmatrix}(1-\mathbf{p}'\cdot\boldsymbol{\sigma}/2m)\,\xi^{\lambda'}\\(1+\mathbf{p}'\cdot\boldsymbol{\sigma}/2m)\,\xi^{\lambda'}\end{pmatrix}^{\dagger}\begin{pmatrix}0 & i\epsilon_{jkl}\sigma^l\\-i\epsilon_{jkl}\sigma^l & 0\end{pmatrix}\begin{pmatrix}(1-\mathbf{p}\cdot\boldsymbol{\sigma}/2m)\,\xi^{\lambda}\\(1+\mathbf{p}\cdot\boldsymbol{\sigma}/2m)\,\xi^{\lambda}\end{pmatrix} \\
&\approx \epsilon_{jkl}\xi^{\dagger,\lambda'}\left[\sigma^l\left(\mathbf{p}\cdot\boldsymbol{\sigma}\right)-\left(\mathbf{p}'\cdot\boldsymbol{\sigma}\right)\sigma^l\right]\xi^{\lambda} \\
&= \epsilon_{jkl}\xi^{\dagger,\lambda'}\left[\mathbf{p}\cdot\hat{\mathbf{x}}_l+i\boldsymbol{\sigma}\cdot(\hat{\mathbf{x}}_l\times\mathbf{p})-\mathbf{p}'\cdot\hat{\mathbf{x}}_l-i\boldsymbol{\sigma}\cdot(\mathbf{p}'\times\hat{\mathbf{x}}_l)\right]\xi^{\lambda} \\
&= 2m\left[\epsilon^{jkl}\left(\frac{\mathbf{q}}{2m}\right)_l\xi^{\dagger,\lambda'}\xi^{\lambda}+i\epsilon^{jkl}\left(\frac{\mathbf{P}}{m}\times\mathbf{s}_u^{\lambda',\lambda}\right)_l\right]
\end{aligned} \tag{A.31}$$

A.5.4 Contracted Momenta

$$\begin{aligned}
\overline{u}^{\lambda'}(p')\not{k}u^{\lambda}(p) &= k_\mu u^{\dagger,\lambda'}(p')\gamma^0\gamma^\mu u^{\lambda}(p) \\
&= k_\mu\overline{u}(p')\gamma^\mu u(p) \\
&\approx (m_k,-\mathbf{k})\begin{pmatrix}2m_u\xi^{\dagger,s'}\xi^s\\\mathbf{P}\xi^{\dagger,s'}\xi^s+2i\mathbf{q}\times\mathbf{s}_u^{s',s}\end{pmatrix} \\
&\approx 2m_u m_k\xi^{\dagger,s'}\xi^s
\end{aligned} \tag{A.32}$$

A.6 Second Order NR-Limit of Lorentz Structures

The procedure to calculate the limit of different Lorentz structures to second order is the same as to first order, with only two differences: use the spinor that is expanded to second order and discard every term that is third order or higher in momentum. Given some structure, go through the following steps:

1. Write out the term such that all components (spinors and γ-matrices) are separated.
2. If necessary, simplify the γ-matrices using different identities.
3. Take the NR limit of the spinors, include the second order momentum terms, and write out the γ-matrices in terms of their matrix representation. Taking the NR limit of the spinor is, in this section, the same as substituting the expression for the spinor derived in Appendix A.4.
4. Multiply the spinors and γ-matrices and discard all third order and higher order momentum terms.
5. Separate the relativistic normalization pre-factor from the rest of the expression (not necessary).

A.6.1 Scalar

$$\begin{aligned}\overline{u}^{\lambda'}(p')u^{\lambda}(p) &= u^{\dagger,\lambda}(p')\gamma^0 u^{\lambda}(p)\\ &\approx m\begin{pmatrix}\left(1-\mathbf{p}'\cdot\boldsymbol{\sigma}/2m+\mathbf{p}'^2/8m^2\right)\xi^{\lambda'}\\ \left(1+\mathbf{p}'\cdot\boldsymbol{\sigma}/2m+\mathbf{p}'^2/8m^2\right)\xi^{\lambda'}\end{pmatrix}^{\dagger}\begin{pmatrix}0 & I_2\\ I_2 & 0\end{pmatrix}\begin{pmatrix}\left(1-\mathbf{p}\cdot\boldsymbol{\sigma}/2m+\mathbf{p}^2/8m^2\right)\xi^{\lambda}\\ \left(1+\mathbf{p}\cdot\boldsymbol{\sigma}/2m+\mathbf{p}^2/8m^2\right)\xi^{\lambda}\end{pmatrix}\\ &\approx 2m\xi^{\dagger,\lambda'}\left[1+\frac{\mathbf{p}^2+\mathbf{p}'^2}{8m^2}-\frac{\mathbf{p}'\cdot\mathbf{p}}{4m^2}-\frac{i}{4m^2}\boldsymbol{\sigma}\cdot(\mathbf{p}'\times\mathbf{p})\right]\xi^{\lambda}\\ &= 2m\left[\xi^{\dagger,\lambda'}\xi^{\lambda}+\frac{\mathbf{q}^2}{8m^2}\xi^{\dagger,\lambda'}\xi^{\lambda}-\frac{i}{4m^2}\mathbf{s}_u^{\lambda',\lambda}\cdot(\mathbf{P}\times\mathbf{q})\right]\end{aligned} \tag{A.33}$$

A.6.2 Pseudo-Scalar

$$\begin{aligned}\overline{u}^{\lambda'}(p')\gamma^5 u^{\lambda}(p) &= u^{\dagger,\lambda'}(p')\gamma^5 u^{\lambda}(p)\\ &\approx m\begin{pmatrix}\left(1-\mathbf{p}'\cdot\boldsymbol{\sigma}/2m+\mathbf{p}'^2/8m^2\right)\xi^{\lambda'}\\ \left(1+\mathbf{p}'\cdot\boldsymbol{\sigma}/2m+\mathbf{p}'^2/8m^2\right)\xi^{\lambda'}\end{pmatrix}^{\dagger}\begin{pmatrix}0 & I_2\\ -I_2 & 0\end{pmatrix}\begin{pmatrix}\left(1-\mathbf{p}\cdot\boldsymbol{\sigma}/2m+\mathbf{p}^2/8m^2\right)\xi^{\lambda}\\ \left(1+\mathbf{p}\cdot\boldsymbol{\sigma}/2m+\mathbf{p}^2/8m^2\right)\xi^{\lambda}\end{pmatrix}\\ &\approx 2m\left[\frac{\mathbf{q}}{m}\cdot\mathbf{s}_u^{\lambda',\lambda}\right]\end{aligned} \tag{A.34}$$

A.6.3 Vector

$$\begin{aligned}\overline{u}^{\lambda'}(p')\gamma^0 u^{\lambda}(p) &= u^{\dagger,\lambda'}(p')\gamma^0\gamma^0 u^{\lambda}(p)\\ &\approx m\begin{pmatrix}\left(1-\mathbf{p}'\cdot\boldsymbol{\sigma}/2m+\mathbf{p}'^2/8m^2\right)\xi^{\lambda'}\\ \left(1+\mathbf{p}'\cdot\boldsymbol{\sigma}/2m+\mathbf{p}'^2/8m^2\right)\xi^{\lambda'}\end{pmatrix}^{\dagger}\begin{pmatrix}\left(1-\mathbf{p}\cdot\boldsymbol{\sigma}/2m+\mathbf{p}^2/8m^2\right)\xi^{\lambda}\\ \left(1+\mathbf{p}\cdot\boldsymbol{\sigma}/2m+\mathbf{p}^2/8m^2\right)\xi^{\lambda}\end{pmatrix}\\ &\approx 2m\xi^{\dagger,\lambda'}\left[1+\frac{\mathbf{p}^2+\mathbf{p}'^2}{8m^2}+\frac{(\mathbf{p}'\cdot\boldsymbol{\sigma})(\mathbf{p}\cdot\boldsymbol{\sigma})}{4m^2}\right]\xi^{\lambda}\\ &= 2m\xi^{\dagger,\lambda'}\left[1+\frac{\mathbf{p}^2+\mathbf{p}'^2+2\mathbf{p}'\cdot\mathbf{p}}{8m^2}+\frac{i}{4m^2}\boldsymbol{\sigma}\cdot(\mathbf{p}'\times\mathbf{p})\right]\xi^{\lambda}\\ &= 2m\left[\xi^{\dagger,\lambda'}\xi^{\lambda}+\frac{\mathbf{P}^2}{8m^2}\xi^{\dagger,\lambda'}\xi^{\lambda}+\frac{i}{4m^2}\mathbf{s}_u^{\lambda',\lambda}\cdot(\mathbf{P}\times\mathbf{q})\right]\end{aligned} \tag{A.35}$$

$$
\begin{aligned}
\overline{u}^{\lambda'}(p')\gamma^i u^{\lambda}(p) &= u^{\dagger,\lambda'}(p')\gamma^0\gamma^i u^{\lambda}(p) \\
&\approx m \begin{pmatrix} \left(1-\mathbf{p}'\cdot\boldsymbol{\sigma}/2m+\mathbf{p}'^2/8m^2\right)\xi^{\lambda'} \\ \left(1+\mathbf{p}'\cdot\boldsymbol{\sigma}/2m+\mathbf{p}'^2/8m^2\right)\xi^{\lambda'} \end{pmatrix}^{\dagger} \begin{pmatrix} -\sigma^i & 0 \\ 0 & \sigma^i \end{pmatrix} \begin{pmatrix} \left(1-\mathbf{p}\cdot\boldsymbol{\sigma}/2m+\mathbf{p}^2/8m^2\right)\xi^{\lambda} \\ \left(1+\mathbf{p}\cdot\boldsymbol{\sigma}/2m+\mathbf{p}^2/8m^2\right)\xi^{\lambda} \end{pmatrix} \\
&\approx 2m\xi^{\dagger,\lambda'}\left[\sigma^i\frac{\mathbf{p}\cdot\boldsymbol{\sigma}}{2m}+\frac{\mathbf{p}'\cdot\boldsymbol{\sigma}}{2m}\sigma^i\right]\xi^{\lambda} \\
&= 2m\xi^{\dagger,\lambda'}\left[\frac{\mathbf{p}\cdot\hat{\mathbf{x}}_i}{2m}+\frac{i}{2m}\boldsymbol{\sigma}\cdot(\hat{\mathbf{x}}_i\times\mathbf{p})+\frac{\mathbf{p}'\cdot\hat{\mathbf{x}}_i}{2m}+\frac{i}{2m}\boldsymbol{\sigma}\cdot(\mathbf{p}'\times\hat{\mathbf{x}}_i)\right]\xi^{\lambda} \\
&= 2m\left[\frac{\mathbf{P}}{2m}\cdot\hat{\mathbf{x}}_i\xi^{\dagger,\lambda'}\xi^{\lambda}+\hat{\mathbf{x}}_i\cdot\left(\frac{i\mathbf{q}}{m}\times\mathbf{s}_u^{\lambda',\lambda}\right)\right]
\end{aligned}
\tag{A.36}
$$

A.6.4 Axial-Vector

$$
\begin{aligned}
\overline{u}^{\lambda'}(p')\gamma^0\gamma^5 u^{\lambda}(p) &= u^{\dagger,\lambda'}(p')\gamma^0\gamma^0\gamma^5 u^{\lambda}(p) \\
&\approx m \begin{pmatrix} \left(1-\mathbf{p}'\cdot\boldsymbol{\sigma}/2m+\mathbf{p}'^2/8m^2\right)\xi^{\lambda'} \\ \left(1+\mathbf{p}'\cdot\boldsymbol{\sigma}/2m+\mathbf{p}'^2/8m^2\right)\xi^{\lambda'} \end{pmatrix}^{\dagger} \begin{pmatrix} -I_2 & 0 \\ 0 & I_2 \end{pmatrix} \begin{pmatrix} \left(1-\mathbf{p}\cdot\boldsymbol{\sigma}/2m+\mathbf{p}^2/8m^2\right)\xi^{\lambda} \\ \left(1+\mathbf{p}\cdot\boldsymbol{\sigma}/2m+\mathbf{p}^2/8m^2\right)\xi^{\lambda} \end{pmatrix} \\
&\approx 2m\xi^{\dagger,\lambda'}\left[\frac{\mathbf{p}\cdot\boldsymbol{\sigma}}{2m}+\frac{\mathbf{p}'\cdot\boldsymbol{\sigma}}{2m}\right]\xi^{\lambda} \\
&= 2m\left[\frac{\mathbf{P}}{m}\cdot\mathbf{s}_u^{\lambda',\lambda}\right]
\end{aligned}
\tag{A.37}
$$

$$
\begin{aligned}
\overline{u}^{\lambda'}(p')\gamma^i\gamma^5 u^{\lambda}(p) &= u^{\dagger,\lambda'}(p')\gamma^0\gamma^i\gamma^5 u^{\lambda}(p) \\
&\approx m \begin{pmatrix} \left(1-\mathbf{p}'\cdot\boldsymbol{\sigma}/2m+\mathbf{p}'^2/8m^2\right)\xi^{\lambda'} \\ \left(1+\mathbf{p}'\cdot\boldsymbol{\sigma}/2m+\mathbf{p}'^2/8m^2\right)\xi^{\lambda'} \end{pmatrix}^{\dagger} \begin{pmatrix} \sigma^i & 0 \\ 0 & \sigma^i \end{pmatrix} \begin{pmatrix} \left(1-\mathbf{p}\cdot\boldsymbol{\sigma}/2m+\mathbf{p}^2/8m^2\right)\xi^{\lambda} \\ \left(1+\mathbf{p}\cdot\boldsymbol{\sigma}/2m+\mathbf{p}^2/8m^2\right)\xi^{\lambda} \end{pmatrix} \\
&\approx 2m\xi^{\dagger,\lambda'}\left[\sigma^i+\sigma^i\frac{\mathbf{p}^2+\mathbf{p}'^2}{8m^2}+\frac{(\mathbf{p}'\cdot\boldsymbol{\sigma})\,\sigma^i\,(\mathbf{p}\cdot\boldsymbol{\sigma})}{4m^2}\right]\xi^{\lambda} \\
&= 2m\left[2s_u^{i,\lambda',\lambda}+s_u^{i,\lambda',\lambda}\frac{\mathbf{q}^2}{4m^2}-\frac{1}{4m^2}\left(\mathbf{q}\cdot\mathbf{s}_u^{\lambda',\lambda}\right)(\mathbf{q}\cdot\hat{\mathbf{x}}_i)\right. \\
&\left.+\frac{1}{4m^2}\left(\mathbf{P}\cdot\mathbf{s}_u^{\lambda',\lambda}\right)(\mathbf{P}\cdot\hat{\mathbf{x}}_i)+\frac{i}{8m^2}\hat{\mathbf{x}}_i\cdot(\mathbf{q}\times\mathbf{P})\,\xi^{\dagger,\lambda'}\xi^{\lambda}\right]
\end{aligned}
\tag{A.38}
$$

A.6.5 Tensor

$$\overline{u}^{\lambda'}(p')\sigma^{00}u^{\lambda}(p) = 0 \tag{A.39}$$

$$\overline{u}^{\lambda'}(p')\sigma^{ii}u^{\lambda}(p) = 0 \tag{A.40}$$

$$\begin{aligned}
\overline{u}^{\lambda'}(p')\sigma^{i0}u^{\lambda}(p) &\approx im\begin{pmatrix}\left(1-\mathbf{p}'\cdot\boldsymbol{\sigma}/2m+\mathbf{p}'^2/8m^2\right)\xi^{\lambda'}\\ \left(1+\mathbf{p}'\cdot\boldsymbol{\sigma}/2m+\mathbf{p}'^2/8m^2\right)\xi^{\lambda'}\end{pmatrix}^{\dagger}\begin{pmatrix}0 & -\sigma^i\\ \sigma^i & 0\end{pmatrix}\begin{pmatrix}\left(1-\mathbf{p}\cdot\boldsymbol{\sigma}/2m+\mathbf{p}^2/8m^2\right)\xi^{\lambda}\\ \left(1+\mathbf{p}\cdot\boldsymbol{\sigma}/2m+\mathbf{p}^2/8m^2\right)\xi^{\lambda}\end{pmatrix}\\
&\approx 2im\xi^{\dagger,\lambda'}\left[-\sigma^i\frac{\mathbf{p}\cdot\boldsymbol{\sigma}}{2m}+\frac{\mathbf{p}'\cdot\boldsymbol{\sigma}}{2m}\sigma^i\right]\xi^{\lambda}\\
&= 2im\xi^{\dagger,\lambda'}\left[-\frac{\mathbf{p}\cdot\hat{\mathbf{x}}_i}{2m}-\frac{i}{2m}\boldsymbol{\sigma}\cdot(\hat{\mathbf{x}}_i\times\mathbf{p})+\frac{\mathbf{p}'\cdot\hat{\mathbf{x}}_i}{2m}+\frac{i}{2m}\boldsymbol{\sigma}\cdot(\mathbf{p}'\times\hat{\mathbf{x}}_i)\right]\xi^{\lambda}\\
&= 2m\left[-\frac{i\mathbf{q}}{2m}\cdot\hat{\mathbf{x}}_i\xi^{\dagger,\lambda'}\xi^{\lambda}+\hat{\mathbf{x}}_i\cdot\left(\frac{\mathbf{P}}{m}\times\mathbf{s}_u^{\lambda',\lambda}\right)\right]
\end{aligned}\tag{A.41}$$

$$\begin{aligned}
\overline{u}^{\lambda'}(p')\sigma^{ij}u^{\lambda}(p) &\approx m\begin{pmatrix}\left(1-\mathbf{p}'\cdot\boldsymbol{\sigma}/2m+\mathbf{p}'^2/8m^2\right)\xi^{\lambda'}\\ \left(1+\mathbf{p}'\cdot\boldsymbol{\sigma}/2m+\mathbf{p}'^2/8m^2\right)\xi^{\lambda'}\end{pmatrix}^{\dagger}\begin{pmatrix}0 & \epsilon_{ijk}\sigma^k\\ \epsilon_{ijk}\sigma^k & 0\end{pmatrix}\begin{pmatrix}\left(1-\mathbf{p}\cdot\boldsymbol{\sigma}/2m+\mathbf{p}^2/8m^2\right)\xi^{\lambda}\\ \left(1+\mathbf{p}\cdot\boldsymbol{\sigma}/2m+\mathbf{p}^2/8m^2\right)\xi^{\lambda}\end{pmatrix}\\
&\approx 2m\epsilon_{ijk}\xi^{\dagger,\lambda'}\left[\sigma^k+\sigma^k\frac{\mathbf{p}^2}{8m^2}+\frac{\mathbf{p}'^2}{8m^2}\sigma^k-\frac{(\mathbf{p}'\cdot\boldsymbol{\sigma})\,\sigma^k\,(\mathbf{p}\cdot\boldsymbol{\sigma})}{4m^2}\right]\xi^{\lambda}\\
&= 2m\left[\epsilon_{ijk}\hat{\mathbf{x}}_k\cdot\left(2\mathbf{s}_u^{\lambda',\lambda}+\frac{\mathbf{P}^2}{4m^2}\mathbf{s}_u^{\lambda',\lambda}+\frac{i}{8m^2}\mathbf{P}\times\mathbf{q}\xi^{\dagger,\lambda'}\xi^{\lambda}+\mathbf{q}\frac{\mathbf{q}\cdot\mathbf{s}_u^{\lambda',\lambda}}{4m^2}-\mathbf{P}\frac{\mathbf{P}\cdot\mathbf{s}_u^{\lambda',\lambda}}{4m^2}\right)\right]
\end{aligned}\tag{A.42}$$

Note: $i\neq j$. For the tensor Lorentz structure with a γ^5 we will use the identity relating $\sigma^{\mu\nu}\gamma^5$ to $\sigma^{\mu\nu}$.

A.6.6 Contracted momenta

$$\begin{aligned}
\overline{u}^{\lambda'}(p')\not{k}u^{\lambda}(p) &= k_\mu u^{\dagger,\lambda'}(p')\gamma^0\gamma^\mu u^{\lambda}(p)\\
&= k_\mu\overline{u}^{\lambda}(p')\gamma^\mu u^{\lambda}(p)\\
&\approx \left(m_k(1+\mathbf{k}^2/2m_k^2),-\mathbf{k}\right)\begin{pmatrix}2m_u\xi^{\dagger,\lambda'}\xi^s+\mathbf{P}^2\xi^{\dagger,\lambda'}\xi^{\lambda}/4m_u+i\mathbf{s}_u^{\lambda',\lambda}\cdot(\mathbf{P}\times\mathbf{q})/2m_u\\ \mathbf{P}\xi^{\dagger,\lambda'}\xi^{\lambda}+2i\mathbf{q}\times\mathbf{s}_u^{\lambda',\lambda}\end{pmatrix}\\
&= 2m_um_k\xi^{\dagger,\lambda'}\xi^{\lambda}\left(1+\frac{\mathbf{k}^2}{2m_k^2}+\frac{\mathbf{P}^2}{8m_u^2}-\frac{\mathbf{k}\cdot\mathbf{P}}{2m_um_k}\right)+m_ki\mathbf{s}_u^{\lambda',\lambda}\cdot\left(\frac{\mathbf{P}}{2m_u}\times\mathbf{q}\right)\\
&- 2i\mathbf{k}\cdot\left(\mathbf{q}\times\mathbf{s}_u^{\lambda',\lambda}\right)
\end{aligned}\tag{A.43}$$

A.7 Second Order NR-Limit of Operators

Terms that are of higher than second order in momentum are discarded and are not shown in the calculations below. These calculations are fairly straightforward, since one can just multiply the Lorentz structures derived in Appendix A.6 (or Appendix A.5 if one only needs the first order terms). For every operator go through the following steps:

1. Take the NR-limit of the operator by substituting the expressions of the NR-limit of the Lorentz structures in the operator. Remember that the expressions in Table A.1 and Table A.2 are only valid in these forms for the DM particle. To obtain an expression for the SM fermion, take in these expressions $\mathbf{P}\to\mathbf{K}$ and $\mathbf{q}\to-\mathbf{q}$.

2. Multiply the Lorentz structures and discard every term that is third order (or second order if one needs only the first order expansion).

3. Write every term in terms of the building block expectation value $\langle \mathcal{O}_i \rangle$.

A.7.1 (Pseudo)Scalar-(Pseudo)Scalar

$$\begin{aligned}
\left(\overline{N}^{s'}(k')\, N^{s}(k)\right)\left(\overline{\chi}^{r'}(p')\chi^{r}(p)\right) &\approx 4m_N m_\chi \left[\xi^{\dagger,s'}\xi^{s} + \frac{\mathbf{q}^2}{8m_N^2}\xi^{\dagger,s'}\xi^{s} + \frac{i}{4m_N^2}\mathbf{s}_N^{s',s}\cdot(\mathbf{K}\times\mathbf{q})\right] \\
&\cdot\left[\xi^{\dagger,r'}\xi^{r} + \frac{\mathbf{q}^2}{8m_\chi^2}\xi^{\dagger,r'}\xi^{r} - \frac{i}{4m_\chi^2}\mathbf{s}_\chi^{r',r}\cdot(\mathbf{P}\times\mathbf{q})\right] \\
&\approx 4m_N m_\chi \left[\xi^{\dagger,s'}\xi^{s}\xi^{\dagger,r'}\xi^{r}\left(1+\frac{\mathbf{q}^2(m_N^2+m_\chi^2)}{8m_N^2 m_\chi^2}\right) - \frac{i}{4m_\chi^2}\mathbf{s}_\chi^{r',r}\cdot(\mathbf{P}\times\mathbf{q})\,\xi^{\dagger,s'}\xi^{s}\right. \\
&\left. + \frac{i}{4m_N^2}\mathbf{s}_N^{s',s}\cdot(\mathbf{K}\times\mathbf{q})\,\xi^{\dagger,r'}\xi^{r}\right] \\
&\overset{\text{CM}}{=} 4m_N m_\chi \left[\langle\mathcal{O}_1\rangle\left(1+\frac{\mathbf{q}^2(m_N^2+m_\chi^2)}{8m_N^2 m_\chi^2}\right) + \frac{\mu m_N}{2m_\chi^2}\langle\mathcal{O}_5\rangle + \frac{\mu}{2m_N}\langle\mathcal{O}_3\rangle\right]
\end{aligned} \tag{A.44}$$

$$\begin{aligned}
\left(\overline{N}^{s'}(k')\gamma^5 N^{s}(k)\right)\left(\overline{\chi}^{r'}(p')\chi^{r}(p)\right) &\approx 4m_N m_\chi \left[-\frac{\mathbf{q}}{m_N}\cdot\mathbf{s}_N^{s',s}\right]\left[\xi^{\dagger,r'}\xi^{r} + \frac{\mathbf{q}^2}{8m_\chi^2}\xi^{\dagger,r'}\xi^{r}\right. \\
&\left. - \frac{i}{4m_\chi^2}\mathbf{s}_\chi^{r',r}\cdot(\mathbf{P}\times\mathbf{q})\right] \\
&\approx 4m_N m_\chi \left[-\frac{\mathbf{q}}{m_N}\cdot\mathbf{s}_N^{s',s}\xi^{\dagger,r'}\xi^{r}\right] \\
&= 4im_N m_\chi \langle\mathcal{O}_{10}\rangle
\end{aligned} \tag{A.45}$$

$$\begin{aligned}
\left(\overline{N}^{s'}(k')N^{s}(k)\right)\left(\overline{\chi}^{r'}(p')\gamma^5\chi^{r}(p)\right) &\approx 4m_N m_\chi \left[\xi^{\dagger,s'}\xi^{s} + \frac{\mathbf{q}^2}{8m_N^2}\xi^{\dagger,s'}\xi^{s}\right. \\
&\left. + \frac{i}{4m_N^2}\mathbf{s}_N^{s',s}\cdot(\mathbf{K}\times\mathbf{q})\right]\left[\frac{\mathbf{q}}{m_\chi}\cdot\mathbf{s}_\chi^{r',r}\right] \\
&\approx 4m_N m_\chi \left[\frac{\mathbf{q}}{m_\chi}\cdot\mathbf{s}_\chi^{r',r}\xi^{\dagger,s'}\xi^{s}\right] \\
&= 4m_N m_\chi \left[-\frac{im_N}{m_\chi}\langle\mathcal{O}_{11}\rangle\right]
\end{aligned} \tag{A.46}$$

$$\begin{aligned}
\left(\overline{N}^{s'}(k')\gamma^5 N^{s}(k)\right)\left(\overline{\chi}^{r'}(p')\gamma^5\chi^{r}(p)\right) &\approx \left[-2\mathbf{q}\cdot\mathbf{s}_N^{s',s}\right]\left[2\mathbf{q}\cdot\mathbf{s}_\chi^{r',r}\right] \\
&\approx -4m_N m_\chi \left[\frac{\mathbf{q}}{m_N}\cdot\mathbf{s}_N^{s',s}\right]\left[\frac{\mathbf{q}}{m_\chi}\cdot\mathbf{s}_\chi^{r',r}\right] \\
&= 4m_N m_\chi \left[-\frac{m_N}{m_\chi}\langle\mathcal{O}_6\rangle\right]
\end{aligned} \tag{A.47}$$

A.7.2 (Axial)Vector-(Axial)Vector

$$
\begin{aligned}
\left(\overline{N}^{s'}(k')\gamma_\mu N^s(k)\right)\left(\overline{\chi}^{r'}(p')\gamma^\mu\chi^r(p)\right) &\approx 4m_N m_\chi\left[\xi^{\dagger,s'}\xi^s+\frac{\mathbf{K}^2}{8m_N^2}\xi^{\dagger,s'}\xi^s\right.\\
&-\frac{i}{4m_N^2}\mathbf{s}_N^{s',s}\cdot(\mathbf{K}\times\mathbf{q}),-\frac{\mathbf{K}}{2m_N}\xi^{\dagger,s}\xi^s+\frac{i\mathbf{q}}{m_N}\times\mathbf{s}_N^{s',s}\Big]\cdot\left[\xi^{\dagger,r'}\xi^r+\frac{\mathbf{P}^2}{8m_\chi^2}\xi^{\dagger,r'}\xi^r\right.\\
&\left.+\frac{i}{4m_\chi^2}\mathbf{s}_\chi^{r',r}\cdot(\mathbf{P}\times\mathbf{q}),\frac{\mathbf{P}}{2m_\chi}\xi^{\dagger,r'}\xi^r+\frac{i\mathbf{q}}{m_\chi}\times\mathbf{s}_\chi^{r',r}\right]\\
&\approx 4m_N m_\chi\left[\xi^{\dagger,s'}\xi^s\xi^{\dagger,r'}\xi^r\left(1+\frac{\mathbf{P}^2}{8m_\chi^2}+\frac{\mathbf{K}^2}{8m_N^2}-\frac{\mathbf{K}}{2m_N}\cdot\frac{\mathbf{P}}{2m_\chi}\right)\right.\\
&+\frac{im_N}{4m_\chi}\mathbf{s}_\chi^{r',r}\cdot\left(\frac{\mathbf{P}}{m_\chi}\times\frac{\mathbf{q}}{m_N}\right)\xi^{\dagger,r'}\xi^r-\frac{i}{4}\mathbf{s}_N^{s',s}\cdot\left(\frac{\mathbf{K}}{m_N}\times\frac{\mathbf{q}}{m_N}\right)\xi^{\dagger,r'}\xi^r\\
&-\frac{im_N}{2m_\chi}\frac{\mathbf{K}}{m_N}\cdot\left(\frac{\mathbf{q}}{m_N}\times\mathbf{s}_\chi^{r',r}\right)\xi^{\dagger,s'}\xi^s+\frac{i}{2}\frac{\mathbf{P}}{m_\chi}\cdot\left(\frac{\mathbf{q}}{m_N}\times\mathbf{s}_N^{s',s}\right)\xi^{\dagger,r'}\xi^r\\
&\left.-\frac{m_N}{m_\chi}\left(\frac{\mathbf{q}}{m_N}\times\mathbf{s}_N^{s',s}\right)\left(\frac{\mathbf{q}}{m_N}\times\mathbf{s}_\chi^{r',r}\right)\right]\\
&\overset{\text{CM}}{=} 4m_N m_\chi\left[\langle\mathcal{O}_1\rangle\left(1+\frac{1}{2}\mathbf{v}_{\text{el}}^{\perp\,2}\right)-\frac{m_N(m_N+2m_\chi)}{2m_\chi(m_N+m_\chi)}\langle\mathcal{O}_5\rangle-\frac{m_\chi+2m_N}{2(m_N+m_\chi)}\langle\mathcal{O}_3\rangle\right.\\
&\left.+\frac{m_N}{m_\chi}\langle\mathcal{O}_6\rangle-\frac{\mathbf{q}^2}{m_N m_\chi}\langle\mathcal{O}_4\rangle\right]
\end{aligned}
\tag{A.48}
$$

To go from the second to the last equal sign, we used the vector identities Eqs. (A.11a) to (A.11c).

$$
\begin{aligned}
\left(\overline{N}^{s'}(k')\gamma_\mu\gamma^5 N^s(k)\right)\left(\overline{\chi}^{r'}(p')\gamma^\mu\chi^r(p)\right) &\approx 4m_N m_\chi\left[\frac{\mathbf{K}}{m_N}\cdot\mathbf{s}_N^{s',s},2\mathbf{s}_N^{s',s}+\mathbf{s}_N^{s',s}\frac{\mathbf{q}^2}{4m_N^2}\right.\\
&\left.-\frac{1}{4m_N^2}\left(\mathbf{q}\cdot\mathbf{s}_N^{s',s}\right)\mathbf{q}+\frac{1}{4m_N^2}\left(\mathbf{K}\cdot\mathbf{s}_N^{s',s}\right)\mathbf{K}+\frac{i}{8m_N^2}\mathbf{K}\times\mathbf{q}\xi^{\dagger,s'}\xi^s\right]\\
&\cdot\left[\xi^{\dagger,r'}\xi^r-\frac{\mathbf{P}^2}{8m_\chi^2}\xi^{\dagger,r'}\xi^r+\frac{i}{4m_\chi^2}\mathbf{s}_\chi^{r',r}\cdot(\mathbf{P}\times\mathbf{q}),-\frac{\mathbf{P}}{2m_\chi}\xi^{\dagger,r'}\xi^r-\frac{i\mathbf{q}}{m_\chi}\times\mathbf{s}_\chi^{r',r}\right]\\
&\approx 4m_N m_\chi\left[\frac{\mathbf{K}}{m_N}\cdot\mathbf{s}_N^{s',s}\xi^{\dagger,r'}\xi^r-\frac{\mathbf{P}}{m_\chi}\cdot\mathbf{s}_N^{s',s}\xi^{\dagger,r'}\xi^r-\frac{2i}{m_\chi}\mathbf{s}_N^{s',s}\cdot\left(\mathbf{q}\times\mathbf{s}_\chi^{r',r}\right)\right]\\
&\overset{\text{CM}}{=} 4m_N m_\chi\left[-2\langle\mathcal{O}_7\rangle-\frac{2m_N}{m_\chi}\langle\mathcal{O}_9\rangle\right]
\end{aligned}
\tag{A.49}
$$

$$
\begin{aligned}
\left(\overline{N}^{s'}(k')\gamma^\mu N^s(k)\right)\left(\overline{\chi}^{r'}(p')\gamma_\mu\gamma^5\chi^r(p)\right) &\approx 4m_N m_\chi\left[\xi^{\dagger,s'}\xi^s-\frac{\mathbf{K}^2}{8m_N^2}\xi^{\dagger,s'}\xi^s\right.\\
&-\frac{i}{4m_N^2}\mathbf{s}_N^{s',s}\cdot(\mathbf{K}\times\mathbf{q}),\frac{\mathbf{K}}{2m_N}\xi^{\dagger,s'}\xi^s-\frac{i\mathbf{q}}{m_N}\times\mathbf{s}_N^{s',s}\Big]\cdot\left[\frac{\mathbf{P}}{m_\chi}\cdot\mathbf{s}_\chi^{r',r},-2\mathbf{s}_\chi^{r',r}\right.\\
&\left.-\mathbf{s}_\chi^{r',r}\frac{\mathbf{q}^2}{4m_\chi^2}-\frac{1}{4m_\chi^2}\left(\mathbf{P}\cdot\mathbf{s}_\chi^{r',r}\right)\mathbf{P}+\frac{1}{4m_\chi^2}\left(\mathbf{q}\cdot\mathbf{s}_\chi^{r',r}\right)\mathbf{q}-\frac{i}{8m_\chi^2}\mathbf{P}\times\mathbf{q}\xi^{\dagger,r'}\xi^r\right]\\
&\approx 4m_N m_\chi\left[\frac{\mathbf{P}}{m_\chi}\cdot\mathbf{s}_\chi^{r',r}\xi^{\dagger,s'}\xi^s-\frac{\mathbf{K}}{m_N}\cdot\mathbf{s}_\chi^{r',r}\xi^{\dagger,s'}\xi^s+\frac{2i}{m_N}\mathbf{s}_\chi^{r',r}\cdot\left(\mathbf{q}\times\mathbf{s}_N^{s',s}\right)\right]\\
&\overset{\text{CM}}{=} 4m_N m_\chi\left[2\langle\mathcal{O}_8\rangle-2\langle\mathcal{O}_9\rangle\right]
\end{aligned}
\tag{A.50}
$$

$$
\begin{aligned}
\left(\overline{N}^{s'}(k')\gamma^{\mu}\gamma^{5}N^{s}(k)\right)\left(\overline{\chi}^{r'}(p')\gamma_{\mu}\gamma^{5}\chi^{r}(p)\right) &\approx 4m_N m_\chi\left[\frac{\mathbf{K}}{m_N}\cdot\mathbf{s}_N^{s',s},2\mathbf{s}_N^{s',s}+\mathbf{s}_N^{s',s}\frac{\mathbf{q}^2}{4m_N^2}\right.\\
&+\frac{1}{4}\left(\frac{\mathbf{K}}{m_N}\cdot\mathbf{s}_N^{s',s}\right)\frac{\mathbf{K}}{m_N}-\frac{1}{4}\left(\frac{\mathbf{q}}{m_N}\cdot\mathbf{s}_N^{s',s}\right)\frac{\mathbf{q}}{m_N}+\frac{i}{8}\frac{\mathbf{K}}{m_N}\times\frac{\mathbf{q}}{m_N}\xi^{\dagger,s'}\xi^{s}\Big]\\
&\cdot\left[\frac{\mathbf{P}}{m_\chi}\cdot\mathbf{s}_\chi^{r',r},-2\mathbf{s}_\chi^{r',r}-\mathbf{s}_\chi^{r',r}\frac{\mathbf{q}^2}{4m_\chi^2}-\frac{1}{4}\left(\frac{\mathbf{P}}{m_\chi}\cdot\mathbf{s}_\chi^{r',r}\right)\frac{\mathbf{P}}{m_\chi}\right.\\
&+\frac{m_N^2}{4m_\chi^2}\left(\frac{\mathbf{q}}{m_N}\cdot\mathbf{s}_\chi^{r',r}\right)\frac{\mathbf{q}}{m_N}+\frac{im_N}{8m_\chi}\frac{\mathbf{P}}{m_\chi}\times\frac{\mathbf{q}}{m_N}\xi^{\dagger,r'}\xi^{r}\Big]\\
&\approx 4m_N m_\chi\left[\left(\frac{\mathbf{K}}{m_N}\cdot\mathbf{s}_N^{s',s}\right)\left(\frac{\mathbf{P}}{m_\chi}\cdot\mathbf{s}_\chi^{r',r}\right)-\left(4+\frac{\mathbf{q}^2}{2m_\chi^2}+\frac{\mathbf{q}^2}{2m_N^2}\right)\mathbf{s}_N^{s's}\cdot\mathbf{s}_\chi^{r',r}\right.\\
&-\frac{1}{2}\left(\frac{\mathbf{P}}{m_\chi}\cdot\mathbf{s}_\chi^{r',r}\right)\left(\mathbf{s}_N^{s',s}\cdot\frac{\mathbf{P}}{m_\chi}\right)+\frac{m_N^2}{2m_\chi^2}\left(\frac{\mathbf{q}}{m_N}\cdot\mathbf{s}_\chi^{r',r}\right)\left(\frac{\mathbf{q}}{m_N}\cdot\mathbf{s}_N^{s',s}\right)\\
&+\frac{im_N}{4m_\chi}\mathbf{s}_N^{s',s}\cdot\left(\frac{\mathbf{P}}{m_\chi}\times\frac{\mathbf{q}}{m_N}\right)\xi^{\dagger,r'}\xi^{r}-\frac{i}{4}\mathbf{s}_\chi^{r',r}\cdot\left(\frac{\mathbf{K}}{m_N}\times\frac{\mathbf{q}}{m_N}\right)\xi^{\dagger,s'}\xi^{s}\\
&\left.-\frac{1}{2}\left(\frac{\mathbf{K}}{m_N}\cdot\mathbf{s}_r^{s',s}\right)\left(\frac{\mathbf{K}}{m_N}\cdot\mathbf{s}_\chi^{r',r}\right)+\frac{1}{2}\left(\frac{\mathbf{q}}{m_N}\cdot\mathbf{s}_N^{s',s}\right)\left(\frac{\mathbf{q}}{m_N}\cdot\mathbf{s}_\chi^{r',r}\right)\right]\\
&\overset{\text{CM}}{=} 4m_N m_\chi\left[-\langle\mathcal{O}_4\rangle\left(4+\frac{\mathbf{q}^2(m_N^2+m_\chi^2)}{2m_\chi^2m_N^2}\right)-\frac{m_N^2}{2m_\chi(m_N+m_\chi)}\langle\mathcal{O}_3\rangle\right.\\
&\left.-\frac{m_\chi}{2(m_N+m_\chi)}\langle\mathcal{O}_5\rangle+\frac{m_\chi^2+m_N^2}{2m_\chi^2}\langle\mathcal{O}_6\rangle-2\langle\mathcal{O}_{16}\rangle\right]
\end{aligned}
\tag{A.51}
$$

A.7.3 Tensor

Let us first analyze which parts are needed. For the pure tensor operator:

$$
\begin{aligned}
\left(\overline{N}^{s'}(k')\sigma^{\mu\nu}N^{s}(k)\right)\left(\overline{\chi}^{r'}(p')\sigma_{\mu\nu}\chi^{r}(p)\right) &= \left(\overline{N}^{r'}(k')\sigma^{ij}N^{s}(k)\right)\left(\overline{\chi}^{s'}(p')\sigma_{ij}\chi^{s}(p)\right)\\
&+2\left(\overline{N}^{s'}(k')\sigma^{i0}N^{s}(k)\right)\left(\overline{\chi}^{r'}(p')\sigma_{i0}\chi^{r}(p)\right)\\
&=\sum_{i,j\neq i}\left(\overline{N}^{s'}(k')\sigma^{ij}u^{s}(k)\right)\left(\overline{\chi}^{r'}(p')\sigma^{ij}\chi^{r}(p)\right)-2\sum_{i}\left(\overline{N}^{s'}(k')\sigma^{i0}N^{s}(k)\right)\left(\overline{\chi}^{r'}(p')\sigma^{i0}\chi^{r}(p)\right)
\end{aligned}
\tag{A.52}
$$

And for the $\sigma^{\mu\nu}\gamma^5$ structures:

$$
\begin{aligned}
\left(\overline{N}^{s'}(k')\sigma^{\mu\nu}\gamma^{5}N^{s}(k)\right)\left(\overline{\chi}^{r'}(p')\sigma_{\mu\nu}\chi^{r}(s)\right) &= \frac{i}{2}\epsilon^{\alpha\beta\mu\nu}\left(\overline{N}^{s'}(k')\sigma_{\alpha\beta}N^{s}(k)\right)\left(\overline{\chi}^{r'}(p')\sigma_{\mu\nu}\chi^{r}(p)\right)\\
&=\frac{i}{2}\left[2\epsilon^{i0\mu\nu}\left(\overline{u}^{s'}(k')\sigma_{i0}u^{s}(p)\right)\left(\overline{\chi}^{r'}(p')\sigma_{\mu\nu}\chi^{r}(p)\right)+\epsilon^{ij\mu\nu}\left(\overline{N}^{s'}(p')\sigma_{ij}N^{r}(p)\right)\left(\overline{\chi}^{r'}(p')\sigma_{\mu\nu}\chi^{r}(p)\right)\right]\\
&=i\epsilon^{ijk0}\left[\left(\overline{N}^{s'}(k')\sigma_{i0}N^{s}(k)\right)\left(\overline{\chi}^{r'}(p')\sigma_{jk}\chi^{r}(p)\right)+\left(\overline{N}^{s'}(k')\sigma_{ij}N^{s}(k)\right)\left(\overline{\chi}^{r'}(p')\sigma_{k0}\chi^{r}(p)\right)\right]\\
&=-i\epsilon^{ijk}\left[\left(\overline{N}^{s'}(k')\sigma_{i0}N^{s}(k)\right)\left(\overline{\chi}^{r'}(p')\sigma_{jk}\chi^{r}(p)\right)+\left(\overline{N}^{s'}(k')\sigma_{ij}N^{s}(k)\right)\left(\overline{\chi}^{r'}(p')\sigma_{k0}\chi^{r}(p)\right)\right]
\end{aligned}
\tag{A.53}
$$

$$\begin{aligned}\left(\overline{N}^{s'}(k')\,\sigma^{\mu\nu}N^{s}(k)\right)\left(\overline{\chi}^{r'}(p')\sigma_{\mu\nu}\gamma^{5}\chi^{r}(p)\right) &= \frac{i}{2}\eta_{\mu\alpha}\eta_{\nu\beta}\epsilon^{\gamma\rho\alpha\beta}\left(\overline{N}^{s'}(k')\sigma^{\mu\nu}N^{s}(k)\right)\left(\overline{\chi}^{r'}(p')\sigma_{\gamma\rho}\chi^{r}(p)\right)\\ &= \frac{i}{2}\epsilon^{\gamma\rho\alpha\beta}\left(\overline{N}^{s'}(k')\sigma_{\alpha\beta}N^{s}(k)\right)\left(\overline{\chi}^{r'}(p')\sigma_{\gamma\rho}\chi^{r}(p)\right)\\ &= \frac{i}{2}\epsilon^{\alpha\beta\mu\nu}\left(\overline{N}^{s'}(k')\sigma_{\alpha\beta}N^{s}(k)\right)\left(\overline{\chi}^{r'}(p')\sigma_{\mu\nu}\chi^{r}(p)\right)\end{aligned} \tag{A.54}$$

$$\begin{aligned}\left(\overline{N}^{s'}(k')\,\sigma^{\mu\nu}\gamma^{5}N^{s}(k)\right)\left(\overline{\chi}^{r'}(p')\sigma_{\mu\nu}\gamma^{5}\chi^{r}(p)\right) &= -\frac{1}{4}\eta_{\mu\delta}\eta_{\nu\sigma}\epsilon^{\alpha\beta\mu\nu}\epsilon^{\gamma\rho\delta\sigma}\left(\overline{N}^{s'}(k')\sigma_{\alpha\beta}N^{s}(k)\right)\left(\overline{\chi}^{r'}(p')\sigma_{\gamma\rho}\chi^{r}(p)\right)\\ &= -\frac{1}{4}\eta^{\gamma\lambda}\eta^{\rho\kappa}\epsilon^{\alpha\beta\mu\nu}\epsilon_{\lambda\kappa\mu\nu}\left(\overline{N}^{s'}(k')\sigma_{\alpha\beta}N^{s}(k)\right)\left(\overline{\chi}^{r'}(p')\sigma_{\gamma\rho}\chi^{r}(p)\right)\\ &= \frac{1}{4}\eta^{\gamma\lambda}\eta^{\rho\kappa}\left(2\delta^{\alpha\beta}_{\lambda\kappa}\right)\left(\overline{N}^{s'}(k')\sigma_{\alpha\beta}N^{s}(k)\right)\left(\overline{\chi}^{r'}(p')\sigma_{\gamma\rho}\chi^{r}(p)\right)\\ &= \frac{1}{2}\eta^{\gamma\lambda}\eta^{\rho\kappa}\left(\delta^{\alpha}_{\lambda}\delta^{\beta}_{\kappa}-\delta^{\alpha}_{\kappa}\delta^{\beta}_{\lambda}\right)\left(\overline{N}^{s'}(k')\sigma_{\alpha\beta}N^{s}(k)\right)\left(\overline{\chi}^{r'}(p')\sigma_{\gamma\rho}\chi^{r}(p)\right)\\ &= \left(\overline{N}^{s'}(k')\sigma^{\gamma\rho}N^{s}(k)\right)\left(\overline{\chi}^{r'}(p')\sigma_{\gamma\rho}\chi^{r}(p)\right)\end{aligned} \tag{A.55}$$

Using that

$$\epsilon^{i_1\cdots i_s k_1\cdot k_n}\epsilon_{j_1\cdots j_s k_1\cdot k_n} = -n!\delta^{i_1\cdots i_s}_{j_1\cdots j_s} = -n!\det\begin{bmatrix}\delta^{i_1}_{j_1} & \cdots & \delta^{i_1}_{j_s}\\ \vdots & \ddots & \vdots\\ \delta^{i_1}_{j_s} & \cdots & \delta^{i_s}_{j_s}\end{bmatrix} \tag{A.56}$$

This means that only two operators need to be calculated in order to calculate all four operators. Starting with the tensor-tensor operator:

$$\begin{aligned}\left(\overline{N}^{s'}(k')\,\sigma^{\mu\nu}N^{s}(k)\right)\left(\overline{\chi}^{s'}(p')\sigma_{\mu\nu}\chi^{s}(p)\right) &\approx 4m_N m_\chi\left[2\left(2\mathbf{s}_N^{s',s}+\frac{\mathbf{K}^2}{4m_N^2}\mathbf{s}_N^{s',s}-\frac{i}{8m_N^2}\mathbf{K}\times\mathbf{q}\xi^{\dagger,s'}\xi^{s}\right.\right.\\ &+\mathbf{q}\frac{\mathbf{q}\cdot\mathbf{s}_N^{s',s}}{4m_N^2}-\mathbf{K}\frac{\mathbf{K}\cdot\mathbf{s}_N^{s',s}}{4m_N^2}\Bigg)\cdot\left(2\mathbf{s}_\chi^{r',r}+\frac{\mathbf{P}^2}{4m_\chi^2}\mathbf{s}_\chi^{r',r}+\frac{i}{8m_\chi^2}\mathbf{P}\times\mathbf{q}\xi^{\dagger,r'}\xi^{r}-\mathbf{P}\frac{\mathbf{P}\cdot\mathbf{s}_\chi^{r',r}}{4m_\chi^2}\right.\\ &\left.\left.+\mathbf{q}\frac{\mathbf{q}\cdot\mathbf{s}_\chi^{r',r}}{4m_\chi^2}\right)-2\left(\frac{i\mathbf{q}}{2m_N}\xi^{\dagger,s'}\xi^{s}+\left(\frac{\mathbf{K}}{m_N}\times\mathbf{s}_N^{s',s}\right)\right)\left(-\frac{i\mathbf{q}}{2m_\chi}\xi^{\dagger,r'}\xi^{r}+\left(\frac{\mathbf{P}}{m_\chi}\times\mathbf{s}_\chi^{r',r}\right)\right)\right]\\ &\approx 4m_N m_\chi\left[\mathbf{s}_N^{s',s}\cdot\mathbf{s}_\chi^{r',r}\left(8+\frac{\mathbf{P}^2}{m_\chi^2}+\frac{\mathbf{K}^2}{m_N^2}\right)+\frac{im_N}{2m_\chi}\mathbf{s}_N^{s',s}\cdot\left(\frac{\mathbf{P}}{m_\chi}\times\frac{\mathbf{q}}{m_N}\right)\xi^{\dagger,r'}\xi^{r}\right.\\ &-\frac{\mathbf{q}^2}{2m_N m_\chi}\xi^{\dagger,s'}\xi^{s}\xi^{\dagger,r'}\xi^{r}-\left(\mathbf{s}_N^{s',s}\cdot\frac{\mathbf{P}}{m_\chi}\right)\left(\mathbf{s}_\chi^{r',r}\cdot\frac{\mathbf{P}}{m_\chi}\right)-\left(\mathbf{s}_\chi^{r',r}\cdot\frac{\mathbf{K}}{m_N}\right)\left(\mathbf{s}_N^{s',s}\cdot\frac{\mathbf{K}}{m_N}\right)\\ &-\frac{i}{2}\mathbf{s}_\chi^{r',r}\cdot\left(\frac{\mathbf{K}}{m_N}\times\frac{\mathbf{q}}{m_N}\right)\xi^{\dagger,s'}\xi^{s}+\frac{m_\chi^2+m_N^2}{m_\chi^2}\left(\mathbf{s}_\chi^{r',r}\cdot\frac{\mathbf{q}}{m_N}\right)\left(\mathbf{s}_N^{s',s}\cdot\frac{\mathbf{q}}{m_N}\right)\\ &\left.-\frac{i\mathbf{q}}{m_N}\cdot\left(\frac{\mathbf{P}}{m_\chi}\times\mathbf{s}_\chi^{r',r}\right)\xi^{\dagger,s'}\xi^{s}+\frac{i\mathbf{q}}{m_\chi}\cdot\left(\frac{\mathbf{K}}{m_N}\times\mathbf{s}_N^{s',s}\right)\xi^{\dagger,r'}\xi^{r}-2\left(\frac{\mathbf{K}}{m_N}\times\mathbf{s}_N^{s',s}\right)\left(\frac{\mathbf{P}}{m_\chi}\times\mathbf{s}_\chi^{r',r}\right)\right]\\ &\overset{\text{CM}}{=} 4m_N m_\chi\left[\langle\mathcal{O}_4\rangle\left(8+4\mathbf{v}_{\text{el}}^{\perp\,2}\right)-\frac{\mathbf{q}^2}{2m_N m_\chi}\langle\mathcal{O}_1\rangle+\frac{m_N^2+m_\chi^2}{m_\chi^2}\langle\mathcal{O}_6\rangle-4\langle\mathcal{O}_{16}\rangle\right.\\ &\left.-\frac{m_\chi+2m_N}{m_N+m_\chi}\langle\mathcal{O}_5\rangle-\frac{m_N(2m_\chi+m_N)}{m_\chi(m_N+m_\chi)}\langle\mathcal{O}_3\rangle\right]\end{aligned} \tag{A.57}$$

$$\begin{aligned}
\left(\overline{N}^{s'}(k')\,\sigma^{\mu\nu}\gamma^5 N^s(k)\right)\left(\overline{\chi}^{r'}(p')\sigma_{\mu\nu}\chi^r(p)\right) &\approx -4m_N m_\chi i\epsilon^{ijk}\left[\left\{\hat{\mathbf{x}}_i\cdot\left(-\frac{i\mathbf{q}}{2m_N}\xi^{\dagger,s'}\xi^s-\frac{\mathbf{K}}{m_N}\times\mathbf{s}_N^{s',s}\right)\right\}\cdot\right.\\
&\left\{\epsilon_{jkl}\hat{\mathbf{x}}_l\cdot\left(2\mathbf{s}_\chi^{r',r}+\frac{\mathbf{P}^2}{4m_\chi^2}\mathbf{s}_\chi^{r',r}+\frac{i}{8m_\chi^2}\mathbf{P}\times\mathbf{q}\xi^{\dagger,r'}\xi^r-\mathbf{P}\frac{\mathbf{P}\cdot\mathbf{s}_\chi^{r',r}}{4m_\chi^2}+\mathbf{q}\frac{\mathbf{q}\cdot\mathbf{s}_\chi^{r',r}}{4m_\chi^2}\right)\right\}\\
&+\left\{\epsilon_{ijm}\hat{\mathbf{x}}_m\cdot\left(2\mathbf{s}_N^{s',s}+\frac{\mathbf{K}^2}{4m_N^2}\mathbf{s}_N^{s',s}-\frac{i}{8m_N^2}\mathbf{K}\times\mathbf{q}\xi^{\dagger,s'}\xi^s+\mathbf{q}\frac{\mathbf{q}\cdot\mathbf{s}_N^{s',s}}{4m_N^2}-\mathbf{K}\frac{\mathbf{K}\cdot\mathbf{s}_N^{s',s}}{4m_N^2}\right)\right\}\cdot\\
&\left.\left\{\hat{\mathbf{x}}_k\cdot\left(\frac{i\mathbf{q}}{2m_\chi}\xi^{\dagger,r'}\xi^r-\frac{\mathbf{P}}{m_\chi}\times\mathbf{s}_\chi^{r',r}\right)\right\}\right]\\
&\approx -8m_N m_\chi i\left[-\frac{i\mathbf{q}}{m_N}\cdot\mathbf{s}_\chi^{r',r}\xi^{\dagger,s'}\xi^s-2\mathbf{s}_\chi^{r',r}\cdot\left(\frac{\mathbf{K}}{m_N}\times\mathbf{s}_N^{s',s}\right)+\frac{i\mathbf{q}}{m_\chi}\cdot\mathbf{s}_N^{s',s}\xi^{\dagger,r'}\xi^r\right.\\
&\left.-2\mathbf{s}_N^{s',s}\cdot\left(\frac{\mathbf{P}}{m_\chi}\times\mathbf{s}_\chi^{r',r}\right)\right]\\
&=4m_N m_\chi\left[2i\left\langle\mathcal{O}_{11}\right\rangle+8i\left\langle\mathcal{O}_{12}\right\rangle-\frac{2im_N}{m_\chi}\left\langle\mathcal{O}_{10}\right\rangle\right]
\end{aligned}\tag{A.58}$$

$$\left(\overline{N}^{s'}(k')\sigma^{\mu\nu}N^s(k)\right)\left(\overline{\chi}^{r'}(p')\sigma_{\mu\nu}\gamma^5\chi^r(p)\right)\approx 4m_N m_\chi\left[2i\left\langle\mathcal{O}_{11}\right\rangle+8i\left\langle\mathcal{O}_{12}\right\rangle-\frac{2im_N}{m_\chi}\left\langle\mathcal{O}_{10}\right\rangle\right]\tag{A.59}$$

A.7.4 Contracted Momenta

$$\begin{aligned}
\left(\overline{N}^{s'}(k')\,N^s(k)\right)\left(\chi^{r'}(p')\not{k}\chi^r(p)\right) &\approx \left[2m_N\xi^{\dagger,s'}\xi^s+\frac{\mathbf{q}^2}{4m_N}\xi^{\dagger,s'}\xi^s+\frac{i}{2m_N}\mathbf{s}_N^{s',s}\cdot(\mathbf{K}\times\mathbf{q})\right]\\
&\cdot\left[2m_\chi m_N\xi^{\dagger,r'}\xi^r\left(1+\frac{\mathbf{k}^2}{2m_N^2}+\frac{\mathbf{P}^2}{8m_\chi^2}-\frac{\mathbf{k}\cdot\mathbf{P}}{2m_N m_\chi}\right)+m_N i\mathbf{s}_\chi^{r',r}\cdot\left(\frac{\mathbf{P}}{2m_\chi}\times\mathbf{q}\right)\right.\\
&\left.-2i\mathbf{k}\cdot\left(\mathbf{q}\times\mathbf{s}_\chi^{r',r}\right)\right]\\
&\approx 4m_N^2 m_\chi\xi^{\dagger,s'}\xi^s\xi^{\dagger,r'}\xi^r\left(1+\frac{\mathbf{k}^2}{2m_N^2}+\frac{\mathbf{P}^2}{8m_\chi^2}-\frac{\mathbf{k}\cdot\mathbf{P}}{2m_N m_\chi}+\frac{\mathbf{q}^2}{8m_N^2}\right)\\
&+im_\chi m_N^2\mathbf{s}_N^{s',s}\cdot\left(\frac{\mathbf{K}}{m_N}\times\frac{\mathbf{q}}{m_N}\right)\xi^{\dagger,r'}\xi^r\\
&+2m_N^3 i\mathbf{s}_\chi^{r',r}\cdot\left(-\frac{\mathbf{P}}{m_\chi}\times\frac{\mathbf{q}}{m_N}+2\mathbf{v}_{\text{el}}^\perp\times\frac{\mathbf{q}}{m_N}\right)\xi^{\dagger,s'}\xi^s\\
&\overset{\text{CM}}{=}4m_N^2 m_\chi\left\langle\mathcal{O}_1\right\rangle\left(1+\frac{1}{2}\left(\mathbf{v}_{\text{el}}^\perp+\frac{\mathbf{q}}{2m_N}\right)^2+\frac{\mathbf{q}^2}{8m_N^2}\right)\\
&-2m_N^3\frac{2m_\chi-\mu}{m_\chi}\left\langle\mathcal{O}_5\right\rangle+2m_\chi m_N\mu\left\langle\mathcal{O}_3\right\rangle
\end{aligned}\tag{A.60}$$

Using that

$$\frac{\mathbf{k}}{m_N}=-\mathbf{v}_{\text{el}}^\perp-\frac{\mathbf{q}}{2m_N}+\frac{\mathbf{P}}{2m_\chi}\tag{A.61}$$

$$\begin{aligned}
\left(\overline{N}^{s'}(k')\not{p}N^{s}(k)\right)\left(\chi^{r'}(p')\chi^{r}(p)\right) &\approx \left[2m_N m_\chi \xi^{\dagger,s'}\xi^{s}\left(1+\frac{\mathbf{p}^2}{2m_\chi^2}+\frac{\mathbf{K}^2}{8m_N^2}-\frac{\mathbf{p}\cdot\mathbf{K}}{2m_N m_\chi}\right)\right.\\
&\left.-m_\chi i\mathbf{s}_N^{s',s}\cdot\left(\frac{\mathbf{K}}{2m_N}\times\mathbf{q}\right)+2i\mathbf{p}\cdot\left(\mathbf{q}\times\mathbf{s}_N^{s',s}\right)\right]\\
&\cdot\left[2m_\chi\xi^{\dagger,r'}\xi^{r}+\frac{\mathbf{q}^2}{4m_\chi}\xi^{\dagger,r'}\xi^{r}-\frac{i}{2m_\chi}\mathbf{s}_\chi^{r',r}\cdot(\mathbf{P}\times\mathbf{q})\right]\\
&\approx 4m_N m_\chi^2\xi^{\dagger,s'}\xi^{s}\xi^{\dagger,r'}\xi^{r}\left(1+\frac{\mathbf{p}^2}{2m_\chi^2}+\frac{\mathbf{K}^2}{8m_N^2}-\frac{\mathbf{p}\cdot\mathbf{K}}{2m_N m_\chi}+\frac{\mathbf{q}^2}{8m_\chi^2}\right)\\
&+im_N\mathbf{s}_\chi^{r',r}\cdot(\mathbf{q}\times\mathbf{P})-im_\chi^2\mathbf{s}_N^{s',s}\cdot\left(\frac{\mathbf{K}}{m_N}\times\mathbf{q}\right)-4im_\chi\mathbf{s}_N^{s',s}\cdot(\mathbf{q}\times\mathbf{p})\\
&\overset{\text{CM}}{=} 4m_N m_\chi^2\left\langle\mathcal{O}_1\right\rangle\left(1+\frac{1}{2}\left(\mathbf{v}_{\text{el}}^{\perp}+\frac{\mathbf{q}}{2m_\chi}\right)^2+\frac{\mathbf{q}^2}{8m_\chi^2}\right)\\
&-2m_\chi^2(2m_N-\mu)\left\langle\mathcal{O}_3\right\rangle+2\mu m_N^2\left\langle\mathcal{O}_5\right\rangle
\end{aligned}\tag{A.62}$$

Using that

$$\frac{\mathbf{p}}{m_\chi}=\mathbf{v}_{\text{el}}^{\perp}+\frac{\mathbf{q}}{2m_\chi}+\frac{\mathbf{K}}{2m_N}\tag{A.63}$$

$$\begin{aligned}
\left(\overline{N}^{s'}(k')\not{p}N^{s}(k)\right)\left(\chi^{r'}(p')\not{k}\chi^{r}(p)\right) &\approx \left[2m_N m_\chi \xi^{\dagger,s'}\xi^{s}\left(1+\frac{\mathbf{p}^2}{2m_\chi^2}+\frac{\mathbf{K}^2}{8m_N^2}-\frac{\mathbf{p}\cdot\mathbf{K}}{2m_N m_\chi}\right)\right.\\
&\left.-m_\chi i\mathbf{s}_N^{s',s}\cdot\left(\frac{\mathbf{K}}{2m_N}\times\mathbf{q}\right)+2i\mathbf{p}\cdot\left(\mathbf{q}\times\mathbf{s}_N^{s',s}\right)\right]\\
&\cdot\left[2m_\chi m_N\xi^{\dagger,r'}\xi^{r}\left(1+\frac{\mathbf{k}^2}{2m_N^2}+\frac{\mathbf{P}^2}{8m_\chi^2}-\frac{\mathbf{k}\cdot\mathbf{P}}{2m_N m_\chi}\right)+m_N i\mathbf{s}_\chi^{r',r}\cdot\left(\frac{\mathbf{P}}{2m_\chi}\times\mathbf{q}\right)\right.\\
&\left.-2i\mathbf{k}\cdot\left(\mathbf{q}\times\mathbf{s}_\chi^{r',r}\right)\right]\\
&\approx 4m_N^2 m_\chi^2\xi^{\dagger,s'}\xi^{s}\xi^{\dagger,r'}\xi^{\dagger}\left(1+\frac{1}{2}\left((\mathbf{v}_{\text{el}}^{\perp})^2+\frac{\mathbf{q}}{2m_\chi}\right)^2+\frac{1}{2}\left((\mathbf{v}_{\text{el}}^{\perp})^2+\frac{\mathbf{q}}{2m_N}\right)^2\right)\\
&+2im_N m_\chi^2\xi^{\dagger,s'}\xi^{s}\mathbf{s}_\chi^{r',r}\cdot\left(\left[\frac{\mathbf{P}}{2m_\chi}-\frac{2\mathbf{k}}{m_N}\right]\times\mathbf{q}\right)-2im_N m_\chi^2\xi^{\dagger,r'}\xi^{r}\mathbf{s}_N^{s',s}\cdot\left(\left[\frac{\mathbf{K}}{2m_N}-\frac{2\mathbf{p}}{m_\chi}\right]\times\mathbf{q}\right)\\
&\overset{\text{CM}}{=} 4m_N^2 m_\chi^2\xi^{\dagger,s'}\xi^{s}\xi^{\dagger,r'}\xi^{\dagger}\left(1+\frac{1}{2}\left((\mathbf{v}_{\text{el}}^{\perp})^2+\frac{\mathbf{q}}{2m_\chi}\right)^2+\frac{1}{2}\left((\mathbf{v}_{\text{el}}^{\perp})^2+\frac{\mathbf{q}}{2m_N}\right)^2\right)\\
&+2m_N^3(2m_\chi-\mu)\left\langle\mathcal{O}_5\right\rangle-2m_N m_\chi^2(2m_N-\mu)\left\langle\mathcal{O}_3\right\rangle
\end{aligned}\tag{A.64}$$

$$\begin{aligned}
\left(\overline{N}^{s'}(k')\not{p}\gamma^5 N^{s}(k)\right)\left(\overline{\chi}^{r'}(p')\chi^{r}(p)\right) &\approx \left[2m_\chi\mathbf{K}\cdot\mathbf{s}_N^{s',s}-4m_N\mathbf{p}\cdot\mathbf{s}_N^{s',s}\right]\\
&\cdot\left[2m_\chi\xi^{\dagger,r'}\xi^{r}+\frac{\mathbf{q}^2}{4m_\chi}\xi^{\dagger,r'}\xi^{r}-\frac{i}{2m_N}\mathbf{s}_\chi^{r',r}\cdot(\mathbf{P}\times\mathbf{q})\right]\\
&\approx 4m_\chi^2\left(\mathbf{K}\cdot\mathbf{s}_N^{s',s}\right)\xi^{\dagger,r'}\xi^{r}-8m_\chi m_N\left(\mathbf{p}\cdot\mathbf{s}_N^{s',s}\right)\xi^{\dagger,r'}\xi^{r}\\
&=-4m_\chi m_N\left(\mathbf{q}+2m_\chi\mathbf{v}_{\text{el}}^{\perp}\right)\cdot\mathbf{s}_N^{s',s}\xi^{\dagger,r'}\xi^{r}\\
&=4m_\chi m_N\left[im_N\left\langle\mathcal{O}_{10}\right\rangle-2m_\chi\left\langle\mathcal{O}_7\right\rangle\right]
\end{aligned}\tag{A.65}$$

$$\begin{aligned}
\left(\overline{N}^{s'}(k')\gamma^5 N^s(k)\right)\left(\overline{\chi}^{r'}(p')\not{k}\chi^r(p)\right) &\approx \left[-2\mathbf{q}\cdot\mathbf{s}_N^{s',s}\right] \\
&\cdot\left[2m_\chi m_N\xi^{\dagger,r'}\xi^r\left(1+\frac{\mathbf{k}^2}{2m_N^2}+\frac{\mathbf{P}^2}{8m_\chi^2}-\frac{\mathbf{k}\cdot\mathbf{P}}{2m_N m_\chi}\right)+m_N i\mathbf{s}_\chi^{r',r}\cdot\left(\frac{\mathbf{P}}{2m_\chi}\times\mathbf{q}\right)\right. \\
&\left.-2i\mathbf{k}\cdot\left(\mathbf{q}\times\mathbf{s}_\chi^{r',r}\right)\right] \\
&\approx -4m_\chi m_N\left(\mathbf{q}\cdot\mathbf{s}_N^{s',s}\right)\xi^{\dagger,r'}\xi^r \\
&= -4m_\chi m_N\left[-im_N\left\langle\mathcal{O}_{10}\right\rangle\right]
\end{aligned} \tag{A.66}$$

$$\begin{aligned}
\left(\overline{N}^{s'}(k')\not{p}\gamma^5 N^s(k)\right)\left(\overline{\chi}^{r'}(p')\not{k}\chi^r(p)\right) &\approx \left[2m_\chi\mathbf{K}\cdot\mathbf{s}_N^{s',s}-4m_N\mathbf{p}\cdot\mathbf{s}_N^{s',s}\right] \\
&\cdot\left[2m_\chi m_N\xi^{\dagger,r'}\xi^r\left(1+\frac{\mathbf{k}^2}{2m_N^2}+\frac{\mathbf{P}^2}{8m_\chi^2}-\frac{\mathbf{k}\cdot\mathbf{P}}{2m_N m_\chi}\right)+m_N i\mathbf{s}_\chi^{r',r}\cdot\left(\frac{\mathbf{P}}{2m_\chi}\times\mathbf{q}\right)\right. \\
&\left.-2i\mathbf{k}\cdot\left(\mathbf{q}\times\mathbf{s}_\chi^{r',r}\right)\right] \\
&\approx 8m_\chi^2 m_N^2\left(\frac{\mathbf{K}}{2m_N}-\frac{\mathbf{p}}{m_\chi}\right)\cdot\mathbf{s}_N^{s',s}\xi^{\dagger,r'}\xi^r \\
&= 4m_\chi m_N\left[im_N^2\left\langle\mathcal{O}_{10}\right\rangle-2m_\chi m_N\left\langle\mathcal{O}_7\right\rangle\right]
\end{aligned} \tag{A.67}$$

$$\begin{aligned}
\left(\overline{N}^{s'}(k')\not{p}N^s(k)\right)\left(\overline{\chi}^{r'}(p')\gamma^5\chi^r(p)\right) &\approx \left[2m_N m_\chi\xi^{\dagger,s'}\xi^s\left(1+\frac{\mathbf{p}^2}{2m_\chi^2}+\frac{\mathbf{K}^2}{8m_N^2}-\frac{\mathbf{p}\cdot\mathbf{K}}{2m_N m_\chi}\right)\right. \\
&\left.-m_\chi i\mathbf{s}_N^{s',s}\cdot\left(\frac{\mathbf{K}}{2m_N}\times\mathbf{q}\right)+2i\mathbf{p}\cdot\left(\mathbf{q}\times\mathbf{s}_N^{s',s}\right)\right]\cdot\left[2\mathbf{q}\cdot\mathbf{s}_\chi^{r',r}\right] \\
&\approx 4m_N m_\chi\left(\mathbf{q}\cdot\mathbf{s}_\chi^{r',r}\right)\xi^{\dagger,s'}\xi^s \\
&= 4m_\chi m_N\left[-im_N\left\langle\mathcal{O}_{11}\right\rangle\right]
\end{aligned} \tag{A.68}$$

$$\begin{aligned}
\left(\overline{N}^{s'}(k')N^s(k)\right)\left(\overline{\chi}^{r'}(p')\not{k}\gamma^5\chi^r(p)\right) &\approx \left[2m_N\xi^{\dagger,s'}\xi^s+\frac{\mathbf{q}^2}{4m_N}\xi^{\dagger,s'}\xi^s+\frac{i}{2m_N}\mathbf{s}_N^{s',s}\cdot(\mathbf{K}\times\mathbf{q})\right] \\
&\cdot\left[2m_N\mathbf{P}\cdot\mathbf{s}_\chi^{r',r}-4m_\chi\mathbf{k}\cdot\mathbf{s}_\chi^{r',r}\right] \\
&\approx 4m_N\left(m_N\mathbf{P}-2m_\chi\mathbf{k}\right)\cdot\mathbf{s}_\chi^{r',r}\xi^{\dagger,s'}\xi^s \\
&= 4m_N m_\chi\left[-im_N\left\langle\mathcal{O}_{11}\right\rangle+2m_N\left\langle\mathcal{O}_8\right\rangle\right]
\end{aligned} \tag{A.69}$$

$$\begin{aligned}
\left(\overline{N}^{s'}(k')\not{p}N^s(k)\right)\left(\overline{\chi}^{r'}(p')\not{k}\gamma^5\chi^r(p)\right) &\approx \left[2m_N m_\chi\xi^{\dagger,s'}\xi^s\left(1+\frac{\mathbf{p}^2}{2m_\chi^2}+\frac{\mathbf{K}^2}{8m_N^2}-\frac{\mathbf{p}\cdot\mathbf{K}}{2m_N m_\chi}\right)\right. \\
&\left.-m_\chi i\mathbf{s}_N^{s',s}\cdot\left(\frac{\mathbf{K}}{2m_N}\times\mathbf{q}\right)+2i\mathbf{p}\cdot\left(\mathbf{q}\times\mathbf{s}_N^{s',s}\right)\right]\cdot\left[2m_N\mathbf{P}\cdot\mathbf{s}_\chi^{r',r}-4m_\chi\mathbf{k}\cdot\mathbf{s}_\chi^{r',r}\right] \\
&\approx 4m_\chi m_N\left(m_N\mathbf{P}-2m_\chi\mathbf{k}\right)\cdot\mathbf{s}_\chi^{r',r}\xi^{\dagger,s'}\xi^s \\
&= 4m_\chi m_N\left[-im_\chi m_N\left\langle\mathcal{O}_{11}\right\rangle+2m_\chi m_N\left\langle\mathcal{O}_8\right\rangle\right]
\end{aligned} \tag{A.70}$$

$$\begin{aligned}
\left(\overline{N}^{s'}(k')\not{p}\gamma^5 N^s(k)\right)\left(\overline{\chi}^{r'}(p')\gamma^5\chi^r(p)\right) &\approx \left[2m_\chi\mathbf{K}\cdot\mathbf{s}_N^{s',s}-4m_N\mathbf{p}\cdot\mathbf{s}_N^{s',s}\right]\cdot\left[2\mathbf{q}\cdot s_\chi^{r',r}\right] \\
&= 4m_\chi m_N\left(\frac{\mathbf{q}}{m_N}\cdot s_\chi^{r',r}\right)\left(-m_N\frac{\mathbf{q}}{m_\chi}-2m_N\mathbf{v}_{\mathrm{el}}^{\perp}\right)\cdot s_N^{s',s} \\
&= 4m_\chi m_N\left[-\frac{m_N^2}{m_\chi}\left\langle\mathcal{O}_6\right\rangle+2im_N\left\langle\mathcal{O}_{14}\right\rangle\right]
\end{aligned} \tag{A.71}$$

$$\begin{aligned}\left(\overline{N}^{s'}(k')\gamma^5 N^s(k)\right)\left(\overline{\chi}^{r'}(p')\not{k}\gamma^5\chi^r(p)\right) &\approx \left[-2\mathbf{q}\cdot\mathbf{s}_N^{s',s}\right]\cdot\left[2m_N\mathbf{P}\cdot\mathbf{s}_\chi^{r'r}-4m_\chi\mathbf{k}\cdot\mathbf{s}_\chi^{r',r}\right]\\ &= -8m_\chi m_N\left(\mathbf{q}\cdot\mathbf{s}_N^{s',s}\right)\left(\frac{\mathbf{q}}{2m_N}+\mathbf{v}_{\rm el}^{\perp}\right)\cdot\mathbf{s}_\chi^{r',r}\\ &= -4m_\chi m_N\left[m_N\left\langle\mathcal{O}_6\right\rangle-2im_N\left\langle\mathcal{O}_{13}\right\rangle\right]\end{aligned} \tag{A.72}$$

$$\begin{aligned}\left(\overline{N}^{s'}(k')\not{p}\gamma^5 N^s(k)\right)\left(\overline{\chi}^{r'}(p')\not{k}\gamma^5\chi^r(p)\right) &\approx \left[2m_\chi\mathbf{K}\cdot\mathbf{s}_N^{s',s}-4m_N\mathbf{p}\cdot\mathbf{s}_N^{s',s}\right]\\ &\cdot\left[2m_N\mathbf{P}\cdot\mathbf{s}_\chi^{r',r}-4m_\chi\mathbf{k}\cdot\mathbf{s}_\chi^{r',r}\right]\\ &= 16m_\chi^2m_N^2\left[-\frac{\mathbf{q}}{2m_\chi}\cdot\mathbf{s}_N^{s',s}-\mathbf{v}_{\rm el}^{\perp}\cdot\mathbf{s}_N^{s',s}\right]\left[\frac{\mathbf{q}}{2m_N}\cdot\mathbf{s}_\chi^{r',r}+\mathbf{v}_{\rm el}^{\perp}\cdot\mathbf{s}_\chi^{r',r}\right]\\ &= 4m_\chi m_N\left[-m_N^2\left\langle\mathcal{O}_6\right\rangle+2im_N^2\left\langle\mathcal{O}_{13}\right\rangle+2im_\chi m_N\left\langle\mathcal{O}_{14}\right\rangle-4m_\chi m_N\left\langle\mathcal{O}_{16}\right\rangle\right]\end{aligned} \tag{A.73}$$

A.8 Boosted Frame

$$\begin{aligned}u(\tilde{p}) &= \begin{pmatrix}\sqrt{\tilde{p}\cdot\sigma}\xi\\ \sqrt{\tilde{p}\cdot\overline{\sigma}}\xi\end{pmatrix}\\ &= \begin{pmatrix}\sqrt{\tilde{E}-\tilde{\mathbf{p}}\cdot\boldsymbol{\sigma}}\xi\\ \sqrt{\tilde{E}+\tilde{\mathbf{p}}\cdot\boldsymbol{\sigma}}\xi\end{pmatrix}\\ &\approx \sqrt{m}\begin{pmatrix}\left(1-\tilde{\mathbf{p}}\cdot\boldsymbol{\sigma}/2m+\tilde{\mathbf{p}}^2/8m^2\right)\xi\\ \left(1+\tilde{\mathbf{p}}\cdot\boldsymbol{\sigma}/2m+\tilde{\mathbf{p}}^2/8m^2\right)\xi\end{pmatrix}\\ &\approx \sqrt{m}\begin{pmatrix}\left(1-[\mathbf{p}+2m\mathbf{v}]\cdot\boldsymbol{\sigma}/2m+[\mathbf{p}+2m\mathbf{v}]^2/8m^2\right)\xi\\ \left(1+[\mathbf{p}+2m\mathbf{v}]\cdot\boldsymbol{\sigma}/2m+[\mathbf{p}+2m\mathbf{v}]^2/8m^2\right)\xi\end{pmatrix}\end{aligned} \tag{A.74}$$

APPENDIX B

Loop Integral Calculations

B.1 Loop Integral

After multiplying Eqs. (3.21) and (3.22) and Eqs. (3.21) and (3.23), simplyfing and writing in terms of Passarino-Veltman tensor integrals one obtains the loop integrals for the first and second diagram, respectively.

$$
\begin{aligned}
256i\pi^2 f_a^4 I_1 = &-\left[\overline{\chi}(p')\left(c_{\chi\chi}^V - c_{\chi\chi}^A\gamma^5\right)^2\gamma^\mu\chi(p)\right]\left[\overline{u}(k')\left(c_{tu}^V - c_{tu}^A\gamma^5\right)^2\gamma^\nu u(k)\right]\left[B_{\mu\nu}(-q,m_a,m_a)\right.\\
&\left.+m_t^2 C_{\mu\nu}(k,-q,m_a,m_t,m_a)\right]\\
&+2m_t m_u\left((c_{tu}^V)^2-(c_{tu}^A)^2\right)\left[\overline{\chi}(p')\left(c_{\chi\chi}^V - c_{\chi\chi}^A\gamma^5\right)^2\gamma^\mu\chi(p)\right]\left[\overline{u}(k')\gamma^\nu u(k)\right]C_{\mu\nu}(k,-q,m_a,m_t,m_a)\\
&-m_t\left((c_{tu}^V)^2-(c_{tu}^A)^2\right)\left[\overline{\chi}(p')\left(c_{\chi\chi}^V - c_{\chi\chi}^A\gamma^5\right)^2\gamma^\mu\chi(p)\right]\left[\overline{u}(k')u(k)\right]\left[B_\mu(-q,m_a,m_a)\right.\\
&\left.+(m_t^2-m_u^2)C_\mu(k,-q,m_a,m_t,m_a)\right]\\
&+m_u\left[\overline{\chi}(p')\left(c_{\chi\chi}^V - c_{\chi\chi}^A\gamma^5\right)^2\gamma^\mu\chi(p)\right]\left[\overline{u}(k')\left(c_{tu}^V + c_{tu}^A\gamma^5\right)^2 u(k)\right]\left[B_\mu(-q,m_a,m_a)\right.\\
&\left.+(m_t^2-m_u^2)C_\mu(k,-q,m_a,m_t,m_a)\right]\\
&-m_u^2\left[\overline{\chi}(p')\left(c_{\chi\chi}^V - c_{\chi\chi}^A\gamma^5\right)^2\gamma^\mu\chi(p)\right]\left[\overline{u}(k')\left(c_{tu}^V + c_{tu}^A\gamma^5\right)^2\gamma^\nu u(k)\right]C_{\mu\nu}(k,-q,m_a,m_t,m_a)\\
\\
&-2m_\chi c_{\chi\chi}^A\left[\overline{\chi}(p')\left(c_{\chi\chi}^A + c_{\chi\chi}^V\gamma^5\right)\chi(p)\right]\left[\overline{u}(k')\left(c_{tu}^V - c_{tu}^A\gamma^5\right)^2\gamma^\nu u(k)\right]\left[B_\nu(-q,m_a,m_a)\right.\\
&\left.+m_t^2 C_\nu(k,-q,m_a,m_t,m_a)\right]\\
&+4m_\chi m_t m_u c_{\chi\chi}^A\left((c_{tu}^V)^2-(c_{tu}^A)^2\right)\left[\overline{\chi}(p')\left(c_{\chi\chi}^A + c_{\chi\chi}^V\gamma^5\right)\chi(p)\right]\left[\overline{u}(k')\gamma^\nu u(k)\right]C_\nu(k,-q,m_a,m_t,m_a)\\
&-2m_\chi m_t c_{\chi\chi}^A\left((c_{tu}^V)^2-(c_{tu}^A)^2\right)\left[\overline{\chi}(p')\left(c_{\chi\chi}^A + c_{\chi\chi}^V\gamma^5\right)\chi(p)\right]\left[\overline{u}(k')u(k)\right]\left[B_0(-q,m_a,m_a)\right.\\
&\left.+(m_t^2-m_u^2)C_0(k,-q,m_a,m_t,m_a)\right]\\
&+2m_\chi m_u c_{\chi\chi}^A\left[\overline{\chi}(p')\left(c_{\chi\chi}^A + c_{\chi\chi}^V\gamma^5\right)\chi(p)\right]\left[\overline{u}(k')\left(c_{tu}^V + c_{tu}^A\gamma^5\right)^2 u(k)\right]\left[B_0(-q,m_a,m_a)\right.
\end{aligned}
$$

$$
\begin{aligned}
&+(m_t^2-m_u^2)C_0(k,-q,m_a,m_t,m_a)\big]\\
&-2m_\chi m_u^2 c^A_{\chi\chi}\left[\overline{\chi}(p')\left(c^A_{\chi\chi}+c^V_{\chi\chi}\gamma^5\right)\chi(p)\right]\left[\overline{u}(k')\left(c^V_{tu}+c^A_{tu}\gamma^5\right)^2\gamma^\nu u(k)\right]C_\nu(k,-q,m_a,m_t,m_a)\\
&\\
&-4m_\chi^2(c^A_{\chi\chi})^2\left[\overline{\chi}(p')\gamma^\mu\chi(p)\right]\left[\overline{u}(k')\left(c^V_{tu}-c^A_{tu}\gamma^5\right)^2\gamma^\nu u(k)\right]\left[C_{\mu\nu}(-q,-p,m_a,m_a,m_\chi)\right.\\
&\left.+m_t^2D_{\mu\nu}(k,-q,-p,m_a,m_t,m_a,m_\chi)\right]\\
&+8m_\chi^2m_tm_u(c^A_{\chi\chi})^2\left((c^V_{tu})^2-(c^A_{tu})^2\right)\left[\overline{\chi}(p')\gamma^\mu\chi(p)\right]\left[\overline{u}(k')\gamma^\nu u(k)\right]D_{\mu\nu}(k,-q,-p,m_a,m_t,m_a,m_\chi)\\
&-4m_\chi^2m_t(c^A_{\chi\chi})^2\left((c^V_{tu})^2-(c^A_{tu})^2\right)\left[\overline{\chi}(p')\gamma^\mu\chi(p)\right]\left[\overline{u}(k')u(k)\right]\left[C_\mu(-q,-p,m_a,m_a,m_\chi)\right.\\
&\left.+(m_t^2-m_a^2)D_\mu(k,-q,-p,m_a,m_t,m_a,m_\chi)\right]\\
&+4m_\chi^2m_u(c^A_{\chi\chi})^2\left[\overline{\chi}(p')\gamma^\mu\chi(p)\right]\left[\overline{u}(k')\left(c^V_{tu}+c^A_{tu}\gamma^5\right)^2u(k)\right]\left[C_\mu(-q,-p,m_a,m_a,m_\chi)\right.\\
&\left.+(m_t^2-m_u^2)D_\mu(k,-q,-p,m_a,m_t,m_a,m_\chi)\right]\\
&-4m_\chi^2m_u^2(c^A_{\chi\chi})^2\left[\overline{\chi}(p')\gamma^\mu\chi(p)\right]\left[\overline{u}(k')\left(c^V_{tu}+c^A_{tu}\gamma^5\right)^2\gamma^\nu u(k)\right]D_{\mu\nu}(k,-q,-p,m_a,m_t,m_a,m_\chi)
\end{aligned}
\tag{B.1}
$$

$$
\begin{aligned}
256i\pi^2f_a^4I_2=&\left[\overline{\chi}(p')\left(c^V_{\chi\chi}-c^A_{\chi\chi}\gamma^5\right)^2\gamma^\mu\chi(p)\right]\left[\overline{u}(k')\left(c^V_{tu}-c^A_{tu}\gamma^5\right)^2\gamma^\nu u(k)\right]\left[B_{\mu\nu}(-q,m_a,m_a)\right.\\
&\left.+m_t^2C_{\mu\nu}(-k',-q,m_a,m_t,m_a)\right]\\
&-2m_tm_u\left((c^V_{tu})^2-(c^A_{tu})^2\right)\left[\overline{\chi}(p')\left(c^V_{\chi\chi}-c^A_{\chi\chi}\gamma^5\right)^2\gamma^\mu\chi(p)\right]\left[\overline{u}(k')\gamma^\nu u(k)\right]C_{\mu\nu}(-k',-q,m_a,m_t,m_a)\\
&-m_t\left((c^V_{tu})^2-(c^A_{tu})^2\right)\left[\overline{\chi}(p')\left(c^V_{\chi\chi}-c^A_{\chi\chi}\gamma^5\right)^2\gamma^\mu\chi(p)\right]\left[\overline{u}(k')u(k)\right]\left[B_\mu(-q,m_a,m_a)\right.\\
&\left.+(m_t^2-m_u^2)C_\mu(-k',-q,m_a,m_t,m_a)\right]\\
&+m_u\left[\overline{\chi}(p')\left(c^V_{\chi\chi}-c^A_{\chi\chi}\gamma^5\right)^2\gamma^\mu\chi(p)\right]\left[\overline{u}(k')\left(c^V_{tu}-c^A_{tu}\gamma^5\right)^2u(k)\right]\left[B_\mu(-q,m_a,m_a)\right.\\
&\left.+(m_t^2-m_u^2)C_\mu(-k',-q,m_a,m_t,m_a)\right]\\
&+m_u^2\left[\overline{\chi}(p')\left(c^V_{\chi\chi}-c^A_{\chi\chi}\gamma^5\right)^2\gamma^\mu\chi(p)\right]\left[\overline{u}(k')\left(c^V_{tu}+c^A_{tu}\gamma^5\right)^2\gamma^\nu u(k)\right]C_{\mu\nu}(-k',-q,m_a,m_t,m_a)\\
&\\
&+2m_\chi c^A_{\chi\chi}\left[\overline{\chi}(p')\left(c^A_{\chi\chi}+c^V_{\chi\chi}\gamma^5\right)\chi(p)\right]\left[\overline{u}(k')\left(c^V_{tu}-c^A_{tu}\gamma^5\right)^2\gamma^\nu u(k)\right]\left[B_\nu(-q,m_a,m_a)\right.\\
&\left.+m_t^2C_\nu(-k',-q,m_a,m_t,m_a)\right]\\
&-4m_\chi m_tm_uc^A_{\chi\chi}\left((c^V_{tu})^2-(c^A_{tu})^2\right)\left[\overline{\chi}(p')\left(c^A_{\chi\chi}+c^V_{\chi\chi}\gamma^5\right)\chi(p)\right]\left[\overline{u}(k')\gamma^\nu u(k)\right]C_\nu(-k',-q,m_a,m_t,m_a)\\
&-2m_\chi m_tc^A_{\chi\chi}\left((c^V_{tu})^2-(c^A_{tu})^2\right)\left[\overline{\chi}(p')\left(c^A_{\chi\chi}+c^V_{\chi\chi}\gamma^5\right)\chi(p)\right]\left[\overline{u}(k')u(k)\right]\left[B_0(-q,m_a,m_a)\right.\\
&\left.+(m_t^2-m_u^2)C_0(-k',-q,m_a,m_t,m_a)\right]\\
&+2m_\chi m_uc^A_{\chi\chi}\left[\overline{\chi}(p')\left(c^A_{\chi\chi}+c^V_{\chi\chi}\gamma^5\right)\chi(p)\right]\left[\overline{u}(k')\left(c^V_{tu}-c^A_{tu}\gamma^5\right)^2u(k)\right]\left[B_0(-q,m_a,m_a)\right.\\
&\left.+(m_t^2-m_u^2)C_0(-k',-q,m_a,m_t,m_a)\right]\\
&+2m_\chi m_u^2c^A_{\chi\chi}\left[\overline{\chi}(p')\left(c^A_{\chi\chi}+c^V_{\chi\chi}\gamma^5\right)\chi(p)\right]\left[\overline{u}(k')\left(c^V_{tu}+c^A_{tu}\gamma^5\right)^2\gamma^\nu u(k)\right]C_\nu(-k',-q,m_a,m_t,m_a)\\
&\\
&+4m_\chi^2(c^A_{\chi\chi})^2\left[\overline{\chi}(p')\gamma^\mu\chi(p)\right]\left[\overline{u}(k')\left(c^V_{tu}-c^A_{tu}\gamma^5\right)^2\gamma^\nu u(k)\right]\left[C_{\mu\nu}(-q,-p,m_a,m_a,m_\chi)\right.
\end{aligned}
$$

$$
\begin{aligned}
&+m_t^2 D_{\mu\nu}(-k',-q,-p,m_a,m_t,m_a,m_\chi)\big] \\
&-8m_\chi^2 m_t m_u (c^A_{\chi\chi})^2\left((c^V_{tu})^2-(c^A_{tu})^2\right)[\overline{\chi}(p')\gamma^\mu\chi(p)]\,[\overline{u}(k')\gamma^\nu u(k)]\,D_{\mu\nu}(-k',-q,-p,m_a,m_t,m_a,m_\chi) \\
&-4m_\chi^2 m_t (c^A_{\chi\chi})^2\left((c^V_{tu})^2-(c^A_{tu})^2\right)[\overline{\chi}(p')\gamma^\mu\chi(p)]\,[\overline{u}(k')u(k)]\,[C_\mu(-q,-p,m_a,m_a,m_\chi) \\
&+(m_t^2-m_u^2)D_\mu(-k',m_a,m_t,m_a,m_\chi)\big] \\
&+4m_\chi^2 m_u (c^A_{\chi\chi})^2[\overline{\chi}(p')\gamma^\mu\chi(p)]\left[\overline{u}(k')\left(c^V_{tu}-c^A_{tu}\gamma^5\right)^2 u(k)\right][C_\mu(-q,-p,m_a,m_a,m_\chi) \\
&+(m_t^2-m_u^2)D_\mu(-k',-q,-p,m_a,m_t,m_a,m_\chi)\big] \\
&+4m_\chi^2 m_u^2 (c^A_{\chi\chi})^2[\overline{\chi}(p')\gamma^\mu\chi(p)]\left[\overline{u}(k')\left(c^V_{tu}+c^A_{tu}\gamma^5\right)^2\gamma^\nu u(k)\right]D_{\mu\nu}(-k',-q,-p,m_a,m_t,m_a,m_\chi)
\end{aligned}
\tag{B.2}
$$

Here

$$
\left(c^V\pm c^A\gamma^5\right)^2=(c^V)^2+(c^A)^2\pm 2c^Vc^A\gamma^5. \tag{B.3}
$$

Summing the two integrals results in the total loop integral and reads

$$
\begin{aligned}
256i\pi^2 f_a^4\mathcal{I} &= 256i\pi^2 f_a^4(I_1+I_2) \\
&= -(c^V_{\chi\chi})^2[\overline{\chi}(p')\gamma^\mu\chi(p)] \\
&\times\big\{\left((m_t-m_u)^2(c^V_{tu})^2+(m_t+m_u)^2(c^A_{tu})^2\right)[\overline{u}(k')\gamma^\nu u(k)]\,[C_{\mu\nu}(k,-q,m_a,m_t,m_a) \\
&-C_{\mu\nu}(-k',-q,m_a,m_t,m_a)] \\
&-2(m_t^2-m_u^2)c^V_{tu}c^A_{tu}\left[\overline{u}(k')\gamma^5\gamma^\nu u(k)\right][C_{\mu\nu}(k,-q,m_a,m_t,m_a)-C_{\mu\nu}(-k',-q,m_a,m_t,m_a)] \\
&+\left((m_t-m_u)(c^V_{tu})^2-(m_t+m_u)(c^A_{tu})^2\right)[\overline{u}(k')u(k)] \\
&\times\left[2B_\mu(-q,m_a,m_a)+(m_t^2-m_u^2)C_\mu(k,-q,m_a,m_t,m_a)+(m_t^2-m_u^2)C_\mu(-k',-q,m_a,m_t,m_a)\right] \\
&-2m_u(m_t^2-m_u^2)c^V_{tu}c^A_{tu}\left[\overline{u}(k')\gamma^5u(k)\right][C_\mu(k,-q,m_a,m_t,m_a)-C_\mu(-k',-q,m_a,m_t,m_a)]\big\} \\
&+2c^V_{\chi\chi}c^A_{\chi\chi}\left[\overline{\chi}(p')\gamma^5\gamma^\mu\chi(p)\right] \\
&\times\big\{\left((m_t-m_u)^2(c^V_{tu})^2+(m_t+m_u)^2(c^A_{tu})^2\right)[\overline{u}(k')\gamma^\nu u(k)]\,[C_{\mu\nu}(k,-q,m_a,m_t,m_a) \\
&-C_{\mu\nu}(-k',-q,m_a,m_t,m_a)] \\
&-2(m_t^2-m_u^2)c^V_{tu}c^A_{tu}\left[\overline{u}(k')\gamma^5\gamma^\nu u(k)\right][C_{\mu\nu}(k,-q,m_a,m_t,m_a)-C_{\mu\nu}(-k',-q,m_a,m_t,m_a)] \\
&+2\left((m_t-m_u)(c^V_{tu})^2-(m_t+m_u)(c^A_{tu})^2\right)[\overline{u}(k')u(k)]\,B_\mu(-q,m_a,m_a) \\
&+(m_t^2-m_u^2)\left((m_t-m_u)(c^V_{tu})^2-(m_t+m_u)(c^A_{tu})^2\right)[\overline{u}(k')u(k)]\,[C_\mu(k,-q,m_a,m_t,m_a) \\
&+C_\mu(-k',-q,m_a,m_t,m_a)] \\
&-2m_u(m_t^2-m_u^2)c^V_{tu}c^A_{tu}\left[\overline{u}(k')\gamma^5u(k)\right][C_\mu(k,-q,m_a,m_t,m_a)-C_\mu(-k',-q,m_a,m_t,m_a)]\big\} \\
&-2m_\chi c^V_{\chi\chi}c^A_{\chi\chi}\left[\overline{\chi}(p')\gamma^5\chi(p)\right] \\
&\times\big\{\left((m_t-m_u)^2(c^V_{tu})^2+(m_t+m_u)^2(c^A_{tu})^2\right)[\overline{u}(k')\gamma^\nu u(k)]\,[C_\nu(k,-q,m_a,m_t,m_a) \\
&-C_\nu(-k',-q,m_a,m_t,m_a)] \\
&-2(m_t^2-m_u^2)c^V_{tu}c^A_{tu}\left[\overline{u}(k')\gamma^5\gamma^\nu u(k)\right][C_\nu(k,-q,m_a,m_t,m_a)-C_\nu(-k',-q,m_a,m_t,m_a)] \\
&+\left((m_t-m_u)(c^V_{tu})^2-(m_t+m_u)(c^A_{tu})^2\right)[\overline{u}(k')u(k)]\,[2B_0(-q,m_a,m_a) \\
&+(m_t^2-m_u^2)C_0(k,-q,m_a,m_t,m_a)+(m_t^2-m_u^2)C_0(-k',-q,m_a,m_t,m_a)] \\
&-2m_u(m_t^2-m_u^2)c^V_{tu}c^A_{tu}\left[\overline{u}(k')\gamma^5u(k)\right][C_0(k,-q,m_a,m_t,m_a)-C_0(-k',-q,m_a,m_t,m_a)]\big\}
\end{aligned}
$$

$$
\begin{aligned}
&- (c^A_{\chi\chi})^2 \left[\overline{\chi}(p')\gamma^\mu\chi(p)\right] \\
&\times \left\{ \left((m_t - m_u)^2 (c^V_{tu})^2 + (m_t + m_u)^2 (c^A_{tu})^2\right) \left[\overline{u}(k')\gamma^\nu u(k)\right] \right. \\
&\times \left[C_{\mu\nu}(k, -q, m_a, m_t, m_a) - C_{\mu\nu}(-k', -q, m_a, m_t, m_a) + 4m_\chi^2 D_{\mu\nu}(k, -q, -p, m_a, m_t, m_a, m_\chi)\right. \\
&\left. -4m_\chi^2 D_{\mu\nu}(-k', -q, -p, m_a, m_t, m_a, m_\chi)\right] \\
&- 2(m_t^2 - m_u^2) c^V_{tu} c^A_{tu} \left[\overline{u}(k')\gamma^5\gamma^\nu u(k)\right] \\
&\times \left[C_{\mu\nu}(k, -q, m_a, m_t, m_a) - C_{\mu\nu}(-k', -q, m_a, m_t, m_a) + 4m_\chi^2 D_{\mu\nu}(k, -q, -p, m_a, m_t, m_a, m_\chi)\right. \\
&\left. -4m_\chi^2 D_{\mu\nu}(-k', -q, -p, m_a, m_t, m_a, m_\chi)\right] \\
&+ \left((m_t - m_u)(c^V_{tu})^2 - (m_t + m_u)(c^A_{tu})^2\right) \left[\overline{u}(k')u(k)\right] \\
&\times \left[2B_\mu(-q, m_a, m_a) + (m_t^2 - m_u^2) C_\mu(k, -q, m_a, m_t, m_a) + (m_t^2 - m_u^2) C_\mu(-k', -q, m_a, m_t, m_a)\right. \\
&+8m_\chi^2 C_\mu(-q, -p, m_a, m_a, m_\chi) + 4m_\chi^2 (m_t^2 - m_u^2) D_\mu(k, -q, -p, m_a, m_t, m_a, m_\chi) \\
&\left. +4m_\chi^2 (m_t^2 - m_u^2) D_\mu(-k', -q, -p, m_a, m_t, m_a, m_\chi)\right] \\
&- 2m_u(m_t^2 - m_u^2) c^V_{tu} c^A_{tu} \left[\overline{u}(k')\gamma^5 u(k)\right] \\
&\times \left[C_\mu(k, -q, m_a, m_t, m_a) - C_\mu(-k', -q, m_a, m_t, m_a) + 4m_\chi^2 D_\mu(k, -q, -p, m_a, m_t, m_a, m_\chi)\right. \\
&\left. -4m_\chi^2 D_\mu(-k', -q, -p, m_a, m_t, m_a, m_\chi)\right] \Big\}
\end{aligned}
$$

$$
\begin{aligned}
&- 2m_\chi (c^A_{\chi\chi})^2 \left[\overline{\chi}(p')\chi(p)\right] \\
&\times \left\{ \left((m_t - m_u)^2 (c^V_{tu})^2 + (m_t + m_u)^2 (c^A_{tu})^2\right) \left[\overline{u}(k')\gamma^\nu u(k)\right] \left[C_\nu(k, -q, m_a, m_t, m_a)\right. \right. \\
&\left. -C_\nu(-k', -q, m_a, m_t, m_a)\right] \\
&- 2(m_t^2 - m_u^2) c^V_{tu} c^A_{tu} \left[\overline{u}(k')\gamma^5\gamma^\nu u(k)\right] \left[C_\nu(k, -q, m_a, m_t, m_a) - C_\nu(-k', -q, m_a, m_t, m_a)\right] \\
&+ \left((m_t - m_u)(c^V_{tu})^2 - (m_t + m_u)(c^A_{tu})^2\right) \left[\overline{u}(k')u(k)\right] \\
&\times \left[2B_0(-q, m_a, m_a) + (m_t^2 - m_u^2) C_0(k, -q, m_a, m_t, m_a) + (m_t^2 - m_u^2) C_0(-k', -q, m_a, m_t, m_a)\right] \\
&\left. -2m_u(m_t^2 - m_u^2) c^V_{tu} c^A_{tu} \left[\overline{u}(k')\gamma^5 u(k)\right] \left[C_0(k, -q, m_a, m_t, m_a) - C_0(-k', -q, m_a, m_t, m_a)\right]\right\}
\end{aligned}
\tag{B.4}
$$

The total loop integral is ordered by Lorentz structure of the DM part.

B.2 Tensor Integral Simplifications

B.2.1 C-Functions

The three-point functions are dependent on two momenta, one of which is the transfer momentum. Using the transfer momentum the C functions in terms of k' can be written in terms of k and vice versa. First, we do this for $C_{\mu\nu}$:

$$
\begin{aligned}
C_{\mu\nu}(-k', -q, m_a, m_t, m_a) &= C_{\mu\nu}(k', q, m_a, m_t, m_a) \\
&= C_{\mu\nu}(k, -q, m_a, m_t, m_a) - q_\mu C_\nu(k, -q, m_a, m_t, m_a) \\
&\quad - q_\nu C_\mu(k, -q, m_a, m_t, m_a) + q_\nu q_\mu C_0(k, -q, m_a, m_t, m_a)
\end{aligned}
\tag{B.5}
$$

For the first equality we took $\ell \to -\ell$ and to go from the first to the second line we changed variables $\ell \to \ell - q$. Going through similar steps, we can write

$$C_\mu(-k', -q, m_a, m_t, m_a) = -C_\mu(k', q, m_a, m_t, m_a)$$

$$= -C_\mu(k,-q,m_a,m_t,m_a) + q_\mu C_0(k,-q,m_a,m_t,m_a). \tag{B.6}$$

Similarly for the scalar three-point function:

$$C_0(-k',-q,m_a,m_t,m_a) = C_0(k,q,m_a,m_t,m_a) = C_0(k,-q,m_a,m_t,m_a) \tag{B.7}$$

B.2.2 Expanding the Top-Propagator

Let us start with the rank-two four-point function.

$$\begin{aligned}
&D_{\mu\nu}(k,-q,-p,m_a,m_t,m_a,m_\chi) - D_{\mu\nu}(-k',-q,-p,m_a,m_t,m_a,m_\chi) \\
&\quad\approx D_{\mu\nu}(-k,q,p,m_a,m_t,m_a,m_\chi) - D_{\mu\nu}(k',q,p,m_a,m_t,m_a,m_\chi) \\
&\quad= \frac{1}{i\pi^2}\int d^4\ell \frac{\ell_\mu\ell_\nu}{\left[\ell-m_a^2\right]\left[(\ell+q)-m_a^2\right]\left[(\ell+p)^2-m_\chi^2\right]}\left(\frac{1}{(\ell-k)^2-m_t^2} - \frac{1}{(\ell+k')^2-m_t^2}\right) \\
&\quad\approx \frac{1}{i\pi^2}\int d^4\ell \frac{\ell_\mu\ell_\nu}{\left[\ell-m_a^2\right]\left[(\ell+q)-m_a^2\right]\left[(\ell+p)^2-m_\chi^2\right]\left[\ell^2-m_t^2\right]}\left(1-\frac{k^2-2k\cdot\ell}{\ell^2-m_t^2} - 1 + \frac{k'^2+2k'\cdot\ell}{\ell^2-m_t^2}\right) \\
&\quad= \frac{1}{i\pi^2}\int d^4\ell \frac{\ell_\mu\ell_\nu\left(k'^2-k^2+2(k+k')\cdot\ell\right)}{\left[\ell-m_a^2\right]\left[(\ell+q)-m_a^2\right]\left[(\ell+p)^2-m_\chi^2\right]\left[\ell^2-m_t^2\right]^2}
\end{aligned} \tag{B.8}$$

The up quarks are approximately on-shell and therefore $k'^2 - k^2 \approx 0$. First taking $q \to 0$, it is easy to see that in the small up quark momenta limit, this integral will be negligible because the whole integral is proportional to the up quark momenta.

Next we look at a combination of the three- and four-point functions

$$\begin{aligned}
&2C_\mu(-q,-p,m_a,m_a,m_\chi) + m_t^2 D_\mu(k,-q,-p,m_a,m_t,m_a,m_\chi) + m_t^2 D_\mu(-k',-q,-p,m_a,m_t,m_a,m_\chi) \\
&\quad= -2C_\mu(q,p,m_a,m_a,m_\chi) - m_t^2 D_\mu(-k,q,p,m_a,m_t,m_a,m_\chi) - m_t^2 D_\mu(k',q,p,m_a,m_t,m_a,m_\chi) \\
&\quad= \frac{-1}{i\pi^2}\int d^4\ell \frac{\ell_\mu}{\left[\ell-m_a^2\right]\left[(\ell+q)-m_a^2\right]\left[(\ell+p)^2-m_\chi^2\right]}\left(\frac{m_t^2}{(\ell-k)^2-m_t^2} + \frac{m_t^2}{(\ell+k')^2-m_t^2} + 2\right) \\
&\quad\approx \frac{-1}{i\pi^2}\int d^4\ell \frac{\ell_\mu}{\left[\ell-m_a^2\right]\left[(\ell+q)-m_a^2\right]\left[(\ell+p)^2-m_\chi^2\right]\left[\ell^2-m_t^2\right]} \\
&\quad\times\left(m_t^2 - m_t^2\frac{k^2-2k\cdot\ell}{\ell^2-m_t^2} + m_t^2 - m_t^2\frac{k'^2+2k'\cdot\ell}{\ell^2-m_t^2} + 2(\ell^2-m_t^2)\right) \\
&\quad\approx \frac{-2}{i\pi^2}\int d^4\ell \frac{\ell_\mu\ell^2}{\left[\ell-m_a^2\right]\left[(\ell+q)-m_a^2\right]\left[(\ell+p)^2-m_\chi^2\right]\left[\ell^2-m_t^2\right]^2}
\end{aligned} \tag{B.9}$$

Using `FeynCalc` for the Passarino-Veltman reduction and taking the limit of $q \to 0$, we obtain the following approximation:

$$\begin{aligned}
&2C_\mu(-q,-p,m_a,m_a,m_\chi) + m_t^2 D_\mu(k,-q,-p,m_a,m_t,m_a,m_\chi) + m_t^2 D_\mu(-k',-q,-p,m_a,m_t,m_a,m_\chi) \\
&\quad\approx \frac{p_\mu}{m_\chi^2(m_t^2-m_a^2)^2}\left[m_a^2\left(m_a^2-2m_t^2\right)B_0(p,m_a,m_\chi) + m_a^2\left(m_t^2-m_a^2\right)B_0(0,m_a,m_a)\right. \\
&\quad\left. -m_a^4(m_t^2-m_a^2)C_0(0,p,m_a,m_a,m_\chi) + m_t^4 B_0(p,m_t,m_\chi) + m_t^2 A_0(m_a) - m_t^2 A_0(m_t)\right]
\end{aligned} \tag{B.10}$$

Third, we look at the rank-one three point function:

$$C_\nu(k,-q,m_a,m_a,m_t) = \frac{1}{i\pi^2}\int d^4\ell \frac{\ell_\nu}{\left[\ell^2-m_a^2\right]\left[(\ell-q)^2-m_a^2\right]\left[(\ell+k)^2-m_t^2\right]}$$

$$\approx \frac{1}{i\pi^2}\int d^4\ell \frac{\ell_\nu}{[\ell^2-m_a^2]\,[(\ell-q)^2-m_a^2]\,[\ell^2-m_t^2]}\left(1-\frac{k^2+2k\cdot\ell}{\ell^2-m_t^2}\right)$$
$$\approx \frac{1}{i\pi^2}\int d^4\ell \frac{\ell_\nu}{[\ell^2-m_a^2]\,[(\ell-q)^2-m_a^2]\,[\ell^2-m_t^2]} \tag{B.11}$$

Using partial fractions and writing the result in terms of the Passarino-Veltman functions we obtain

$$C_\nu(k,-q,m_a,m_t,m_a) = \frac{1}{m_t^2-m_a^2}\left(B_\nu(-q,m_t,m_a)-B_\nu(-q,m_a,m_a)\right) \tag{B.12}$$

The reduction of these two functions is $-q_\mu B_1$, with the right parameters for each function. When contracted with the up quark vector currents, this results to a zero contribution.

Last, the scalar three-point function can be done in a similar way

$$\begin{aligned} C_0(k,-q,m_a,m_t,m_a) &= \frac{1}{i\pi^2}\int d^4\ell \frac{1}{[\ell^2-m_a^2]\,[(\ell-q)^2-m_a^2]\,[(\ell+k)^2-m_t^2]} \\ &\approx \frac{1}{i\pi^2}\int d^4\ell \frac{1}{[\ell^2-m_a^2]\,[(\ell-q)^2-m_a^2]\,[\ell^2-m_t^2]}\left(1-\frac{k^2+2k\cdot\ell}{\ell^2-m_t^2}\right) \\ &\approx \frac{1}{i\pi^2}\int d^4\ell \frac{1}{[\ell^2-m_a^2]\,[(\ell-q)^2-m_a^2]\,[\ell^2-m_t^2]} \\ &= \frac{1}{m_t^2-m_a^2}\left(B_0(-q,m_t,m_a)-B_0(-q,m_a,m_a)\right) \end{aligned} \tag{B.13}$$

Taking the limit of $q^2 \to 0$ gives

$$C_0(k,-q,m_a,m_a,m_t) \approx \frac{1}{m_t^2-m_a^2}\left(\frac{A_0(m_t)-A_0(m_a)}{m_t^2-m_a^2}-\frac{d}{dm_a^2}A_0(m_a)\right) \tag{B.14}$$

B.3 Limiting Cases

Starting with the limit $m_a \to 0$, we first note that the two-point function contains the factor $r_{a\chi}$. So before taking the limit of the two-point function, the limit of this factor $r_{a\chi}$ has to be known. It is for now only needed to check whether $r_{a\chi}$ is finite and nonzero, such that the terms containing $r_{a\chi}$ are also finite:

$$\begin{aligned} \lim_{m_a\to 0} r_{a\chi} &= \lim_{m_a\to 0}\frac{m_a^2-i\epsilon+\sqrt{(m_a^2-i\epsilon)^2-4m_a^2m_\chi^2}}{2m_am_\chi} \\ &= \lim_{m_a\to 0}\left[\frac{m_a}{2m_\chi}+\sqrt{m_a^2/2m_\chi^2-1-i\delta}\right] \end{aligned} \tag{B.15}$$

It is easy to see that $r_{a\chi}$ is finite and nonzero when the ALP is massless.

$$\begin{aligned} \lim_{m_a\to 0} B_0(m_\chi,m_a,m_\chi) = \lim_{m_a\to 0}\Bigg[&\Delta+2-\log\frac{m_am_\chi}{\mu^2} \\ &+\frac{m_a^2-m_\chi^2}{m_\chi^2}\log\frac{m_\chi}{m_a}-\frac{m_a}{m_\chi}\left(\frac{1}{r_{a\chi}}-r_{a\chi}\right)\log r_{a\chi}\Bigg] \end{aligned}$$

$$= \lim_{m_a \to 0} \left[\Delta + 2 - \log \frac{m_\chi^2}{\mu^2} - \frac{m_a^2}{m_\chi^2} \log \frac{m_a}{m_\chi} - \frac{m_a}{m_\chi} \left(\frac{1}{r_{a\chi}} - r_{a\chi} \right) \log r_{a\chi} \right] \tag{B.16}$$

Because $r_{a\chi}$ is finite and nonzero in this limit, the last term in the last line will be zero. The second to last term in the last line has the form $x^2 \ln x$. Although the natural log diverges as $x \to 0$, x^2 goes to zero faster than the natural log diverges. One can also verify this formally by taking the limit as x goes to zero. This term is therefore also zero in the $m_a \to 0$ limit. The first three terms remain finite in this limit, which was enough to check that the term $m_a^2(m_a^2 - 2m_t^2)B_0(m_\chi, m_a, m_\chi)$ is zero in the massless ALP limit. The second term of Eq. (3.48) is not dependent on m_a in any way, so when the ALP is massless only the pre-factor is affected, i.e. the pre-factor cancels with the factor m_t^{-4}. In the last term the derivative of the two-point function is taken. Although the two-point function itself is finite at $m_a = 0$, it is not always guarenteed for an arbitrary function that its derivative is also finite at that point, e.g. $\sqrt{x}$. It is for this term also enough to show that the derivative of the two-point function w.r.t. m_a^2 is finite, because the pre-factor is zero in massless ALP limit. We know that $r_{a\chi}$ remains finite, so next we have to check that $dr_{a\chi}/dm_a$ remains finite as well, or rather $m_a \frac{dr_{a\chi}}{dm_a}$. The derivative is multiplied by m_a before taking the limit, because then it is dimensionless and there is a factor of m_a available as can be seen in Eq. (3.41). Going through similar steps as for $r_{a\chi}$, this becomes

$$\begin{aligned} \lim_{m_a \to 0} m_a \frac{dr_{a\chi}}{dm_a} &= \lim_{m_a \to 0} m_a \left[-\frac{r_{a\chi}}{m_a} + \frac{2m_a \left(r_{a\chi} - \frac{m_\chi}{m_a} \right)}{\sqrt{(m_a^2 - i\epsilon)^2 - 4m_a^2 m_\chi^2}} \right] \\ &= \lim_{m_a \to 0} \left[-\frac{m_a}{2m_\chi} - \sqrt{m_a^2/2m_\chi^2 - 1} + \frac{m_a r_{a\chi} - m_\chi}{m_\chi \sqrt{m_a^2 - 1}} \right] \end{aligned} \tag{B.17}$$

It is straightforward to see that this remains finite in this limit. Since $r_{a\chi}$ is finite and nonzero and $m_a \frac{dr_{a\chi}}{dm_a}$ is finite as $m_a \to 0$, and $x^2 \log x \to 0$ in the limit as x goes to zero, $m_a^2 \frac{d}{m_a^2} B_0(m_\chi, m_a, m_\chi)$ is finite in the massless ALP limit. Therefore, the third line in Eq. (3.48) is zero in the limit as $m_a \to 0$. The only term that survives is $B_0(m_\chi, m_t, m_\chi)$. Because the other two two-point function terms are zero, the integral in the massless ALP limit has the following analytical expression:

$$\lim_{m_a \to 0} \mathcal{I} \approx \frac{i m_\chi m_t}{4\pi^2 f_a^4} \left(c_{\chi\chi}^A \right)^2 \left(\left(c_{tu}^V \right)^2 - \left(c_{tu}^A \right)^2 \right) \left[\overline{\chi}(p')\chi(p) \right] \left[\overline{u}(k')u(k) \right] B_0(m_\chi, m_t, m_\chi). \tag{B.18}$$

The loop integral, and thus also the cross section, will become a nonzero constant if the ALP mass is small or if the ALP is massless.

Instead of the ALP being massless, the ALP could also be very heavy, requiring us to take the limit $m_a \to \infty$. Again starting with $r_{a\chi}$:

$$\begin{aligned} \lim_{m_a \to \infty} r_{a\chi} &= \lim_{m_a \to \infty} \frac{m_a^2 - i\epsilon + \sqrt{(m_a^2 - i\epsilon)^2 - 4m_a^2 m_\chi^2}}{2m_a m_\chi} \\ &= \lim_{m_a \to \infty} \left(\frac{m_a}{m_\chi} - \frac{m_\chi}{m_a} \right) \end{aligned} \tag{B.19}$$

So $r_{a\chi} \approx m_a/m_\chi - m_\chi/m_a$ in the infinite ALP mass limit. Knowing this behavior, the derivative

of $dr_{a\chi}/dm_a$ can easily be approximated as well:

$$\lim_{m_a\to\infty} m_a \frac{dr_{a\chi}}{dm_a} = \lim_{m_a\to\infty} \left[-r_{a\chi} + \frac{2m_a^2\left(r_{a\chi} - \frac{m_\chi}{m_a}\right)}{\sqrt{(m_a^2 - i\epsilon)^2 - 4m_a^2 m_\chi^2}} \right]$$
$$= \lim_{m_a\to\infty} \left[-\frac{m_a}{m_\chi} + \frac{2m_a}{m_\chi} + \frac{m_\chi}{m_a} \right] \tag{B.20}$$

Hence, $m_a \frac{dr_{a\chi}}{dm_a} \approx \frac{m_a}{m_\chi} + \frac{m_\chi}{m_a}$ in this limit. Looking at Eq. (3.48) the pre-factors that are dependent on the ALP mass will cancel with the denominator pre-factor. The term not dependent on the ALP mass, $m_t^4 B_0(m_\chi, m_t, m_\chi)/m_a^4$, will be zero as $m_a \to \infty$. It is, therefore, only needed to check the behavior of $B_0(m_\chi, m_a, m_\chi)$ and of its derivative w.r.t. m_a^2. After a quick calculation the proportionality of the two-point function in this limit is

$$\lim_{m_a\to\infty} B_0(m_\chi, m_a, m_\chi) \propto \lim_{m_a\to\infty} -\log\frac{m_a^2}{\mu^2} \tag{B.21}$$

Similarly for the derivative

$$\lim_{m_a\to\infty} 2m_a^2 \frac{d}{dm_a^2} B_0(m_\chi, m_a, m_\chi) = -2 \tag{B.22}$$

With this we conclude that

$$\lim_{m_a\to\infty} \mathcal{I} \propto -\log\frac{m_a^2}{\mu^2}. \tag{B.23}$$

This means that the integral has a log-divergence for large ALP masses, which is expected from the two-point function.

Now looking at the supposed pole at the mass of the top quark. We identify that as $m_a \to m_t$ the integral $\mathcal{I}$ becomes of the form $\frac{0}{0}$, which means that L'Hôpital's rule can be used to evaluate this limit. Differentiating the numerator and denominator, and simplifying the expression the limit becomes:

$$\lim_{m_a\to m_t} \mathcal{I} \propto \lim_{m_a\to m_t} \left[B_0(m_\chi, m_a, m_\chi) + 2m_a^2 \frac{d}{dm_a^2} B_0(m_\chi, m_a, m_\chi) + \frac{m_a^4}{2} \frac{d^2}{d(m_a^2)^2} B_0(m_\chi, m_a, m_\chi) \right] \tag{B.24}$$

All two-point functions and their derivatives w.r.t. m_a^2 are well-defined for $m_a = m_t$. Since all functions are well-defined, we see that the integral is finite for $m_a = m_t$.

Next we are taking the limit $m_\chi \to \infty$. Going through similar steps, in this limit $r_{a\chi}$ is finite, nonzero and independent of m_χ. This means that

$$\lim_{m_\chi\to\infty} B_0(m_\chi, m_a, m_\chi) \propto -\log\frac{m_\chi^2}{\mu^2} \tag{B.25}$$

$$\lim_{m_\chi\to\infty} B_0(m_\chi, m_t, m_\chi) \propto -\log\frac{m_\chi^2}{\mu^2} \tag{B.26}$$

$$\lim_{m_\chi\to\infty} m_a^2 \frac{d}{dm_a^2} B_0(m_\chi, m_a, m_\chi) \to 0 \tag{B.27}$$

The overall DM mass dependence of $\mathcal{I}$ is then $m_\chi \log m_\chi^2$.

In the limit $m_\chi \to 0$, the factor $r_{a\chi} = \frac{m_a}{m_\chi} - \frac{m_\chi}{m_a}$ and therefore $\frac{dr_{a\chi}}{dm_a} = \frac{1}{m_\chi} + \frac{m_\chi}{m_a^2}$. The factor $r_{t\chi}$ must have the same value, only with m_t instead of m_a. Then, taking the pre-factor of m_χ into account

$$\lim_{m_\chi \to 0} m_\chi B_0(m_\chi, m_a, m_\chi) = \lim_{m_\chi \to 0} m_\chi \left[\Delta + 1 - \log \frac{m_\chi^2}{\mu^2} \right] \to 0 \tag{B.28}$$

$$\lim_{m_\chi \to 0} m_\chi B_0(m_\chi, m_t, m_\chi) = \lim_{m_\chi \to 0} m_\chi \left[\Delta + 1 - \log \frac{m_\chi^2}{\mu^2} \right] \to 0 \tag{B.29}$$

$$\lim_{m_\chi \to 0} m_\chi m_a^2 \frac{d}{dm_a^2} B_0(m_\chi, m_a, m_\chi) \to -m_\chi \to 0 \tag{B.30}$$

Thus in the limit as the DM particles are massless, the integral goes to zero as well.

Bibliography

[1]M. S. Turner, 'Λ CDM: Much More Than We Expected, but Now Less Than What We Want', Found. Phys. **48**, 1261–1278 (2018).

[2]P. Bull et al., 'Beyond ΛCDM: Problems, solutions, and the road ahead', Phys. Dark Univ. **12**, 56–99 (2016).

[3]G. R. Blumenthal, S. M. Faber, J. R. Primack and M. J. Rees, 'Formation of Galaxies and Large Scale Structure with Cold Dark Matter', Nature **311**, edited by M. A. Srednicki, 517–525 (1984).

[4]G. Bertone and D. Hooper, 'History of dark matter', Rev. Mod. Phys. **90**, 045002 (2018).

[5]K. Garrett and G. Duda, 'Dark Matter: A Primer', Adv. Astron. **2011**, 968283 (2011).

[6]K. G. Begeman, A. H. Broeils and R. H. Sanders, 'Extended rotation curves of spiral galaxies: dark haloes and modified dynamics', Monthly Notices of the Royal Astronomical Society **249**, 523–537 (1991).

[7]M. Lisanti, 'Lectures on Dark Matter Physics', in Theoretical Advanced Study Institute in Elementary Particle Physics: New Frontiers in Fields and Strings (2017), pp. 399–446.

[8]R. H. Wechsler and J. L. Tinker, 'The Connection between Galaxies and their Dark Matter Halos', Ann. Rev. Astron. Astrophys. **56**, 435–487 (2018).

[9]J. A. Tyson, G. P. Kochanski and I. P. Dell'Antonio, 'Detailed mass map of cl 0024+1654 from strong lensing', The Astrophysical Journal **498**, L107 (1998).

[10]M. Bradač et al., 'A direct empirical proof of the existence of dark matter', The Astrophysical Journal **648**, L109 (2006).

[11]C. X.-R. Observatory, *1e 0657-56: nasa finds direct proof of dark matter*, Accessed: 2024-12-04, (2006) `https://chandra.harvard.edu/photo/2006/1e0657/`.

[12]W. Y. Wong, 'Cosmological Recombination', PhD thesis (British Columbia U., 2008).

[13]Y. Akrami et al. (Planck), 'Planck 2018 results - iv. diffuse component separation', Astron. Astrophys. **641**, A4 (2020).

[14]P. A. R. Ade et al. (Planck), 'Planck 2015 results. XIII. Cosmological parameters', Astron. Astrophys. **594**, A13 (2016).

[15]D. F. Jackson Kimball and D. Budker, 'Introduction to dark matter', in *The search for ultralight bosonic dark matter*, edited by D. F. Jackson Kimball and K. van Bibber (Springer International Publishing, Cham, 2023), pp. 1–30.

[16]N. Aghanim et al. (Planck), 'Planck 2018 results. VI. Cosmological parameters', Astron. Astrophys. **641**, [Erratum: Astron.Astrophys. 652, C4 (2021)], A6 (2020).

[17]G. Arcadi, M. Dutra, P. Ghosh, M. Lindner, Y. Mambrini, M. Pierre, S. Profumo and F. S. Queiroz, 'The waning of the WIMP? A review of models, searches, and constraints', Eur. Phys. J. C **78**, 203 (2018).

[18]O. F. Piattella, *Lecture Notes in Cosmology*, UNITEXT for Physics (Springer, Cham, 2018).

[19]T. Binder, T. Bringmann, M. Gustafsson and A. Hryczuk, 'Dark matter relic abundance beyond kinetic equilibrium', Eur. Phys. J. C **81**, 577 (2021).

[20]P. Gondolo and G. Gelmini, 'Cosmic abundances of stable particles: improved analysis', Nuclear Physics B **360**, 145–179 (1991).

[21]D. Abercrombie et al., 'Dark Matter benchmark models for early LHC Run-2 Searches: Report of the ATLAS/CMS Dark Matter Forum', Phys. Dark Univ. **27**, edited by A. Boveia, C. Doglioni, S. Lowette, S. Malik and S. Mrenna, 100371 (2020).

[22]C. W. Fabjan and F. Gianotti, 'Calorimetry for particle physics', Rev. Mod. Phys. **75**, 1243–1286 (2003).

[23]M. Felcini, *Search for dark matter particle production at the lhc*, 2024.

[24]J. M. Gaskins, 'A review of indirect searches for particle dark matter', Contemp. Phys. **57**, 496–525 (2016).

[25]D. S. Akerib et al. (LZ), 'The LUX-ZEPLIN (LZ) Experiment', Nucl. Instrum. Meth. A **953**, 163047 (2020).

[26]E. Aprile et al. (XENON), 'The XENONnT dark matter experiment', Eur. Phys. J. C **84**, 784 (2024).

[27]P. Agnes et al. (DarkSide), 'Search for Dark-Matter–Nucleon Interactions via Migdal Effect with DarkSide-50', Phys. Rev. Lett. **130**, 101001 (2023).

[28]D. Huang et al. (PandaX), 'Search for Dark-Matter–Nucleon Interactions with a Dark Mediator in PandaX-4T', Phys. Rev. Lett. **131**, 191002 (2023).

[29]J. Aalbers et al. (LZ), 'First Dark Matter Search Results from the LUX-ZEPLIN (LZ) Experiment', Phys. Rev. Lett. **131**, 041002 (2023).

[30]V. Barger, W.-Y. Keung and G. Shaughnessy, 'Spin Dependence of Dark Matter Scattering', Phys. Rev. D **78**, 056007 (2008).

[31]C. A. J. O'Hare, 'New Definition of the Neutrino Floor for Direct Dark Matter Searches', Phys. Rev. Lett. **127**, 251802 (2021).

[32]E. Aprile, 'The xenon program for dark matter direct detection', Nuclear Physics B **1003**, Special Issue of Nobel Symposium 182 on Dark Matter, 116463 (2024).

[33]P. Di Gangi, 'The xenon road to direct detection of dark matter at lngs: the xenon project', Universe **7**, 10.3390/universe7080313 (2021).

[34]R. Penco, 'An Introduction to Effective Field Theories', (2020).

[35]A. V. Manohar, 'Introduction to Effective Field Theories', edited by S. Davidson, P. Gambino, M. Laine, M. Neubert and C. Salomon, 10.1093/oso/9780198855743.003.0002 (2018).

[36]A. L. Fitzpatrick, W. Haxton, E. Katz, N. Lubbers and Y. Xu, 'The Effective Field Theory of Dark Matter Direct Detection', JCAP **02**, 004 (2013).

[37]E. Del Nobile, 'Complete lorentz-to-galileo dictionary for direct dark matter detection', Physical Review D **98**, 10.1103/physrevd.98.123003 (2018).

[38]B. A. Dobrescu and I. Mocioiu, 'Spin-dependent macroscopic forces from new particle exchange', Journal of High Energy Physics **2006**, 005–005 (2006).

[39]M. E. Peskin and D. V. Schroeder, *An introduction to quantum field theory*, 1st ed. (CRC Press, 2019).

[40]M. Bauer, M. Neubert, S. Renner, M. Schnubel and A. Thamm, 'The Low-Energy Effective Theory of Axions and ALPs', JHEP **04**, 063 (2021).

[41]D. J. E. Marsh, 'Axions and ALPs: a very short introduction', in 13th Patras Workshop on Axions, WIMPs and WISPs (2018), pp. 59–74.

[42]R. J. Crewther, P. Di Vecchia, G. Veneziano and E. Witten, 'Chiral Estimate of the Electric Dipole Moment of the Neutron in Quantum Chromodynamics', Phys. Lett. B **88**, [Erratum: Phys.Lett.B 91, 487 (1980)], 123 (1979).

[43]J. M. Pendlebury et al., 'Revised experimental upper limit on the electric dipole moment of the neutron', Phys. Rev. D **92**, 092003 (2015).

[44]R. D. Peccei and H. R. Quinn, 'CP conservation in the presence of pseudoparticles', Phys. Rev. Lett. **38**, 1440–1443 (1977).

[45]R. D. Peccei and H. R. Quinn, 'Constraints imposed by CP conservation in the presence of pseudoparticles', Phys. Rev. D **16**, 1791–1797 (1977).

[46]S. Weinberg, 'A new light boson?', Phys. Rev. Lett. **40**, 223–226 (1978).

[47]F. Wilczek, 'Problem of strong P and T invariance in the presence of instantons', Phys. Rev. Lett. **40**, 279–282 (1978).

[48]C. Eröncel, 'Axion-like-particle dark matter beyond the standard paradigm', in (Jan. 2025).

[49]S. Allen, A. Blackburn, O. Cardenas, Z. Messenger, N. H. Nguyen and B. Shuve, 'Electroweak axion portal to dark matter', Phys. Rev. D **110**, 095010 (2024).

[50]M. Bauer, M. Neubert, S. Renner, M. Schnubel and A. Thamm, 'Flavor probes of axion-like particles', JHEP **09**, 056 (2022).

[51]A. Stadler and F. Gross, 'Covariant spectator theory: foundations and applications', Few-Body Systems **49**, 91–110 (2011).

[52]M. Peña, G. Ramalho and F. Gross, 'Electromagnetic structure of the baryon within the covariant spectator theory', Few-Body Systems **49**, 111–119 (2011).

[53]G. Passarino and M. Veltman, 'One-loop corrections for e+e- annihilation into $+-$ in the weinberg model', Nuclear Physics B **160**, 151–207 (1979).

[54]G. Devaraj and R. G. Stuart, 'Reduction of one loop tensor form-factors to scalar integrals: A General scheme', Nucl. Phys. B **519**, 483–513 (1998).

[55]C. Anastasiou, J. Karlen and M. Vicini, 'Tensor reduction of loop integrals', JHEP **12**, 169 (2023).

[56]A. Denner, 'Techniques for calculation of electroweak radiative corrections at the one loop level and results for W physics at LEP-200', Fortsch. Phys. **41**, 307–420 (1993).

[57]V. Shtabovenko, R. Mertig and F. Orellana, 'FeynCalc 10: Do multiloop integrals dream of computer codes?', Comput. Phys. Commun. **306**, 109357 (2025).

[58]V. Shtabovenko, R. Mertig and F. Orellana, 'FeynCalc 9.3: New features and improvements', Comput. Phys. Commun. **256**, 107478 (2020).

[59]V. Shtabovenko, R. Mertig and F. Orellana, 'New Developments in FeynCalc 9.0', Comput. Phys. Commun. **207**, 432–444 (2016).

[60]R. Mertig, M. Böhm and A. Denner, 'Feyn calc - computer-algebraic calculation of feynman amplitudes', Computer Physics Communications **64**, 345–359 (1991).

[61]S. Navas et al. (Particle Data Group), 'Review of particle physics', Phys. Rev. D **110**, 030001 (2024).

[62]J. Martin Camalich, M. Pospelov, P. N. H. Vuong, R. Ziegler and J. Zupan, 'Quark Flavor Phenomenology of the QCD Axion', Phys. Rev. D **102**, 015023 (2020).

[63]T. Ferber, A. Filimonova, R. Schäfer and S. Westhoff, 'Displaced or invisible? ALPs from B decays at Belle II', JHEP **04**, 131 (2023).

[64]E. Cortina Gil et al. (NA62), 'Search for a feebly interacting particle X in the decay $K^+ \to \pi^+ X$', JHEP **03**, 058 (2021).

[65]N. Carrasco, P. Lami, V. Lubicz, L. Riggio, S. Simula and C. Tarantino, '$K \to \pi$ semileptonic form factors with $N_f = 2 + 1 + 1$ twisted mass fermions', Phys. Rev. D **93**, 114512 (2016).

[66]N. Gubernari, A. Kokulu and D. van Dyk, '$B \to P$ and $B \to V$ Form Factors from B-Meson Light-Cone Sum Rules beyond Leading Twist', JHEP **01**, 150 (2019).

[67]A. Abdel-Rehim, C. Alexandrou, M. Constantinou, K. Hadjiyiannakou, K. Jansen, C. Kallidonis, G. Koutsou and A. Vaquero Aviles-Casco (ETM), 'Direct Evaluation of the Quark Content of Nucleons from Lattice QCD at the Physical Point', Phys. Rev. Lett. **116**, 252001 (2016).

[68]A. Freitas, S. Westhoff and J. Zupan, 'Integrating in the Higgs Portal to Fermion Dark Matter', JHEP **09**, 015 (2015).

[69]G. Aad et al. (ATLAS), 'Determination of the strong coupling constant from transverse energy−energy correlations in multijet events at $\sqrt{s} = 13$ TeV with the ATLAS detector', JHEP **07**, 085 (2023).

[70]A. M. Sirunyan et al. (CMS), 'Measurement of the top quark Yukawa coupling from $\mathrm{t\bar{t}}$ kinematic distributions in the dilepton final state in proton-proton collisions at $\sqrt{s} = 13$ TeV', Phys. Rev. D **102**, 092013 (2020).

[71]D. S. Akerib et al. (LZ), 'Projected WIMP sensitivity of the LUX-ZEPLIN dark matter experiment', Phys. Rev. D **101**, 052002 (2020).

[72]E. Aprile et al. (XENON), 'First Dark Matter Search with Nuclear Recoils from the XENONnT Experiment', Phys. Rev. Lett. **131**, 041003 (2023).

[73]E. Aprile et al. (XENON), 'Projected WIMP sensitivity of the XENONnT dark matter experiment', JCAP **11**, 031 (2020).

[74]P. Adari et al. (SENSEI), 'First Direct-Detection Results on Sub-GeV Dark Matter Using the SENSEI Detector at SNOLAB', Phys. Rev. Lett. **134**, 011804 (2025).

[75]B. Carew, A. R. Caddell, T. N. Maity and C. A. J. O'Hare, 'Neutrino fog for dark matter-electron scattering experiments', Phys. Rev. D **109**, 083016 (2024).